

# Compass models: Theory and physical motivations

Zohar Nussinov\*

Department of Physics, Washington University, St. Louis, Missouri 63160, USA

Jeroen van den Brink

Institute for Theoretical Solid State Physics, IFW Dresden, 01069 Dresden, Germany  
and Department of Physics, Technical University Dresden, 01062 Dresden, Germany

(published 12 January 2015)

*Compass models* are theories of matter in which the couplings between the internal spin (or other relevant field) components are inherently spatially (typically, direction) dependent. A simple illustrative example is furnished by the  $90^\circ$  compass model on a square lattice in which only couplings of the form  $\tau_i^x \tau_j^y$  (where  $\{\tau_i^a\}_a$  denote Pauli operators at site  $i$ ) are associated with nearest-neighbor sites  $i$  and  $j$  separated along the  $x$  axis of the lattice while  $\tau_i^y \tau_j^x$  couplings appear for sites separated by a lattice constant along the  $y$  axis. Similar compass-type interactions can appear in diverse physical systems. For instance, compass models describe Mott insulators with orbital degrees of freedom where interactions sensitively depend on the spatial orientation of the orbitals involved as well as the low-energy effective theories of frustrated quantum magnets, and a host of other systems such as vacancy centers, and cold atomic gases. The fundamental interdependence between internal (spin, orbital, or other) and external (i.e., spatial) degrees of freedom which underlies compass models generally leads to very rich behaviors, including the frustration of (semi-)classical ordered states on nonfrustrated lattices, and to enhanced quantum effects, prompting, in certain cases, the appearance of zero-temperature quantum spin liquids. As a consequence of these frustrations, new types of symmetries and their associated degeneracies may appear. These *intermediate symmetries* lie midway between the extremes of global symmetries and local gauge symmetries and lead to effective dimensional reductions. In this article, compass models are reviewed in a unified manner, paying close attention to exact consequences of these symmetries and to thermal and quantum fluctuations that stabilize orders via *order-out-of-disorder* effects. This is complemented by a survey of numerical results. In addition to reviewing past works, a number of other models are introduced and new results established. In particular, a general link between flat bands and symmetries is detailed.

DOI: [10.1103/RevModPhys.87.1](https://doi.org/10.1103/RevModPhys.87.1)

PACS numbers: 71.27.+a, 03.67.Lx

## CONTENTS

I. Introduction and Outline	2	B. Quantum compass models	13
A. Introduction	2	B. Momentum space representations	13
B. Outline of the review	3	1. Dimensional reduction	13
II. Compass Model Overview	3	2. (In)commensurate ground states	14
A. Definition of quantum compass models	3	C. Ising model representations	14
1. $90^\circ$ compass models	4	D. Dynamics: Equation of motion	15
2. Kitaev's honeycomb model	6	V. Physical Motivations and Incarnations	15
3. The XXZ honeycomb compass model	6	A. Orbital degrees of freedom	16
4. $120^\circ$ compass models	7	1. Atomiclike states in correlated solids	16
B. Hybrid compass models	8	2. Representations of orbital states	17
III. Generalized and Extended Compass Models	8	3. Orbital-orbital interactions	18
A. Kugel-Khomskii spin-orbital models	8	a. $e_g$ -orbital-only Hamiltonians	19
B. Classical, higher- $D$ , and large- $n$ generalizations	9	b. Compass and Kitaev Hamiltonians	20
C. Other extended compass models	10	c. $t_{2g}$ orbital-only Hamiltonian	21
1. Arbitrary angle	10	4. Spin-spin and orbital-orbital interactions	22
2. Plaquette and checkerboard (sub)lattices	11	5. Compass Hubbard models	23
3. Longer-range and ring interactions	11	6. Lattice-mediated interactions	23
IV. Compass Model Representations	12	7. Charge transfer effects through ligand sites	24
A. Continuum representation	12	B. Cold atom systems	24
1. Classical compass models	12	1. Engineering tunneling amplitudes	25
		2. Bosonic gases with orbital degree of freedom	25
		3. Fermionic gases with orbital degree of freedom	25
		4. Fermions in an optical lattice	26
		5. Spin interactions on a lattice	26

\*Current address: Department of Condensed Matter Physics, Weizmann Institute of Science, Rehovot 76100, Israel.

6. Three-flavor compass models	27	3. The classical 90° model on a cubic lattice	48
C. Chiral degrees of freedom in frustrated magnets	27	4. The quantum 90° model on a cubic lattice	48
1. Nonuniform trimerized kagome lattice antiferromagnet	27	B. Classical 120° model	49
2. Uniform kagome antiferromagnet	28	C. Discrete classical 120° compass model	49
VI. Symmetries of Compass Models	29	D. Extended 120° model	50
A. Global, topological, and intermediate symmetries and invariances	29	1. Classical extended 120° model	50
B. Exact and emergent symmetries	30	2. Quantum extended 120° model	50
C. Consequences of intermediate symmetry	31	E. Honeycomb lattice 120° compass models	50
1. Degeneracy of spectrum	31	1. Classical model	50
2. Dimensional reduction	31	2. Quantum model	51
a. Theorem on dimensional reduction	31	F. Checkerboard lattice compass models	51
b. Corollaries	31	G. Arbitrary-angle compass models	52
D. Symmetries of the 90° compass model	32	H. XXZ honeycomb compass model	52
1. Exact discrete intermediate symmetries	32	I. Plaquette orbital model	52
2. Exact discrete global symmetries	33	1. Exact symmetries	52
3. Emergent intermediate discrete symmetries: Cubic 90° model	33	2. Classical ground states and emergent symmetries	52
4. Emergent continuous global symmetries	34	3. Finite-temperature order out of disorder	53
E. Emergent symmetries: Classical cubic 120° compass model	34	J. Gell-Mann matrix compass models	53
1. Emergent continuous global symmetries	34	1. Cubic lattice Gell-Mann matrix compass model	53
2. Emergent discrete $d = 2$ symmetries	34	2. Diamond lattice Gell-Mann matrix compass model	53
F. Emergent symmetries: Classical honeycomb 120° compass model	35	K. Symmetric extended compass Hubbard models	54
1. Ground states and emergent intermediate symmetries	35	X. Conclusions	54
2. Emergent local symmetries	35	Acknowledgments	55
G. Emergent symmetries of the triangular 120° compass model	36	Appendix A: The Bond Algebra of the Plaquette Orbital Model	55
H. Three-component Kugel-Khomskii model	36	Appendix B: Gell-Mann Matrices	56
VII. Intermediate Symmetries and Flat Bands in Classical Spin-wave Dispersion	37	Appendix C: Classical and Quantum Fluctuations in the Large- $n$ Limit	56
A. Uniform states as ground states of classical compass models	37	References	57
B. Stratification in classical compass models	38		
C. Flat bands: Momentum space consequences of real space stratified ground states	38		
1. Spin waves of cubic lattice 120° compass model	39		
2. Honeycomb lattice 120° compass model	39		
VIII. Order by Disorder in Compass Models	40		
A. Classical and quantum order out of disorder	40		
B. Cubic lattice 120° compass model	40		
1. Thermal fluctuations	40		
2. Quantum order out of disorder	41		
C. 90° compass models	42		
1. Quantum planar 90° compass models	42		
2. Classical 90° compass models	42		
D. 120° honeycomb model	43		
1. Thermal fluctuations	43		
2. Quantum fluctuations	43		
E. Effect of dilution	43		
F. High-temperature correlations and dimensional reduction	44		
IX. Phases and Phase Transitions in Compass Models	44		
A. 90° compass models	44		
1. Classical square lattice	44		
2. Quantum square lattice 90° compass model	46		
a. Finite-temperature transitions	46		
b. Zero-temperature transitions	46		

## I. INTRODUCTION AND OUTLINE

### A. Introduction

This article reviews compass models. The term “compass models” refers to a family of closely related lattice models involving interacting quantum degrees of freedom (and their classical approximants). Members of this family appear in very different physical contexts. Already more than three decades ago they were first encountered as minimal models to describe interactions between orbital degrees of freedom in strongly correlated electron materials (Kugel and Khomskii, 1982). The name *orbital compass model* was coined at the time, but only in the past decade have these models started to receive wide-spread attention to describe physical properties of materials with orbital degrees of freedom (Tokura and Nagaosa, 2000; van den Brink, 2004; Khaliullin, 2005).

In different guises, these models describe the phase variable in certain superconducting Josephson-junction arrays (Xu and Moore, 2004; Nussinov and Fradkin, 2005) and exchange interactions in ultracold atomic gasses (Duan, Demler, and Lukin, 2003; Wu, 2008). Last but not least, quantum compass models have recently made an entrance onto the scene of quantum information theory as mathematical models for topological quantum computing (Kitaev, 2003): The much-studied Kitaev’s honeycomb model has the structure of a compass model. It is interesting to note that the apparently different fields such as those dealing with orbital degrees of freedom in complex oxides and those studying theoretical

models for quantum computing have compass models in common and can thereby in principle cross fertilize.

In the current work, we review the different incarnations of compass models, their physical motivations, symmetries, ordering, and excitations. One should stress however, that although the investigation of compass models has grown into a considerable area of research, this is an active field of research with still many interesting and open problems, as will become more explicit in the following. In a subsequent review (Nussinov and van den Brink, 2015), we provide an in-depth overview of the relation between orbital models and Kitaev's models for quantum computation.

## B. Outline of the review

We start by introducing and defining, in Sec. II, various compass models. Next, in Sec. III, we discuss viable extensions of more typical compass models including, e.g., ring exchange and extensions to general spatial dimensions. While the most common representation of compass models is that on a lattice, other representations are noteworthy.

In Sec. IV, we introduce previously largely unstudied continuum model representations that are suited for field-theoretic treatments, introduce general momentum space representations, and illustrate how this naturally suggests the presence of dimensional reductions in compass models. We furthermore discuss classical incommensurate ground states and the representation of a quantum compass model as an unusual *anisotropic* classical Ising model. In Sec. IV.D, the general equations of motion associated with compass theories are presented; these equations capture the quintessential anisotropic character of the compass models.

In Sec. V we survey the physical contexts that motivate compass models and derive them for special cases. This includes situations where the compass degrees of freedom represent orbital degrees of freedom (Sec. V.A). We review how they emerge, how they interact, and how they are described mathematically in terms of orbital Hamiltonians. Most typical representations rely on SU(2) algebra but we also discuss SU(3) Gell-Mann and other matrix forms that are better suited for the description of certain orbital systems. In Sec. V.B we proceed with a review of the realization of compass models in cold atomic systems. We conclude our general discussion of incarnations of compass models in general physical systems in Sec. V.C, where we discuss how the effective low-energy theories in chiral frustrated magnets (such as the kagome and triangular antiferromagnets) are of the compass model type.

In Sec. VI, we turn to one of the most common unifying features of compass models: the *intermediate symmetries* that they exhibit. We explain what these symmetries are and place them in perspective to the two extremes of global and local gauge symmetries. We discuss precise consequences of these symmetries, notably those concerning effective dimensional reductions, briefly allude to relations to topological quantum orders, and illustrate how these symmetries arise in the various compass models.

In Sec. VII, we introduce *new results*: an exact relation between intermediate symmetries and band structures. In particular, we illustrate how flat bands can arise and are protected by the existence of these symmetries and demonstrate

how this is materialized in various compass models. One common and important consequence of intermediate symmetries is the presence of a subextensive exponentially large ground-state degeneracy. We discuss situations where this degeneracy is exact and ones in which it emerges in various limits.

In Sec. VIII, we review how low-temperature orders in various compass models nevertheless appear and are stabilized by fluctuations or, as they are often termed, *order-out-of-disorder* effects. As we will explain, orders in classical compass models that we study are, rigorously, stabilized by thermal fluctuations. This ordering tendency is further bolstered by quantum zero-point fluctuations. Because of an exact equivalence between the large- $n$  and high-temperature limits, the low-temperature behavior of compass models is supplanted by exact results at high temperatures as reviewed in Sec. VIII.F. Following the review of these earlier analytic results concerning the limiting behaviors at both low and high temperatures, we finally turn in Sec. IX to numerical results concerning the phases and transitions in various compass model systems.

## II. COMPASS MODEL OVERVIEW

### A. Definition of quantum compass models

In order to define quantum compass models, we start by considering a lattice with sites on which quantum degrees of freedom exist. Throughout this review the total number of lattice sites is denoted by  $N$ . Each lattice site has a vector pointing to it that is denoted by  $\mathbf{r}$ . When square (or cubic) lattices are involved, these are considered of dimension  $N = L \times L$  (or  $N = L \times L \times L$ ). On more general lattices,  $L$  denotes the typical linear dimension (i.e., linear extent along one of the crystal axes). We set the lattice constant to unity. The spatial dimensionality of the lattice is denoted by  $D$  (e.g.,  $D = 2$  for the square and honeycomb lattices,  $D = 3$  in cubic and pyrochlore lattices, etc.).

Depending on the physical problems at hand, we will refer to these degrees of freedom at the lattice sites as spins, pseudospins, or orbitals. We denote these degrees of freedom by  $\tau_i$ , where  $i$  labels the lattice sites and  $\tau \equiv (1/2)(\sigma^x, \sigma^y, \sigma^z)$ , where  $\sigma^x$ ,  $\sigma^y$ , and  $\sigma^z$  are the Pauli matrices. In terms of the creation ( $c_\alpha^\dagger$ ) and annihilation ( $c_\alpha$ ) operators for an electron in state  $\alpha$ , the pseudospin operator  $\tau$  can be expressed as  $\tau = (1/2)\sum_{\alpha\beta} c_\alpha^\dagger \sigma_{\alpha\beta} c_\beta$ , where the sum is over the two different possibilities for each  $\alpha$  and  $\beta$ . Here  $\tau$  is the fundamental  $T = 1/2$  representation of SU(2); for  $T > 1/2$  we will generally employ  $T$  to denote that  $T_x$ ,  $T_y$ , and  $T_z$  triad (or  $T_{1,2,3}$  which we will interchangeably often use).

A representation in terms of Pauli matrices is particularly useful for degrees of freedom that have two flavors, for instance, two possible orientations of a spin (up or down) or two possible orbitals that an electron can occupy, as the Pauli matrices are generators of SU(2), the group of  $2 \times 2$  matrices with determinant 1. For degrees of freedom with  $n$  flavors, we use a representation in terms of the generators of SU( $n$ ), which for the particular case of  $n = 3$  are the eight Gell-Mann matrices  $\lambda_i$ , with  $i = 1 - 8$  (see Appendix B).

The name that one chooses for the degree of freedom (whether spin, pseudospin, color, flavor, or orbital) is, of course, mathematically irrelevant. For SU(2) quantum

compass models it is important that the components of  $\tau$  obey the well-known commutation relation  $[\tau^x, \tau^y] = i\tau^z$ , and its cyclic permutations, and that  $(\tau^\gamma)^2 = 1/4$  for any component  $\gamma = x, y$ , or  $z$ . For SU(3), in the fundamental representation  $\tau$  is the eight-component vector  $\tau = (1/2)\sum_{\alpha\beta} c_\alpha^\dagger \lambda_{\alpha\beta} c_\beta$ , with the commutation relations governed by the Gell-Mann matrices.

Compass models are characterized by the specific form that the interaction between the degrees of freedom assumes: (i) there is an interaction only between certain *vector components* of  $\tau$  and (ii) on different bonds in the lattice, different vector components interact. When, for instance, a site  $i$  is linked to nearest-neighbor sites  $j$  and  $k$ , the interaction along the lattice link  $\langle ij \rangle$  can be of the type  $\tau_i^y \tau_j^x$ , whereas on the link  $\langle ik \rangle$  it is  $\tau_i^y \tau_k^y$ . In the following specific Hamiltonians corresponding to various quantum compass models are introduced, in particular, the  $90^\circ$  compass models, Kitaev's honeycomb model,  $120^\circ$  compass models, and a number of generalizations thereof.

### 1. $90^\circ$ compass models

A basic realization of a quantum compass model can be set up on a two-dimensional square lattice, where every site has two horizontal and two vertical bonds. If one defines the interaction along horizontal ( $H$ ) lattice links  $\langle ij \rangle_H$  to be  $J\tau_i^x \tau_j^x$  and along the vertical ( $V$ ) links  $\langle ij \rangle_V$  to be  $J\tau_i^y \tau_j^y$ , we have constructed the so-called two-dimensional  $90^\circ$  quantum compass model, also known as the planar  $90^\circ$  orbital compass model; see Fig. 1. Its Hamiltonian is given by

$$H_{\square}^{90^\circ} = -J_x \sum_{\langle ij \rangle_H} \tau_i^x \tau_j^x - J_y \sum_{\langle ij \rangle_V} \tau_i^y \tau_j^y. \quad (1)$$

The isotropic variant of this system has equal couplings along the vertical and horizontal directions ( $J_x = J_y = J$ ). The minus signs that appear in this Hamiltonian were chosen such that the interactions between the pseudospins  $\tau$  tend to stabilize uniform ground states with ‘ferro’ pseudospin order. (In  $D = 2$  the  $90^\circ$  compass models with ferro and ‘antiferro’ interactions are directly related by symmetry; see Sec. II.A.4.) For clarity, we note that the isotropic two-dimensional compass model is very different from the two-dimensional Ising model

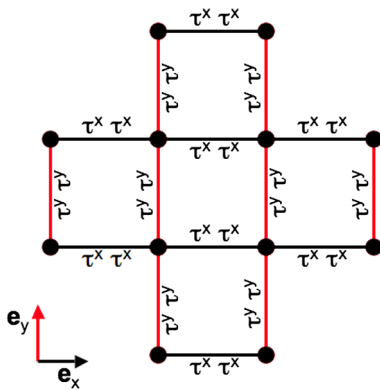


FIG. 1 (color online). The planar  $90^\circ$  compass model on a square lattice: The interaction of (pseudo)spin degrees of freedom  $\tau = (\tau^x, \tau^y)$  along horizontal bonds that are connected by the unit vector  $e_x$  is  $\tau_r^x \tau_{r+e_x}^x$ . Along vertical bonds  $e_y$ , it is  $\tau_r^y \tau_{r+e_y}^y$ .

$$H_{\square}^{\text{Ising}} = -J \sum_{\langle ij \rangle_H} \tau_i^x \tau_j^x - J \sum_{\langle ij \rangle_V} \tau_i^y \tau_j^y = -J \sum_{\langle ij \rangle} \tau_i^x \tau_j^x,$$

where on each horizontal and vertical vertex of the square lattice the interaction is the same and of the form  $\tau_i^x \tau_j^x$ —it is also very different from the two-dimensional XY model

$$H_{\square}^{XY} = -J \sum_{\langle ij \rangle_H, \langle ij \rangle_V} (\tau_i^x \tau_j^x + \tau_i^y \tau_j^y),$$

because also in this case on all bonds the interaction terms in the Hamiltonian are of the same form, i.e.,  $(\tau_i \cdot \tau_j)$ .

One can rewrite the  $90^\circ$  compass Hamiltonian in a more compact form by introducing the unit vectors  $e_x$  and  $e_y$  that denote the bonds along the  $x$  and  $y$  directions in the two-dimensional (2D) lattice, so that

$$H_{\square}^{90^\circ} = -J \sum_{\mathbf{r}} (\tau_{\mathbf{r}}^x \tau_{\mathbf{r}+e_x}^x + \tau_{\mathbf{r}}^y \tau_{\mathbf{r}+e_y}^y), \quad (2)$$

where the sum over  $\mathbf{r}$  represents the sum over lattice sites and every bond is counted only once. With this notation the compass model Hamiltonian can be cast in the more general form

$$H_{\square}^{90^\circ} = -J \sum_{\mathbf{r}, \gamma} \tau_{\mathbf{r}}^\gamma \tau_{\mathbf{r}+e_\gamma}^\gamma, \quad (3)$$

where for the  $90^\circ$  square lattice compass model  $H_{\square}^{90^\circ}$ , we have  $\gamma = 1, 2$ ,  $\{\tau^\gamma\} = \{\tau^1, \tau^2\} = \{\tau^x, \tau^y\}$ , and  $\{e_\gamma\} = \{e_1, e_2\} = \{e_x, e_y\}$ .

This generalized notation allows for different compass models and the more well-known models such as the Ising or Heisenberg model to be cast in the same form; see Table I. For instance, the two-dimensional square lattice Ising model  $H_{\square}^{\text{Ising}}$  corresponds to  $\gamma = 1, 2$  with  $\{\tau^\gamma\} = \{\tau^x, \tau^x\}$  and  $\{e_\gamma\} = \{e_x, e_y\}$ . The Ising model on a three-dimensional cubic lattice is then given by  $\gamma = 1, \dots, 3$ ,  $\{\tau^\gamma\} = \{\tau^x, \tau^x, \tau^x\}$ , and  $\{e_\gamma\} = \{e_x, e_y, e_z\}$ . The XY model on a square lattice  $H_{\square}^{XY}$  corresponds to Eq. (4) with  $\gamma = 1, \dots, 4$ ,  $\{\tau^\gamma\} = \{\tau^x, \tau^y, \tau^x, \tau^y\}$ , and  $\{e_\gamma\} = \{e_x, e_x, e_y, e_y\}$ . Another example is the square lattice Heisenberg model, where  $\gamma = 1, \dots, 6$ ,  $\{\tau^\gamma\} = \{\tau^x, \tau^y, \tau^z, \tau^x, \tau^y, \tau^z\}$ , and  $\{e_\gamma\} = \{e_x, e_x, e_x, e_y, e_y, e_y\}$ , so that in this case  $\sum_{\gamma} \tau_{\mathbf{r}}^\gamma \tau_{\mathbf{r}+e_\gamma}^\gamma = \sum_{\gamma} \tau_{\mathbf{r}} \cdot \tau_{\mathbf{r}+e_\gamma}$ .

This class of compass models can be further generalized in a straightforward manner by allowing for a coupling strength  $J_\gamma$  between the pseudospins  $\tau^\gamma$  that depends on the direction of the bond  $\gamma$  [anisotropic compass models (Nussinov and Fradkin, 2005)] and by adding a field  $h_\gamma$  that couples to  $\tau^\gamma$  linearly (Nussinov and Ortiz, 2008; Scarola, Whaley, and Troyer, 2009). This generalized class of compass models is then defined by the Hamiltonian

$$\mathcal{H}_{\text{compass}} = - \sum_{\mathbf{r}, \gamma} (J_\gamma \tau_{\mathbf{r}}^\gamma \tau_{\mathbf{r}+e_\gamma}^\gamma + h_\gamma \tau_{\mathbf{r}}^\gamma). \quad (4)$$

From a historical viewpoint the three-dimensional  $90^\circ$  compass model is particularly interesting. Denoted by  $H_{3\text{D}}^{90^\circ}$ , it is customarily defined on a cubic lattice and given by

TABLE I. Generalized notation that casts compass models and more well-known Hamiltonians such as the Ising,  $XY$ , or Heisenberg models in the same form. Additional spatial anisotropies can be introduced, for instance, by coupling constants  $J_\gamma$  that depend on the bond direction  $\mathbf{e}_\gamma$ . Doing so changes the strengths of the interaction on different links, but not the form of those interactions: these are determined by how different vector components of  $\boldsymbol{\tau}_r$  and  $\boldsymbol{\tau}_{r+\mathbf{e}_\gamma}$  couple.

$\{\tau^\gamma\}$	$\{\mathbf{e}_\gamma\}$	Model name	Symbol	Dimension
$\{\tau^x\}$	$\{\mathbf{e}_x\}$	Ising chain	$H_1^{\text{Ising}}$	1
$\{\tau^x, \tau^y\}$	$\{\mathbf{e}_x, \mathbf{e}_y\}$	$XY$ chain	$H_1^{XY}$	1
$\{\tau^x, \tau^y, \tau^z\}$	$\{\mathbf{e}_x, \mathbf{e}_y, \mathbf{e}_z\}$	Heisenberg chain	$H_1^{\text{Heis}}$	1
$\{\tau^x, \tau^y\}$	$\{\mathbf{e}_x, \mathbf{e}_y\}$	Square Ising	$H_{\square}^{\text{Ising}}$	2
$\{\tau^x, \tau^y, \tau^z\}$	$\{\mathbf{e}_x, \mathbf{e}_y, \mathbf{e}_z\}$	Cubic Ising	$H_{3\square}^{\text{Ising}}$	3
$\{\tau^x, \tau^y, \tau^z, \tau^x, \tau^y\}$	$\{\mathbf{e}_x, \mathbf{e}_x, \mathbf{e}_y, \mathbf{e}_y\}$	Square $XY$	$H_{\square}^{XY}$	2
$\{\tau^x, \tau^y, \tau^z, \tau^x, \tau^y, \tau^z\}$	$\{\mathbf{e}_x, \mathbf{e}_x, \mathbf{e}_y, \mathbf{e}_y, \mathbf{e}_z, \mathbf{e}_z\}$	Square Heisenberg	$H_{\square}^{\text{Heis}}$	2
$\{\tau^x, \tau^y\}$	$\{\mathbf{e}_x, \mathbf{e}_y\}$	Square $90^\circ$ compass	$H_{\square}^{90^\circ}$	2
$\{\tau^x, \tau^y, \tau^z\}$	$\{\mathbf{e}_x, \mathbf{e}_y, \mathbf{e}_z\}$	Cubic $90^\circ$ compass	$H_{3\square}^{90^\circ}$	3
$\{\frac{\tau^x+\sqrt{3}\tau^y}{2}, \frac{\tau^x-\sqrt{3}\tau^y}{2}\}$	$\{\mathbf{e}_x, \mathbf{e}_y\}$	Square $120^\circ$ compass	$H_{\square}^{120^\circ}$	2
With $\{\theta_\gamma\} = \{0, 2\pi/3, 4\pi/3\}$ :				
$\{\tau^x, \tau^x, \tau^x\}$	$\mathbf{e}_x \cos \theta_\gamma + \mathbf{e}_y \sin \theta_\gamma$	Honeycomb Ising	$H_{\circlearrowleft}^{\text{Ising}}$	2
$\{\tau^x, \tau^y, \tau^z\}$	$\mathbf{e}_x \cos \theta_\gamma + \mathbf{e}_y \sin \theta_\gamma$	Honeycomb Kitaev	$H_{\circlearrowleft}^{\text{Kitaev}}$	2
$\{\tau^x, \tau^x, \tau^z\}$	$\mathbf{e}_x \cos \theta_\gamma + \mathbf{e}_y \sin \theta_\gamma$	Honeycomb $XXZ$	$H_{\circlearrowleft}^{XXZ}$	2
$\pi^\gamma = \tau^x \cos \theta_\gamma + \tau^y \sin \theta_\gamma$	$\{\mathbf{e}_x, \mathbf{e}_y, \mathbf{e}_z\}$	Cubic $120^\circ$	$H_{3\square}^{120^\circ}$	3
$\pi^\gamma$	$\mathbf{e}_x \cos \theta_\gamma + \mathbf{e}_y \sin \theta_\gamma$	Honeycomb $120^\circ$	$H_{\circlearrowleft}^{120^\circ}$	2
With $\{\theta_\gamma\} = \{0, 2\pi/3, 4\pi/3\}$ and $\eta = \pm 1$ :				
$\{\tau^x, \tau^y, \tau^z\}$	$\eta \mathbf{e}_x \cos \frac{\theta_\gamma}{2} + \eta \mathbf{e}_y \sin \frac{\theta_\gamma}{2}$	Triangular Kitaev	$H_{\Delta}^{\text{Kitaev}}$	2
$\pi^\gamma$	$\eta \mathbf{e}_x \cos \frac{\theta_\gamma}{2} + \eta \mathbf{e}_y \sin \frac{\theta_\gamma}{2}$	Triangular $120^\circ$	$H_{\Delta}^{120^\circ}$	2

$\mathcal{H}_{\text{compass}}$  [Eq. (4)] where  $\gamma$  spans three Cartesian directions:  $\gamma = 1, \dots, 3$  with  $\{\tau^\gamma\} = \{\tau^x, \tau^y, \tau^z\}$ ,  $J_\gamma = J = 1$ ,  $h_\gamma = 0$ , and  $\{\mathbf{e}_\gamma\} = \{\mathbf{e}_x, \mathbf{e}_y, \mathbf{e}_z\}$ , so that

$$H_{3\square}^{90^\circ} = -J \sum_r (\tau_r^x \tau_{r+\mathbf{e}_x}^x + \tau_r^y \tau_{r+\mathbf{e}_y}^y + \tau_r^z \tau_{r+\mathbf{e}_z}^z). \quad (5)$$

Thus, by allowing  $\gamma$  to assume values  $\gamma = 1, 2, 3$  the square lattice  $90^\circ$  compass model of Eq. (3) is trivially extended to three spatial dimensions. Similarly, by allowing  $\gamma = 1, 2, \dots, D$ , it can be extended to arbitrary spatial dimension  $D$  (which we return to in later sections). The structure

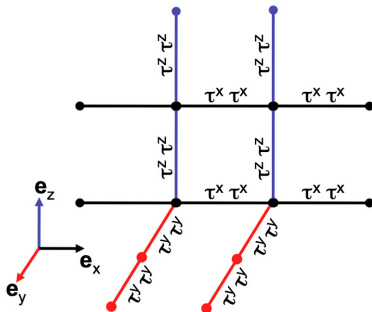


FIG. 2 (color online). The  $90^\circ$  compass model on a cubic lattice: The interaction of (pseudo)spin degrees of freedom  $\boldsymbol{\tau} = (\tau^x, \tau^y, \tau^z)$  along horizontal bonds that are connected by the unit vector  $\mathbf{e}_x$  is  $J\tau_i^x \tau_{i+\mathbf{e}_x}^x$ . On bonds connected by  $\mathbf{e}_y$  it is  $J\tau_i^y \tau_{i+\mathbf{e}_y}^y$  and along the vertical bonds it is  $J\tau_i^z \tau_{i+\mathbf{e}_z}^z$ .

of  $H_{3\square}^{90^\circ}$  is schematically indicated in Fig. 2. This compass model is actually the one originally proposed by Kugel and Khomskii (1982) in the context of orbital ordering. At that time it was noted that even if the interaction on each individual bond is Ising-like, the overall symmetry of the model is considerably more complicated, as is reviewed in Sec. V.A.

In alternative notations for compass model Hamiltonians, one introduces the unit vector  $\mathbf{n}$  connecting neighboring lattice sites  $i$  and  $j$ . Along the three Cartesian axes on a cubic lattice, for instance,  $\mathbf{n}$  equals  $\mathbf{e}_x = (1, 0, 0)$ ,  $\mathbf{e}_y = (0, 1, 0)$ , or  $\mathbf{e}_z = (0, 0, 1)$ . With this one can express  $\tau^x$  as  $\tau^x = \boldsymbol{\tau} \cdot \mathbf{e}_x$ , so that with this vector notation

$$H_{3\square}^{90^\circ} = -\sum_{r,\gamma} \tau_r^\gamma \tau_{r+\mathbf{e}_\gamma}^\gamma = -\sum_{ij} (\boldsymbol{\tau}_i \cdot \mathbf{n})(\boldsymbol{\tau}_j \cdot \mathbf{n}). \quad (6)$$

This elegant vector form stresses the compass nature of the interactions between the pseudospins. This notation, however, does not always generalize easily to cases with higher dimensions and/or different lattice geometries. All Hamiltonians in this review are therefore given in terms of  $\tau^\gamma$  operators and are complemented by an expression in vector notation where appropriate.

It is typical for compass models that even the ground-state structure is nontrivial. For a system governed by  $H_{3\square}^{90^\circ}$ , pairs of pseudospins on lattice links parallel to the  $x$  axis, for instance, favor pointing their pseudospins  $\boldsymbol{\tau}$  along  $x$  so that the expectation value  $\langle \tau^x \rangle \neq 0$ ; see Fig. 3. Similarly, on bonds

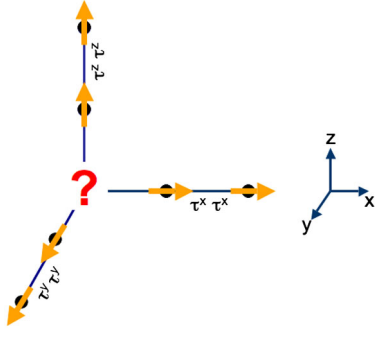


FIG. 3 (color online). Frustration in the  $90^\circ$  compass model on a cubic lattice. The interactions between pseudospins  $\tau$  are such that the pseudospins tend to align their components  $\tau^x$ ,  $\tau^y$ , and  $\tau^z$  along the  $x$ ,  $y$ , and  $z$  axes, respectively. This causes mutually exclusive ordering patterns.

parallel to the  $y$  direction, it is advantageous for the pseudospins to align along the  $y$  direction, so that  $\langle \tau^y \rangle \neq 0$ . It is clear that at a site the bonds along  $x$ ,  $y$ , and  $z$  cannot be satisfied at the same time. Therefore the interactions are strongly frustrated. The form of the interaction in Eq. (6) bears a resemblance to the dipole-dipole interactions between magnetic needles that are positioned on a lattice, and hence the name *compass* models.

Such a frustration of interactions is typical of compass models, but, of course, also appears in numerous other systems. Indeed, on a conceptual level, many of the ideas and results that are discussed in this review, such as renditions of thermal and quantum fluctuation-driven ordering effects, unusual symmetries, and ground-state sectors labeled by topological invariants, have similar incarnations in frustrated spin, charge, cold atom, and Josephson-junction-array systems. Although these similarities are mostly conceptual there are also instances where there are exact correspondences. For instance, the two-dimensional  $90^\circ$  compass model is, in fact, dual to the Moore-Lee model describing Josephson coupling between superconducting grains in a square lattice (Moore and Lee, 2004; Xu and Moore, 2004; Nussinov and Fradkin, 2005; Xu and Moore, 2005; Cobanera, Ortiz, and Nussinov, 2010).

## 2. Kitaev's honeycomb model

In 2006, Kitaev introduced a type of compass model that has interesting topological properties and excitations, which are relevant and much studied in the context of topological quantum computing (Kitaev, 2006). The model is defined on a honeycomb lattice and is referred to either as *Kitaev's honeycomb model* or as the *XYZ honeycomb compass model*. The lattice links on a honeycomb lattice may point along three different directions; see Fig. 4. One can label the bonds along these directions by  $\mathbf{e}_1$ ,  $\mathbf{e}_2$ , and  $\mathbf{e}_3$ , where the angle between the three unit lattice vectors is  $120^\circ$ . With these preliminaries, the Kitaev honeycomb model Hamiltonian  $H_{\square}^{\text{Kitaev}}$  reads

$$H_{\square}^{\text{Kitaev}} = -J_x \sum_{\text{bonds } \mathbf{e}_1} \tau_i^x \tau_j^x - J_y \sum_{\text{bonds } \mathbf{e}_2} \tau_i^y \tau_j^y - J_z \sum_{\text{bonds } \mathbf{e}_3} \tau_i^z \tau_j^z.$$

One can reexpress this model in the form of  $H_{\text{compass}}$  introduced previously, where

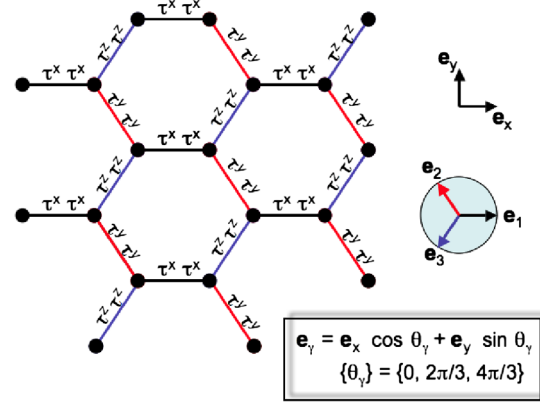


FIG. 4 (color online). Kitaev's compass model on a honeycomb lattice: the interaction of (pseudo)spin degrees of freedom  $\tau = (\tau^x, \tau^y, \tau^z)$  along the three bonds that each site is connected to are  $\tau_r^x \tau_{r+\mathbf{e}_1}^x$ ,  $\tau_r^y \tau_{r+\mathbf{e}_2}^y$ , and  $\tau_r^z \tau_{r+\mathbf{e}_3}^z$ , where the bond vectors of the honeycomb lattice  $\{\mathbf{e}_1, \mathbf{e}_2, \mathbf{e}_3\}$  are  $\{\mathbf{e}_x, -\mathbf{e}_x/2 + \sqrt{3}\mathbf{e}_y/2, -\mathbf{e}_x/2 - \sqrt{3}\mathbf{e}_y/2\}$ , respectively.

$$H_{\square}^{\text{Kitaev}} = - \sum_{r,\gamma} J_{\gamma} \tau_r^{\gamma} \tau_{r+\mathbf{e}_{\gamma}}^{\gamma},$$

with

$$\{\tau^{\gamma}\} = \{\tau^x, \tau^y, \tau^z\}, \quad \{J_{\gamma}\} = \{J_x, J_y, J_z\}, \\ \mathbf{e}_{\gamma} = \mathbf{e}_x \cos \theta_{\gamma} + \mathbf{e}_y \sin \theta_{\gamma}, \quad \{\theta_{\gamma}\} = \{0, 2\pi/3, 4\pi/3\}. \quad (7)$$

It was proven that for large  $J_z$ , the model Hamiltonian  $H_{\square}^{\text{Kitaev}}$  maps onto a square lattice model known as *Kitaev's toric code model* (Kitaev, 2003). These models and their relation to quantum computing are reviewed separately (Nussinov and van den Brink, 2015). To highlight the pertinent interactions and geometry of Kitaev's honeycomb model as a compass model, it may also be termed an *XYZ honeycomb compass model*. This also suggests variants such as the *XXZ honeycomb compass model*, which we define next.

## 3. The XXZ honeycomb compass model

A variation of the Kitaev honeycomb compass Hamiltonian  $H_{\square}^{\text{Kitaev}}$  in Eq. (7) is to consider a compass model where on bonds in two directions there is a  $\tau^x \tau^x$ -type interaction and in the third direction a  $\tau^z \tau^z$  interaction. This model goes under the name of the *XXZ honeycomb compass model* (Nussinov, Ortiz, and Cobanera, 2012a). Explicitly, it is given by the Hamiltonian

$$H_{\square}^{\text{XXZ}} = - \sum_{r,\gamma} J_{\gamma} \tau_r^{\gamma} \tau_{r+\mathbf{e}_{\gamma}}^{\gamma},$$

with

$$\{\tau^{\gamma}\} = \{\tau^x, \tau^x, \tau^z\}, \quad \{J_{\gamma}\} = \{J_x, J_x, J_z\}, \\ \mathbf{e}_{\gamma} = \mathbf{e}_x \cos \theta_{\gamma} + \mathbf{e}_y \sin \theta_{\gamma}, \quad \{\theta_{\gamma}\} = \{0, 2\pi/3, 4\pi/3\}. \quad (8)$$

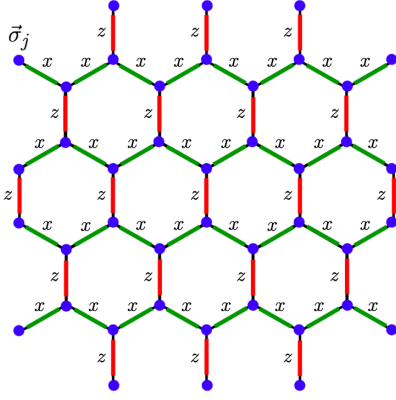


FIG. 5 (color online). Schematic representation of the XXZ honeycomb compass model. From Nussinov, Ortiz, and Cobanera, 2012a.

A schematic is provided in Fig. 5. The key defining feature of this Hamiltonian compared with the original Kitaev model of Sec. II.A.2 is that the interactions along both the diagonal (zigzag)— $x$  and  $y$  directions of the honeycomb lattice are of the  $\tau^x\tau^x$  type (as opposed to both  $\tau^x\tau^x$  and  $\tau^y\tau^y$  in Kitaev's model). As in Kitaev's honeycomb model, all interactions along the vertical ( $z$  direction) are of the  $\tau^z\tau^z$  type. While in Eq. (8) only two couplings  $J_x$  and  $J_z$  appear, the model can, of course, be further generalized to having three different couplings on the three different types of links (and more generally to have nonuniform spatially dependent couplings), while the interactions retain their XXZ form. In all of these cases, an exact duality to a corresponding Ising lattice gauge theory on a square lattice exists, which we elaborate on later (Sec. IX.H).

#### 4. 120° compass models

The 120° compass model has the form of  $H_{\text{compass}}$  [Eq. (4)] and is defined on a general lattice having three distinct lattice directions  $e_\gamma$  for nearest-neighbor links. As for the other compass models on these lattice links different components of  $\tau$  interact. Its particularity is that the three components of  $\tau$  are not orthogonal. Along bond  $\gamma$  the interaction is between the vector components  $\tau^x \cos \theta + \tau^y \sin \theta$  of the two sites connected by the bond, where for the three different links of each site  $\theta = 0, 2\pi/3$ , and  $4\pi/3$ , respectively.

The model was first studied on the cubic lattice (Nussinov *et al.*, 2004; van den Brink, 2004; Biskup, Chayes, and Nussinov, 2005) and later on the honeycomb (Nasu *et al.*, 2008; Wu, 2008; Zhao and Liu, 2008) and pyrochlore lattices (Chern, Perkins, and Hao, 2010). The general 120° Hamiltonian can be denoted as

$$H^{120} = -J \sum_{r,\gamma=1,\dots,3} \hat{n}_r^\gamma \hat{n}_{r+e_\gamma}^\gamma, \quad (9)$$

where  $\hat{n}_r^\gamma$  are the three projections of  $\tau$  along three equally spaced directions on a unit disk in the  $xy$  plane:

$$\begin{aligned} \hat{n}^1 &= \tau^x, \\ \hat{n}^2 &= -(\tau^x - \sqrt{3}\tau^y)/2, \\ \hat{n}^3 &= -(\tau^x + \sqrt{3}\tau^y)/2. \end{aligned} \quad (10)$$

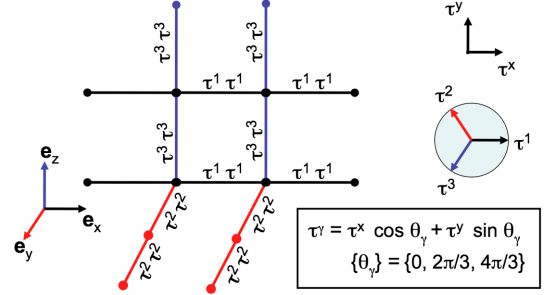


FIG. 6 (color online). The 120° compass model on a cubic lattice: The interaction of (pseudo)spin degrees of freedom  $\tau = (\tau^x, \tau^y, \tau^z)$  along the three bonds that each site is connected to are  $\hat{n}_r^1 \hat{n}_{r+e_x}^1$ ,  $\hat{n}_r^2 \hat{n}_{r+e_y}^2$ , and  $\hat{n}_r^3 \hat{n}_{r+e_z}^3$ , where the different components  $\{\hat{n}^1, \hat{n}^2, \hat{n}^3\}$  of the vector  $\hat{n} = (\tau^x, (-\tau^x + \sqrt{3}\tau^y)/2, (-\tau^x - \sqrt{3}\tau^y)/2)$  interact along the different bonds  $\{e_x, e_y, e_z\}$ .

Hence the name 120° model. In the notation of  $H_{\text{compass}}$  in Eq. (4) the 120° Hamiltonian on a 3D cubic lattice, represented in Fig. 6, takes the form

$$H_{3\Box}^{120} = -J \sum_{r,\gamma} \hat{n}_r^\gamma \hat{n}_{r+e_\gamma}^\gamma,$$

with

$$\begin{aligned} \hat{n}^\gamma &= \tau^x \cos \theta_\gamma + \tau^y \sin \theta_\gamma, \\ \{e_\gamma\} &= \{e_x, e_y, e_z\}, \\ \{\theta_\gamma\} &= \{0, 2\pi/3, 4\pi/3\}. \end{aligned} \quad (11)$$

Like the 90° compass model, the bare 120° model can be extended to include anisotropy of the coupling constants  $J_\gamma$  along the different crystalline directions and external fields (van Rynbach, Todo, and Trebst, 2010). On a honeycomb lattice the 120° Hamiltonian (Nasu *et al.*, 2008; Wu, 2008; Zhao and Liu, 2008) can be thought of as a type of  $H_{3\Box}^{120}$  and  $H_{\text{Kitaev}}^{\text{Kitaev}}$ :

$$H_{3\Box}^{120} = -J \sum_{r,\gamma} \pi_r^\gamma \pi_{r+e_\gamma}^\gamma,$$

with

$$\begin{aligned} \pi^\gamma &= \tau^x \cos \theta_\gamma + \tau^y \sin \theta_\gamma, \\ e_\gamma &= e_x \cos \theta_\gamma + e_y \sin \theta_\gamma, \\ \{\theta_\gamma\} &= \{0, 2\pi/3, 4\pi/3\}. \end{aligned} \quad (12)$$

It is worth highlighting the differences and similarities between the models of Eqs. (11) and (12) on the cubic and honeycomb lattices, respectively. Although the pseudospin operators that appear in these two equations have an identical form, they correspond to different physical links. In the cubic lattice, bonds of the type  $\hat{n}_r^\gamma \hat{n}_{r+e_\gamma}^\gamma$  are associated with links along the Cartesian  $\gamma$  directions; on the honeycomb lattice, bonds of the type  $\pi_r^\gamma \pi_{r+e_\gamma}^\gamma$  correspond to links along the three possible orientations of nearest-neighbor links in the two-dimensional honeycomb lattice.

In 120° compass models the interactions involve only two of the components of  $\tau$  (so that  $n = 2$ ) as opposed to

a three-component ‘‘Heisenberg’’ character of the three-dimensional  $90^\circ$  compass system, having  $n = 3$ . In that sense  $120^\circ$  models are similar  $XY$  models. On bipartite lattices, the ferromagnetic (with  $J > 0$ ) and antiferromagnetic ( $J < 0$ ) variants of the  $120^\circ$  compass model are equivalent to one another up to the standard canonical transformation involving every second site of the bipartite lattice. This can be made explicit by defining the operator

$$U = \prod_{r=\text{odd}} \tau_r^z, \quad (13)$$

with the product taken over all sites  $r$  that belong to, e.g., the *odd* sublattice for which the sum of the components of the lattice site along the three Cartesian directions  $r_x + r_y + r_z$  is an odd integer. The unitary mapping  $U^\dagger H_{120} U$  then effects a change of sign of the interaction constant  $J$  (i.e.,  $J \rightarrow -J$ ). The ferromagnetic and antiferromagnetic square lattice  $90^\circ$  compass models ( $H_{\square}^{90^\circ}$ ) are related to one another in the same way as, similarly, in this case  $n = 2$ . Note that this mapping does not hold for the 3D rendition of the  $90^\circ$  model: in this case the interactions also involve  $\tau^z$  and consequently  $H_{3\Box}^{90^\circ}$  has different low-temperature statistical mechanical properties for  $J > 0$  and  $J < 0$ .

The  $120^\circ$  models have also appeared in various physical contexts on nonbipartite lattices. On the triangular lattice (Mostovoy and Khomskii, 2002; Wu, 2008; Zhao and Liu, 2008), the model is given by

$$H_{3\Delta}^{120} = -\frac{J}{2} \sum_{r,\gamma,\eta} \pi_r^\gamma \pi_{r+\eta e_\gamma}^\gamma,$$

with

$$\begin{aligned} \pi_r^\gamma &= \tau^x \cos \theta_\gamma + \tau^y \sin \theta_\gamma, & e_\gamma &= e_x \cos \frac{\theta_\gamma}{2} + e_y \sin \frac{\theta_\gamma}{2}, \\ \{\theta_\gamma\} &= \{0, 2\pi/3, 4\pi/3\}, & \eta &= \pm 1. \end{aligned} \quad (14)$$

The factor  $1/2$  in front of the summation corrects for the double counting of each bond in the sum over  $r$ ,  $\gamma$ , and  $\eta$ . The triangular model is very similar to the honeycomb lattice model of Eq. (12). The notable difference is that in the triangular lattice there are additional links: In the triangular lattice, each site has six nearest neighbors whereas on the honeycomb lattice, each site has three nearest neighbors. In the Hamiltonian of Eq. (14), nearest-neighbor interactions of the  $\pi^1 \pi^1$  type appear for nearest-neighbor interactions along the rays parallel to the  $e_x$  direction (i.e., they appear from a given site to its two neighbors at angles of zero or  $180^\circ$  relative to the  $e_1$  crystalline directions). Similarly, interactions of the  $\pi^{2,3} \pi^{2,3}$  type appear for rays parallel to the other two crystalline directions.

## B. Hybrid compass models

An interesting and relevant extension of the bare compass models is one in which both usual  $SU(2)$  symmetric Heisenberg-type exchange terms  $\tau_i \cdot \tau_j$  appear in unison with the directional bonds of the bare  $90^\circ$  or  $120^\circ$  compass model, resulting in *compass-Heisenberg* Hamiltonians of the type

$$H = -\sum_{r,\gamma} (J_H \tau_r \cdot \tau_{r+e_\gamma} + J_K \tau_r^\gamma \tau_{r+e_\gamma}^\gamma), \quad (15)$$

where  $J_H$  denotes the coupling constant for the interactions of Heisenberg form and  $J_K$  the coupling constant of the compass or Kitaev terms in the Hamiltonian. For instance, the  $120^\circ$  rendition of this Hamiltonian lattice has been considered on a honeycomb lattice, where it describes exchange interactions between the magnetic moments of  $\text{Ir}^{4+}$  ions in a family of layered iridates  $A_2\text{IrO}_3$  ( $A = \text{Li}, \text{Na}$ )—materials in which the relativistic spin-orbit coupling plays an important role (Chaloupka, Jackeli, and Khaliullin, 2010; Trouselet, Khaliullin, and Horsch, 2011). The hybrid  $90^\circ$  Heisenberg-compass model was introduced in the context of interacting  $t_{2g}$ -orbital degrees of freedom (van den Brink, 2004) and its 2D quantum incarnation was also investigated in the context of quantum computation (Trouselet, Oleś, and Horsch, 2010, 2012). Another physical context in which such a hybrid model appears is modeling the consequences of the presence of orbital degrees of freedom in  $\text{LaTiO}_3$  on the magnetic interactions in this material (Khaliullin, 2001). The resulting Heisenberg-compass and Kitaev-Heisenberg models (Chaloupka, Jackeli, and Khaliullin, 2010; Reuther, Thomale, and Trebst, 2011), their physical motivations, and their conceptual relevance in the area of topological quantum computing are reviewed separately (Nussinov and van den Brink, 2015)

In a similar manner hybrids of Ising and compass models can be constructed. An Ising-compass Hamiltonian of the form  $H_{\square}^{90^\circ} + H_{\square}^{\text{Ising}}$  has, for instance, been introduced and studied by Brzezicki and Oleś (2010).

## III. GENERALIZED AND EXTENDED COMPASS MODELS

Thus far, we have focused solely on a single pseudospin at a given site. It is also possible to consider situations in which more than one pseudospin appears at a site or with a coupling between pseudospins and the usual spin degrees of freedom—a situation equivalent to having two pseudospin degrees of freedom per site. Kugel-Khomskii (KK) models comprise a class of Hamiltonians that are characterized by having both spin and pseudospin (orbital) degrees of freedom on each site. These models are introduced in Sec. III.A, followed by a possible generalization that we briefly discuss which includes multiple pseudospin degrees of freedom. Their physical incarnations are reviewed in detail in Sec. V. We then discuss in Sec. III.B extensions of the quantum compass models introduced earlier to the classical arena, to higher dimensions, and to a large number of spin components  $n$ . In Sec. III.C we collect other compass model extensions.

### A. Kugel-Khomskii spin-orbital models

The situation in which at a site both pseudospin and the usual spin degrees of freedom are present naturally occurs in the realm of orbital physics. It arises when (electron) spins can occupy different orbital states of an ion—the orbital degree of freedom or pseudospin. The spin and orbital degrees of freedom couple to each other because the intersite spin-spin

interaction depends on the orbital states of the two spins involved. Hamiltonians that result from such a coupling of spin and orbital degrees of freedom are generally known as KK model Hamiltonians, named after the authors that first derived (Kugel and Khomskii, 1972, 1973) and reviewed them (Kugel and Khomskii, 1982). Later reviews include those by Tokura and Nagaosa (2000), Khaliullin (2005) Oleś *et al.* (2005), and Oleś (2012).

The physical motivation and incarnations of such KK spin-orbital models are discussed in Sec. V.A. In Sec. V.A.4 they are derived for certain classes of materials from models of their microscopic electronic structure, in particular, from the multiorbital Hubbard model in which the electron-hopping integrals  $t_{i,j}^{\alpha\beta}$  between orbitals  $\alpha$  on lattice site  $i$  and  $\beta$  on site  $j$  and the Coulomb interactions between electrons in orbitals on the same site are the essential ingredients. A KK Hamiltonian then emerges as the low-energy effective model of a multiorbital Hubbard system in the Mott insulating regime, when there is on average an integer number of electrons per site and Coulomb interactions are strong. In that case charge excitations are suppressed because of a large gap and the low-energy dynamics is governed entirely by the spin and orbital degrees of freedom. In this section we introduce the generic structure of KK models. Generally speaking the interaction between spin and orbital degrees of freedom on site  $i$  and neighboring site  $i + e_\gamma$  is the product of the usual spin-spin exchange interactions and compass-type orbital-orbital interactions on this particular bond. The generic structure of the KK models therefore is

$$H^{\text{KK}} = -J_{\text{KK}} \sum_{r,\gamma} H_{r,r+e_\gamma}^{\text{orbital}} H_{r,r+e_\gamma}^{\text{spin}} + \sum_{r,\gamma} \Delta_r^\gamma \tau_r^\gamma. \quad (16)$$

$H_{r,r+e_\gamma}^{\text{orbital}}$  are operators that act on the pseudospin (orbital) degrees of freedom  $\tau_r$  and  $\tau_{r+e_\gamma}$  on sites  $r$  and  $r + e_\gamma$ , and  $H_{r,r+e_\gamma}^{\text{spin}}$  acts on the spins  $S_r$  and  $S_{r+e_\gamma}$  at these same sites. In addition the single-site orbital field  $\Delta_r^\gamma$  is explicitly included. When the interaction between spins is considered to be rotationally invariant so that it depends only on the relative orientation of two spins,  $H_{r,r+e_\gamma}^{\text{spin}}$  takes the simple Heisenberg form  $S_r \cdot S_{r+e_\gamma} + c_S$ . That is,  $H_{r,r+e_\gamma}^{\text{spin}}$  is the usual rotationally invariant interaction between spins when orbital (pseudospin) degrees of freedom are not considered.  $H_{r,r+e_\gamma}^{\text{orbital}}$ , in contrast, is a Hamiltonian of the compass type. KK Hamiltonians can thus be viewed as particular extensions of compass models, where the interaction strength on each bond is determined by the relative orientation of the spins on the two sites connected by the bond.

Electrons in the open  $3d$  shell of, for instance, transition-metal (TM) ions can, depending on the local symmetry of the ion in the lattice and the number of electrons have an orbital degree of freedom. In the case of orbital degrees of freedom of so-called  $e_g$  symmetry, two distinct orbital flavors are present (corresponding to an electron in either a  $3z^2 - r^2$  or an  $x^2 - y^2$  orbital). On a 3D cubic lattice the purely orbital part of the superexchange Hamiltonian  $H_{r,r+e_\gamma}^{\text{orbital}}$  takes the  $120^\circ$  compass form (Kugel and Khomskii, 1982):

$$H_{r,r+e_\gamma}^{\text{orbital}} = \left(\frac{1}{2} + \hat{\pi}_r^\gamma\right) \left(\frac{1}{2} + \hat{\pi}_{r+e_\gamma}^\gamma\right), \quad (17)$$

where  $\hat{\pi}_r^\gamma$  are the orbital pseudospins and, as in the earlier discussion of compass models,  $\gamma$  is the bond corresponding to unit lattice vector  $e_\gamma$ . The pseudospins  $\hat{\pi}_r^\gamma$  are defined in terms of  $\tau_r^\gamma$ ; cf. Eq. (10) as the  $120^\circ$ -type compass variables. If the spin degrees of freedom in the KK Hamiltonian Eq. (16) are considered as forming static and homogeneous bonds, then on the lattice only the orbital exchange part of the Hamiltonian remains active. The Hamiltonian  $\sum_{r,\gamma} H_{r,r+e_\gamma}^{\text{orbital}}$  then reduces to  $H_{3\Box}^{120}$ , up to a constant, as for the  $120^\circ$  compass variables  $\sum_\gamma \tau_r^\gamma = 0$ .

For transition-metal  $3d$  orbitals of  $t_{2g}$  symmetry, there are three orbital flavors ( $xy$ ,  $yz$ , and  $zx$ ), a situation similar to that of the  $p$  orbitals (which have the three flavors  $x$ ,  $y$ , and  $z$ ). As one is dealing with a three-component spinor, the most natural representation of three-flavor compass models is in terms of the generators of the  $SU(3)$  algebra, using the Gell-Mann matrices, which are the  $SU(3)$  analogs of the Pauli matrices for  $SU(2)$ . Such three-flavor compass models also arise in the context of ultracold atomic gases, where they describe the interactions between bosons or fermions with a  $p$ -like orbital degree of freedom (Chern and Wu, 2011), which are further reviewed in Sec. V. In descriptions of transition-metal systems, which we explore in more detail in Sec. V.A, with pseudospin (orbital) and spin degrees of freedom, the usual spin exchange interactions are augmented by both pseudospin interactions and KK-type terms describing pseudospin- (i.e., orbital-) dependent spin exchange interactions.

In principle, even richer situations may arise when, aside from spins, one does not have a single additional pseudospin degree of freedom per site, as in the KK models, but two or more. As far as we are aware, such models have so far not been considered in the literature. The simplest variants involving two pseudospins at all sites give rise to compass-type Hamiltonians of the form

$$H = \sum_{r,\gamma} [J_\gamma \tau_r^\gamma \tau_{r+e_\gamma}^\gamma + J'_\gamma \tau_r^{\gamma'} \tau_{r+e_\gamma}^{\gamma'}] + \sum_{r,\gamma,\gamma'} [V_{\gamma\gamma'} \tau_r^\gamma \tau_{r+e_\gamma}^{\gamma'} + W_{\gamma\gamma'} \tau_r^\gamma \tau_{r+e_\gamma}^\gamma \tau_{r+e_\gamma}^{\gamma'} \tau_{r+e_\gamma}^{\gamma'}] + \dots \quad (18)$$

Such interactions may, of course, be multiplied by a spin-spin interaction as in the Kugel-Khomskii Hamiltonian of Eq. (16).

## B. Classical, higher- $D$ , and large- $n$ generalizations

A generalization to larger pseudospins is possible in all compass models (Mishra *et al.*, 2004; Nussinov *et al.*, 2004; Biskup, Chayes, and Nussinov, 2005) and proceeds by replacing the Pauli operators  $\tau_i^\gamma$  by corresponding angular momentum matrix representations of size  $(2T+1) \times (2T+1)$  with  $T > 1/2$ . The limit  $T \rightarrow \infty$  then corresponds to a classical model. For the classical renditions of the  $H_{\Box}^{90^\circ}$  and  $H_{\Box}^{120^\circ}$  compass models  $\mathbf{T}$  is a two-component ( $n=2$ ) vector of unit length,

$$(T_r^x)^2 + (T_r^y)^2 = 1, \quad (19)$$

on each lattice site  $i$ . This is so simply because in the  $T = 1/2$  model, the operator  $\tau^z$  does not appear in the Hamiltonian. In a similar manner, for  $n = 3$  renditions of the compass model, in, e.g.,  $H_{3\Box}^{90^\circ}$ , the vector  $\mathbf{T}$  has unit norm and three components.

An obvious extension is to consider vectors  $\mathbf{T}$  with a general number of components  $n$ . The  $90^\circ$  compass models [Eq. (5)] generalize straightforwardly to any system having  $n$  independent directions  $\gamma$ . The simplest variant of this type is a hypercubic lattice in  $D = n$  spatial dimensions wherein along each axis  $\gamma$  (all at  $90^\circ$  relative to each other) the interaction is of the form

$$H_{\Box}^{\text{classical } 90^\circ} = -\sum_{r,\gamma} J_\gamma T_r^\gamma T_{r+e_\gamma}^\gamma. \quad (20)$$

(For non- $90^\circ$  models, we more generally set  $T_r^\gamma \equiv \mathbf{T}_r \cdot \mathbf{e}_\gamma$ .) When looked at through this prism, the one-dimensional Ising model can be viewed as a classical one-dimensional ( $D = n = 1$ ) rendition of a compass model.

In the classical arena, when  $\tau$  is replaced by vectors  $\mathbf{T}$  of unit norm, there is a natural generalization of the  $120^\circ$  compass model to hypercubic lattices in arbitrary spatial dimension  $D$ . To formulate this generalization, it is useful to introduce the unit sphere in  $n$  dimensions. In the classical  $120^\circ$  compass model on the  $D = 3$  cubic lattice, the three two-component vectors  $T^\gamma$  are uniformly partitioned on the unit disk (the  $n = 2$  unit sphere). These form  $D$  equally spaced directions  $\mathbf{e}_\gamma$  on the  $n$  unit sphere. The angle  $\theta$  between any pair of differing vectors is therefore the same (and for  $n = 2$  equal to  $2\pi/3$ ). The generic requirement of uniform angular spacing of  $D$  vectors on a sphere in  $n$  dimensions is possible only when  $n = D - 1$ . The angle  $\theta$  between the unit vectors is then given by

$$\mathbf{e}_\gamma \cdot \mathbf{e}_{\gamma'} = \cos \theta = -\frac{1}{D-1}. \quad (21)$$

If  $n = 3$ , for instance, the four equally spaced vectors can be used to describe the interactions on any lattice having four independent directions  $\gamma$ , for instance, the 4D hypercubic one, or the 3D diamond lattice; see Fig. 7.

It is interesting to note that formally, in the limit of high spatial dimension of a hypercubic lattice rendition of the  $120^\circ$

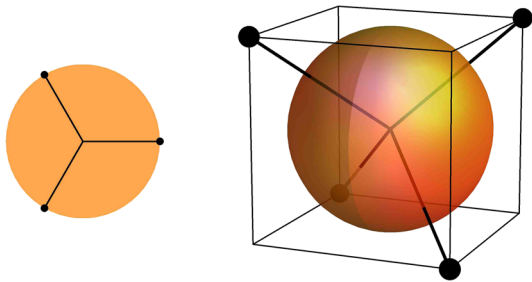


FIG. 7 (color online). Left: A unit disk with three uniformly spaced vectors, the building blocks for the  $120^\circ$  model with  $n = 2$ , on, for instance, a 3D cubic or the 2D honeycomb lattice. Right: Generalization to higher dimensions with four uniformly spaced vectors on the  $n = 3$ -dimensional unit sphere, relevant to a 4D hypercubic lattice, or the 3D diamond lattice.

model, the angle  $\theta \rightarrow 90^\circ$  and the two most prominent types of compass models discussed above (the  $90^\circ$  and  $120^\circ$  compass models) become similar (albeit differing by one dimension of the  $n$ -dimensional unit sphere on which  $\mathbf{T}$  is defined). This is so as the directions  $\hat{e}_\gamma$  become nearly orthogonal.

From here one can return to the quantum arena. The quantum analogs of these  $D$ -dimensional classical compass models (including extensions of the  $120^\circ$  model on a 3D cubic lattice) can be attained by replacing  $\mathbf{T}$  by corresponding quantum operators  $\tau$  that are the generators of spin angular momentum in  $n$ -dimensional space. These are then finite-size representations of the quantum spin angular momentum generators in an  $n$ -dimensional space (e.g., the representations  $T = 1/2, 1, 3/2, \dots$ ) of  $SU(2)$  for a three-component vector just discussed earlier (including the pertinent  $T = 1/2$  representation), representations of  $SU(2) \times SU(2)$  for a four-component  $\tau$ , representations of  $Sp(2)$  and  $SU(4)$  for a five- and six-component  $\tau$ , etc.

These dimensional extensions and definitions of the  $90^\circ$  and  $120^\circ$  models are not unique. One natural  $d = 1$   $90^\circ$  model is the Ising chain. However, another, more interesting “one-dimensional  $90^\circ$  compass model” (sometimes also referred to as the one-dimensional Kitaev model) has been studied in multiple works; see, e.g., Brzezicki, Dziarmaga, and Oleś (2007), Sun, Zhang, and Chen (2008), and You and Tian (2008). In its simplest initial rendition (Brzezicki, Dziarmaga, and Oleś, 2007), this model is defined on a chain in which nearest-neighbor interactions sequentially toggle between the  $\tau_{2i}^x \tau_{2i+1}^x$  and  $\tau_{2i+1}^y \tau_{2i+2}^y$  variants as one proceeds along the chain direction for even or odd numbered bonds. Many aspects of this model have been investigated such as its quench dynamics (Mondal, Sen, and Sengupta, 2008; Divakarian and Dutta, 2009). Such a system is, in fact, dual to the well-studied one-dimensional transverse field Ising model; see, e.g., Brzezicki, Dziarmaga, and Oleś (2007), Eriksson and Johannesson (2009), and Nussinov and Ortiz (2009b). A two-leg ladder rendition of Kitaev’s honeycomb model (and, in particular, the quench dynamics in this system) was investigated by Sen and Vishveshwara (2010) and related ladder models were studied by Feng, Zhang, and Xiang (2007), Saket, Hassan, and Shankar (2010), Lai and Motrunich (2011), and Pedrocchi *et al.* (2012). An interesting two-dimensional realization of the  $120^\circ$  model was further introduced and studied (You and Tian, 2008) wherein only two of the directions  $\gamma$  are active in Eq. (11).

Finally, we comment on these models (in their classical or quantum realization) in the “large- $n$  limit” wherein the number of Cartesian components of the pseudospins  $\mathbf{T}$  becomes large. This limit, albeit seemingly academic, is special. The  $n \rightarrow \infty$  limit has the virtue of being exactly solvable, where it reduces to the “spherical model” (Berlin and Kac, 1952; Stanley, 1968) and further amenable to perturbative corrections in “ $1/n$  expansions” (Ma, 1973). We will return to discuss some aspects of the large- $n$  limit in Sec. VIII.

## C. Other extended compass models

### 1. Arbitrary angle

Several additional extensions of the more standard models have been proposed and studied in various contexts. One of

these includes a generalized angle that need not be  $90^\circ$  or  $120^\circ$  or another special value. Cincio, Dziarmaga, and Oleś (2010) considered a variant of Eq. (9) on the square lattice in which, instead of Eq. (11), one has

$$\begin{aligned}\hat{\pi}_i^x &= \cos(\theta/2)\tau_i^x + \sin(\theta/2)\tau_i^y, \\ \hat{\pi}_i^y &= \cos(\theta/2)\tau_i^x - \sin(\theta/2)\tau_i^y\end{aligned}\quad (22)$$

with a tunable angle  $\theta$ . Compass models with varying angle interactions along particular directions in ladder systems were earlier introduced and solved (Brzezicki and Oleś, 2008, 2009).

Other direction-dependent interactions may be considered to include rotations of spins that have a higher number of components. For instance, Nussinov (2004) studied a model given by the Hamiltonian

$$H = -J \sum_{\langle ij \rangle_\gamma} \mathbf{T}_i \cdot [R_{ij}(\theta) \mathbf{T}_j], \quad (23)$$

where  $R_{ij}(\theta)$  implements a rotation by an angle  $\theta$  around an axis set by the direction of the nearest-neighbor link  $\langle ij \rangle_\gamma$ .

## 2. Plaquette and checkerboard (sub)lattices

Another variant of the compass model form that has been considered, initially introduced to better enable simulation (Wenzel and Janke, 2009), is one in which the angle  $\theta$  is held fixed ( $\theta = 90^\circ$ ) but the distribution of various bonds is permuted over the lattice (Biskup and Kotecky, 2010). Specifically, the *plaquette orbital model* (POM) is defined on the square lattice via

$$H_{\text{POM}} = -J_A \sum_{\langle ij \rangle \in A} \tau_i^x \tau_j^x - J_B \sum_{\langle ij \rangle \in B} \tau_i^y \tau_j^y, \quad (24)$$

where  $A$  and  $B$  denote two plaquette sublattices; see Fig. 8. Bonds are summed over according to whether the physical link  $\langle ij \rangle$  resides in sublattice  $A$  or sublattice  $B$ . Although this system is quite distinct from the models introduced thus far, it does share some common features, including a *bond algebra*

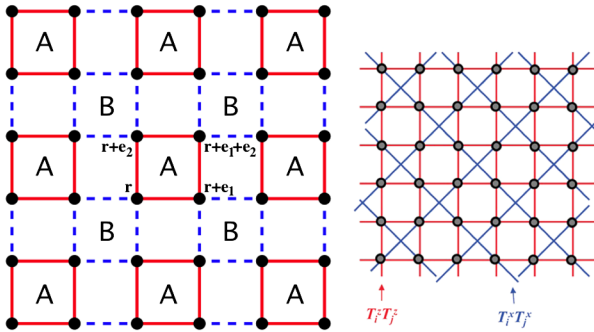


FIG. 8 (color online). Left: The configuration underlying the definition of the plaquette orbital model. Here the  $x$  components of the spins are coupled over the solid edges and the  $z$  components are coupled over the dashed edges. From Biskup and Kotecky, 2010. Right: A schematic representation for the orbital compass model on a checkerboard lattice. From Nasu, Todo, and Ishihara, 2012a.

which, as one can verify in Appendix A is, locally, similar to that of the  $90^\circ$  compass model on the square lattice.

The checkerboard lattice (a two-dimensional variant of the three-dimensional pyrochlore lattice) is composed of corner-sharing crossed plaquettes. This lattice may be regarded as a square lattice in which on every other square plaquette, there are additional diagonal links; see Fig. 8. On this lattice, a compass model may be defined by the following Hamiltonian (Nasu and Ishihara, 2011a; Nasu, Todo, and Ishihara, 2012a):

$$H_{\text{checkerboard}} = -J_x \sum_{\langle ij \rangle} \tau_i^x \tau_j^x - J_z \sum_{\langle ij \rangle} \tau_i^z \tau_j^z. \quad (25)$$

In the first term of Eq. (25), the sum  $\langle ij \rangle$  is over all diagonal (or next-nearest-neighbor) pairs in crossed plaquettes. The second term in Eq. (25) contains the sum  $\langle ij \rangle$ , which is over all nearest-neighbor (i.e., horizontal or vertical) pairs on the lattice.

## 3. Longer-range and ring interactions

In a similar vein, compass models can be defined by pair interactions of varying range and orientation on other general lattices. For instance, in the study of layered oxides, Kargarian, Langari, and Fiete (2012) introduced a hybrid compass model of Kitaev-Heisenberg type with nearest-neighbor and next-neighbor interactions on the honeycomb lattice. One should keep in mind that models in which different spin components couple for different spatial separations may be similar to compass models that we considered in previous sections, yet on enlarged lattices. A case in point is that of a one-dimensional spin system with the Hamiltonian

$$H_{\text{chain}} = -J_x \sum_i \tau_i^x \tau_{i+1}^x - J_z \sum_i \tau_i^z \tau_{i+2}^z. \quad (26)$$

Here the interactions on the chain defined by the Hamiltonian of Eq. (26) are topologically equivalent to a system composed of two parallel chains that are horizontally displaced from one another by half a lattice constant. On one of these chains, we label the sites by odd integers, i.e.,  $i = 1, 3, 5, \dots$ , while the other chain hosts the even sites  $i = 2, 4, \dots$ . On this lattice, the Hamiltonian of Eq. (26) assumes a form similar to that of Eq. (25) when the  $J_x$  interactions appear along diagonally connected sites between the two chains while  $J_z$  coupling occurs between spins that lie on the same chain. Thus, the one-dimensional system with interactions that vary with the range of the coupling between spins is equivalent to a compass model wherein the spin coupling is dependent on the orientation between neighboring spin pairs.

Compass models need not involve only pair interactions. A key feature of models that go beyond pair interactions is that the internal pseudospin components appearing in the interaction terms that depend on an external spatial direction can be extended to any number of interacting pseudospins. A very natural variant was considered by Nasu and Ishihara (2011c) for ring-exchange interactions involving four spins around a basic square plaquette in a cubic lattice. Specifically, these interactions are defined via the Hamiltonian

$$H_{\text{ring}} = K \sum_{[ijkl]_\gamma} (\tau_i^{\gamma+} \tau_j^{\gamma-} \tau_k^{\gamma+} \tau_l^{\gamma-} + \text{H.c.}). \quad (27)$$

In Eq. (27),

$$\tau_i^{\pm\gamma} = \tau_i^\gamma \pm i \frac{\sqrt{3}}{2} \tau_i^\gamma$$

where, as in the  $120^\circ$  model,  $\tau_i^\gamma = \cos(2\pi n_\gamma/3) \tau_i^x - \sin(2\pi n_\gamma/3) \tau_i^y$ . In Eq. (27), the subscript  $[ijkl]_\gamma$  denotes “four neighboring” sites  $[ijkl]$  forming a four-site plaquette that is perpendicular to the cubic lattice direction  $\gamma$ . In the definition of  $\tau_i^\gamma$ ,  $n_\gamma = 1$  for a direction  $\gamma$  parallel to the  $x$  axis (i.e., the plaquette  $[ijkl]$  is orthogonal to the  $x$  direction). Similarly,  $n_\gamma = 2$  or  $3$  for an orientation  $\gamma$  parallel to the cubic lattice  $y$  or  $z$  axis. The physically motivated Hamiltonian of Eq. (27) with its definitions of  $\tau_i^\gamma$  corresponds to a ring exchange of interactions of the  $120^\circ$  type. One may similarly consider extensions for other angles  $\theta$ .

#### IV. COMPASS MODEL REPRESENTATIONS

##### A. Continuum representation

A standard approach in statistical mechanics is to construct effective continuum descriptions of discrete models. A continuum representation of a compass model can be attained by coarse graining its discrete counterpart with pseudospins attached to each point on a lattice. Such coarse-grained continuum representations can offer much insight into the low-energy, long-wavelength behavior and properties of lattice models. We therefore briefly discuss the particular field-theoretic incarnation of compass-type systems, both classical and quantum. The continuum models introduced in this section have previously appeared in the literature.

##### 1. Classical compass models

For a classical pseudospin  $\mathbf{T}$  one defines  $T_r^\gamma = \mathbf{T}_r \cdot \mathbf{n}_\gamma$ , with the angles defining  $\mathbf{n}_\gamma = (\cos \theta_\gamma, \sin \theta_\gamma)$  given by Eq. (11) for the  $120^\circ$  model. Similarly, in the  $90^\circ$  compass model in three dimensions, the three internal pseudospin polarization directions  $\mathbf{n}$  are defined by  $\mathbf{n} = \mathbf{e}_x, \mathbf{e}_y$  or  $\mathbf{e}_z$ . In going over from the discrete lattice model to its continuum representation one uses

$$\begin{aligned} -T_r^\gamma T_{r+\mathbf{e}_\gamma}^\gamma &\rightarrow \frac{a}{2} (T_{r+\mathbf{e}_\gamma}^\gamma - T_r^\gamma)^2 - \frac{a}{2} [(T_{r+\mathbf{e}_\gamma}^\gamma)^2 + (T_r^\gamma)^2] \\ &\rightarrow \frac{a}{2} (\partial_\gamma T^\gamma)^2, \end{aligned} \quad (28)$$

where  $a$  is the lattice constant and the normalization of the pseudovector  $\sum_\gamma (T_r^\gamma)^2$  has been invoked. Classical compass models will be reviewed in detail in Secs. VI–IX. For now, we note that if  $\mathbf{T}$  is a vector of unit norm, then in the  $120^\circ$  model in  $D = 3$  dimensions, regardless of the orientation of that vector on the unit disk,  $\sum_\gamma (T_r^\gamma)^2 = 3/2$  identically. [For a rendition of the  $120^\circ$  model of the form of Eq. (21) in  $D$  dimensions the general result is  $D/(D-1)$ .] In a similar fashion, for the classical  $90^\circ$  model  $\sum_\gamma (T_r^\gamma)^2 = 1$ . The constant value of the sums of  $\sum_\gamma (T_r^\gamma)^2$  leads to rotational symmetry in the ground state manifold. In all such instances,  $\sum_\gamma (T_r^\gamma)^2$  identically amounts to an innocuous constant and as such may be discarded.

In what follows, the “soft-spin” approximation is discussed, in which the “hard-spin” constraint  $\mathbf{T}^2 = 1$  is replaced by a quartic term of order  $\lambda$  that enforces it weakly. Such a term is of the form  $(\lambda/4!)(\mathbf{T}^2 - 1)^2$  with small positive  $\lambda$ . The limit  $\lambda \rightarrow \infty$  corresponds to the hard-spin situation in which the pseudospin is strictly normalized at every point.

With the definition of  $T_r^\gamma$  and simple preliminaries, the continuum-limit Ginzburg-Landau-type free energy in  $D$  spatial dimensions is

$$F = \int d^D x \left[ \sum_\gamma \frac{(\partial_\gamma T^r)^2}{2g} + \frac{r}{2} \mathbf{T}^2 + \frac{\lambda}{4!} (\mathbf{T}^2)^2 \right], \quad (29)$$

with  $g$  an inverse coupling constant and  $r$  a parameter that emulates the effect of temperature,  $r = c(T - T')$  with  $c$  a positive constant and  $T'$  the mean-field temperature. To conform with convention, we will use  $T$  to denote the temperature. Whether  $T$  alludes to the pseudospin or the temperature will be understood from the context. The partition function of the theory is then given by a functional integration over all pseudospin configurations at all lattice sites  $Z = \int D\mathbf{T} e^{-F}$ , where  $\mathbf{T}$  denotes the pseudospin. What differentiates this form from standard field theories is that it does not transform as a simple scalar under rotations. Inspecting Eq. (29), one sees that there is no implicit immediate summation over the repeated index  $\gamma$  in the argument of the square. In Eq. (29), the summation over  $\gamma$  is performed at the end after the squares of the various gradients have been taken. Written long hand for the  $90^\circ$  compass model in two dimensions, the integrand is

$$\left( \frac{\partial T^x}{\partial x} \right)^2 + \left( \frac{\partial T^y}{\partial y} \right)^2. \quad (30)$$

This is to be distinguished from the square of the divergence of  $\mathbf{T}$  (in which the sum over  $\gamma$  would be made prior to taking the square) which would read

$$\left( \frac{\partial T^x}{\partial x} \right)^2 + 2 \frac{\partial T^x}{\partial x} \frac{\partial T^y}{\partial y} + \left( \frac{\partial T^y}{\partial y} \right)^2. \quad (31)$$

This is also different from the square of the gradient of components  $T^\gamma$  and the sums thereof, for which, rather explicitly, one would have for any single component  $\gamma = x$  or  $y$ ,

$$(\nabla T^\gamma)^2 = \left( \frac{\partial T^\gamma}{\partial x} \right)^2 + \left( \frac{\partial T^\gamma}{\partial y} \right)^2. \quad (32)$$

In the present case,  $\mathbf{T}$  indeed represents an internal degree of freedom that does not transform under a rotation of space. By comparison to standard field theories, Eq. (29) manifestly breaks rotational invariance—a feature that is inherited from the original lattice models that it emulates. In Sec. VI the investigations of symmetries as well as of the classical compass models are reviewed in detail.

Continuum limits of other compass theories can similarly be written down. The continuum limits of Heisenberg-compass-type theories on hypercubic lattices are given by the likes of Eq. (29) when these are further augmented by isotropic [i.e.,  $\text{const} \int d^D x \sum_\gamma (\nabla T_\gamma)^2$ ] terms. More complicated theories of the type of Eq. (23) both on the lattice and in

the continuum with arbitrary angle rotations can be mapped onto matter-coupled gauge theories (Nussinov, 2004) in which the strength of the coupling to a gauge theory is set by the rotation angle. Unlike standard rotationally invariant theories in which it can be proven that, barring rare commensurability conditions, all ground states are spirals, in matter-coupled gauge theories and their incarnations in condensed matter systems emulated by Eq. (23), the ground states consist of ordered (Frank-Kasper-type) arrays of “vortices” (Frank and Kasper, 1958, 1959); these vortices are forced in by an external (nondynamic) uniform background field associated with the gauge that implements the compass-type angle-dependent couplings. In the continuum limit theories of such matter-coupled gauge theories, there is a standard minimal coupling between the gauge field and terms linear in the gradients of the pseudospins. Vortex arrays further appear in quite different systems such as the Kitaev-Heisenberg model on the triangular lattice (Roushchatazakis *et al.*, 2013).

## 2. Quantum compass models

As with the usual spin models, the quantum pseudospin systems differ from their classical counterparts by the addition of Berry phase terms. This phase, identical in form to that appearing in spin systems, can be written in both the real time and the imaginary time (Euclidean) formalisms (Fradkin, 1991; Sachdev, 1999). In the quantum arena, one considers the dynamics in imaginary time  $u$  where  $0 \leq u \leq \beta$  with  $\beta$  the inverse temperature. The pseudospin  $T(u)$  evolves on a sphere of radius  $T$  with the boundary conditions that  $T(u=0) = T(u=\beta)$ . Thus, the pseudospin describes a closed trajectory on a sphere of radius  $T$  (the size of the pseudospin). The Berry phase for quantum spin systems [also known as the Wess-Zumino-Witten (WZW) term] is, for each single pseudospin at site  $j$ , given by  $S_j^{\text{WZW}} = -iT A_j$  with  $A_j$  the area of the spherical cap circumscribed by the closed pseudospin trajectory at that site. That is, there is a quantum mechanical (Aharonov-Bohm-type) phase that is associated with a magnetic monopole of strength  $T$  situated at the origin. Denoting the orientation on the unit sphere by  $\mathbf{n}$ , that monopole may be described by a vector potential  $\mathcal{A}$  as a function of  $\mathbf{n}$  that solves  $\epsilon^{abc}(\partial \mathcal{A}^b / \partial n^c) = T n^a$ . The partition function for ferromagnetic variants of the compass models is given by

$$\begin{aligned} Z &= \int Dn^a(x, u) \delta((n^a)^2 - 1) \exp(-S), \\ S &= iT \int_0^\beta du \int d^D x \mathcal{A}^a \frac{dn^a}{du} \\ &\quad + T^2 \int_0^\beta du \int d^D x \sum_\gamma \frac{(\partial_\gamma n^\gamma)^2}{2g}. \end{aligned} \quad (33)$$

As in the classical case, we note that here the summation over  $\gamma$  is performed only after the squares have been taken. As in the so-called “soft-spin” classical model, it is possible to construct approximations in which the  $\delta$  function in Eq. (33) is replaced by soft (i.e., small finite  $\lambda$ ) quartic potentials of the form  $(\lambda/4!)(n^2 - 1)^2$ . In the classical case as well as for  $XY$  quantum systems (such as the  $120^\circ$  compass), the behavior of  $J > 0$  and  $J < 0$  systems is identical. As noted earlier, this is no longer

true in quantum compass systems in which all three components of the spin appear. As for the usual quantum spin systems, the role of the Berry phase terms is quite different for ferromagnetic and antiferromagnetic renditions of the three-component compass models. Although the squared gradient exchange involving  $\mathbf{n}$  can be made similar when looking at the staggered pseudospin on the lattice, the Berry phase term will change upon such staggering and may lead to nontrivial effects.

## B. Momentum space representations

The directional dependence of the interactions in compass models is, of course, manifest also in momentum space. Such a momentum space representation strongly hints that the  $90^\circ$  compass models may exhibit a dimensional reduction (Batista and Nussinov, 2005). On a  $D$ -dimensional lattice, a general pseudospin model having  $n$  components (i.e., one with the classical pseudospin  $T$  having  $n$  Cartesian components at any site) can be Fourier transformed and cast into the form

$$H = \frac{1}{2} \sum_{\mathbf{k}} T^\dagger(\mathbf{k}) \hat{V}(\mathbf{k}) T(\mathbf{k}). \quad (34)$$

In Eq. (34),  $\mathbf{k}$  is the momentum space index, the row vector  $T^\dagger(\mathbf{k}) = (T^1(\mathbf{k}), T^2(\mathbf{k}), \dots, T^n(\mathbf{k}))^*$  with  $*$  representing complex conjugation is the Hermitian conjugate of  $T(\mathbf{k})$ , and  $\hat{V}(\mathbf{k})$  is a momentum space kernel—an  $n \times n$  matrix whose elements depend on the  $D$  components of the momenta  $\mathbf{k}$ .

In usual isotropic spin exchange systems [i.e., those with isotropic interactions of the form  $T_i \cdot T_j$  between (real space) nearest-neighbor lattice sites  $i$  and  $j$ ], the kernel  $\hat{V}(\mathbf{k})$  has a particularly simple form,

$$\hat{V}_{\text{isotropic}} = \left( -2 \sum_{l=1}^D \cos k_l \right) \mathbb{1}_n, \quad (35)$$

with  $k_l$  the  $l$ th Cartesian component of  $\mathbf{k}$  and  $\mathbb{1}_n$  the  $n \times n$  identity matrix. There is a redundancy in the form of Eq. (35) following from spin normalization. At each lattice site  $i$  the sum of the squared projections on the direction  $\gamma$ , i.e.,  $\sum_\gamma (T_i^\gamma)^2$  is a constant so that the double sum over all lattice sites  $i$  and directions  $\gamma \sum_i \sum_\gamma (T_i^\gamma)^2$  is a constant proportional to the total number of sites. From this it follows that  $\sum_{\mathbf{k}} T^\dagger(\mathbf{k}) T(\mathbf{k})$  is a constant. Consequently, any constant term [i.e., any constant (non-momentum-dependent) multiple of the identity matrix] may be added to the right-hand side of Eq. (35). Choosing this constant to be equal to  $2D$ , in the continuum limit, the right-hand side of Eq. (35) disperses as  $\mathbf{k}^2$  for small wave vectors  $\mathbf{k}$ . This is, of course, a manifestation of the usual squared gradient term that appears in standard field theories whose Fourier transform is given by  $\mathbf{k}^2$ . Thus, in the standard isotropic case, the momentum space kernel  $\hat{V}_{\text{isotropic}}$  has a single zero (or lowest-energy state) with a dispersion that rises for small  $\mathbf{k}$  quadratically in all directions.

### 1. Dimensional reduction

The form of the interactions in compass models dramatically differs from that in standard isotropic interactions. As discussed in Sec. VIII.B in greater depth, the directional character of compass systems may lead to a flat momentum

space dispersion in which lines of zeros of  $\hat{V}(\mathbf{k})$  appear, much unlike the typical quadratic dispersion about low-energy modes. In compass models, the coupling between interactions in external space (that of  $D$  dimensions) and the internal space (the  $n$  components of  $\mathbf{T}$ ) leads to a kernel which is more complex than that of isotropic systems. The  $n \times n$  kernel  $\hat{V}$  of Eq. (34) can be written down for all of the compass models that we introduced earlier by replacing any appearance of  $(J_{\gamma\gamma'} T_i^\gamma T_j^{\gamma'})$  in the Hamiltonian where the real space between nearest-neighbor sites  $i$  and  $j$  is separated along the  $l$ th lattice Cartesian direction (on a hypercubic lattice) by a corresponding matrix element of  $\hat{V}$  that is given by  $\langle \gamma | \hat{V} | \gamma' \rangle = 2J_{\gamma\gamma'} \cos k_l$ . By contrast to the usual isotropic spin exchange interactions, the resulting  $\hat{V}$  for compass models is no longer an identity matrix in the internal  $n$ -dimensional space spanning the components of  $\mathbf{T}$ . Rather, each component of  $\hat{V}$  can have a very different dependence on  $\mathbf{k}$ . For the  $90^\circ$  compass models this allows expression of the Hamiltonian in the form of a one-dimensional system in disguise. One sets  $\hat{V}$  to be a diagonal matrix whose diagonal elements are given by

$$\langle \gamma | \hat{V}_{90^\circ} | \gamma \rangle = -2J \cos k_\gamma, \quad (36)$$

where the  $90^\circ$  compass model on an ( $n = D$ )-dimensional hypercubic lattice is recovered. The contrast between Eqs. (35) and (36) is marked and directly captures the directional character of the interactions in the compass model. As in the various compass models (including, trivially, the  $90^\circ$  compass models),  $\sum_i (T_i^\gamma)^2$  is constant at every lattice site  $i$ ; one may as before add to the right-hand side of Eq. (36) any constant times the identity matrix. We may then formally recast Eq. (36) in a form very similar to a one-dimensional variant of Eq. (35)—one which depends on only one momentum space “coordinate” but with that coordinate no longer being a  $k$  but rather a matrix. Toward that end, one may define a diagonal matrix  $\hat{K}$  whose diagonal matrix elements are given by  $(k_1, \dots, k_n)$  and cast Eq. (36) as

$$\hat{V}_{90^\circ} = -2J \cos \hat{K}. \quad (37)$$

In this form, Eq. (37) looks like a one-dimensional ( $D = 1$ ) model in comparison to Eq. (35). The only difference is that instead of having a real scalar quantity  $k$  in 1D, one now formally has a  $(D \times D)$ -dimensional matrix [or a quaternion form for the ( $D = 2$ )-dimensional  $90^\circ$  compass model] but otherwise it looks very similar.

Indeed, to lowest orders in various approximations ( $1/n$ , high-temperature series expansions, etc.) the  $90^\circ$  compass models appears to be one dimensional. This is evident in the spin-wave (SW) spectrum: naively, to lowest orders in all of these approaches, there seems to be a decoupling of excitations along different directions. That is, in the continuum (small- $\mathbf{k}$  limit), one may replace  $2(1 - \cos k_\gamma)$  by  $k_\gamma^2$  and the spectrum for excitations involving  $T^\gamma$  is identical to that of a one-dimensional system parallel to the Cartesian  $\gamma$  direction. This is a manifestation of the unusual gradient terms that appear in the continuum representation of the compass model—Eqs. (28) and (29). In reality, though, the compass

models express the character expected from systems in  $D$  dimensions (not one-dimensional systems) along their finite-temperature phase transitions and universality classes. In the field theory representation of Eq. (29), this occurs due to the quartic term that couples the different pseudospin polarization directions (e.g.,  $T^x$  and  $T^y$ ) to one another. However, an exact remnant of the dimensional reduction suggested by this form still persists in the form of symmetries (Batista and Nussinov, 2005); see Sec. VI.

## 2. (In)commensurate ground states

In what follows here and in later sections, the eigenvalues of  $V(\mathbf{k})$  for each  $\mathbf{k}$  are denoted by  $v_\alpha(\mathbf{k})$  with  $\alpha = 1, 2, \dots, n$  with  $n$  the number of pseudospin components. In rotationally symmetric, isotropic systems when  $v_\alpha(\mathbf{k})$  is independent of the pseudospin index  $\alpha$  and  $\pm \mathbf{q}^*$  are two wave vectors that minimize  $v$ , it is easy to see that two-component spirals (Luttinger and Tisza, 1946; Lyons and Kaplan, 1960; Nussinov *et al.*, 1999; Nussinov, 2001) of the form  $\mathbf{T}(\mathbf{r}) = (\cos \mathbf{q}^* \cdot \mathbf{r}, \sin \mathbf{q}^* \cdot \mathbf{r})$  are classical ground states of the normalized pseudospins  $\mathbf{T}$ . Similar extensions appear for  $n = 3$  (and higher) component pseudospins. It has been proven that for general incommensurate wave vectors  $\mathbf{q}^*$ , all ground states must be spirals of this form (Nussinov *et al.*, 1999; Nussinov, 2001). When the wave vectors that minimize  $v$  are related to one another by commensurability conditions (Nussinov, 2001), then more complicated (e.g., stripe- or checkerboard-type) configurations can arise.

In several compass-type systems that are reviewed here (e.g., the  $90^\circ$  compass model), the interaction kernel  $v$  will still be diagonal in the original internal pseudospin component basis ( $\alpha = 1, 2, \dots, n$ ), yet  $v_\alpha(\mathbf{k})$  are different functions for different  $\alpha$ . Depending on the model at hand, these functions for different components  $\alpha$  may be related to one another by a point group rotation of  $\mathbf{k}$  from one lattice direction to another. We briefly remark on the case when the wave vectors  $\mathbf{q}^*$  that minimize, for each  $\alpha$ , the kernel  $v_\alpha(\mathbf{k})$  are commensurate and allow the construction of Ising-type ground states (Nussinov, 2001) such as commensurate stripes or checkerboard states. In such a case it is possible to construct  $n$ -component ground states by having Ising-type states for each component  $\alpha$ . As reviewed in Secs. VI and VII, the symmetries that compass-type systems exhibit ensure that in many cases there is a multitude of ground states that extend beyond expectations in most other (pseudo)spin systems.

## C. Ising model representations

It is well known that by using a Feynman mapping, one can relate a zero-temperature quantum system in  $D$  spatial dimensions to classical systems in  $D + 1$  dimensions (Sachdev, 1999). In the current context, one can express many of the quantum compass systems as classical Ising models in a dimension one higher. The key idea of such Feynman maps is to work in a classical Ising basis ( $\{\sigma_{i,u}^z\}$ ) at each point in space  $i$  and imaginary time  $u$  and to write the transfer matrix elements of the imaginary time evolution operator between the system and itself at two temporally separated times. The derivation will not be reviewed here; see, e.g., Sachdev (1999).

A simple variant of the Feynman mapping invokes duality considerations (Nussinov and Fradkin, 2005; Cobanera, Ortiz, and Nussinov, 2010, 2011) to another quantum system (Xu and Moore, 2004, 2005) prior to the use of the standard transfer matrix technique. Here we merely quote the results. The two-dimensional  $90^\circ$  compass model of Eq. (4) in the absence of an external field ( $h = 0$ ) maps onto a classical model in  $2 + 1$  dimensions with the action (Nussinov and Fradkin, 2005; Cobanera, Ortiz, and Nussinov, 2011)

$$S = -K \sum_{\square \in (xu) \text{ plane}} \sigma_{r,u}^z \sigma_{r+e_x,u}^z \sigma_{r,u+\Delta u}^z \sigma_{r+e_x,u+\Delta u}^z - J_z \Delta u \sum_r \sigma_{r,u}^z \sigma_{r+e_z,u}^z, \quad (38)$$

with  $K$  a coupling constant that we detailed below. The Ising spins  $\{\sigma_{r,u}^z\}$  are situated at lattice points in the  $(2 + 1)$ -dimensional lattice in space-time. A particular separation  $\Delta u$  along the imaginary time axis has to be specified in performing the mapping of the quantum system onto a classical lattice system in space-time. The coupling constants in Eq. (38) are directly related to those in Eq. (4). We aim to keep the form of Eq. (38) general and cast it in the form of a gauge-type theory (with spins at the vertices of the lattice instead of on links). The plaquette coupling  $K$  in Eq. (38) is related to the coupling constant  $J_x$  of Eq. (4) via a Kramers-Wannier-type of duality,

$$\sinh 2(J_x \Delta u) \sinh 2K = 1. \quad (39)$$

The particular anisotropic directional character of the compass model appears in Eq. (38). Unlike canonical systems in which the form of the interactions is the same in all plaquettes regardless of their orientation, here four-spin interactions appear only for plaquettes that lie parallel to the  $(xu)$  plane—that is, the plane spanned by one of the Cartesian spatial directions ( $x$ ) and the imaginary time axis ( $u$ ). Similarly, exchange interactions [of strength  $(J_z \Delta u)$ ] appear between pairs of spins that are separated along links parallel to the spatial Cartesian  $z$  direction.

The zero-temperature effective classical Ising action of Eq. (38) enables the study of the character of the zero-temperature transition that occurs as  $J_x/J_z$  is varied. From the original compass model of Eq. (1), it is clear that when  $|J_z|$  exceeds  $|J_x|$  there is a preferential orientation of the spins along the  $z$  axis (and, vice versa, when  $|J_x|$  exceeds  $|J_z|$  an ordering along the  $x$  axis is preferred). The point  $J_x = J_z$  (a “self-dual” point for reasons elaborated on later) marks a transition which has been studied by various other means and found to be discontinuous (Dorier, Becca, and Mila, 2005; Chen *et al.*, 2007; Orús, Doherty, and Vidal, 2009), as in the 1D case (Brzezicki, Dziarmaga, and Oleś, 2007).

#### D. Dynamics: Equation of motion

As we now explain, the anisotropic form of the interactions leads to unconventional equations of motion that formally appear similar to those in magnetic systems but are highly anisotropic. In general spin and pseudospin systems, time evolution [both classical (i.e., classical magnetic moments) and quantum] is governed by the equation of motion

$$\frac{\partial \mathbf{T}_i}{\partial t} = \mathbf{T}_i \times \mathbf{h}_i, \quad (40)$$

where  $\mathbf{h}_i$  is the local magnetic (pseudomagnetic) field at site  $i$ . For a stationary field  $\mathbf{h}$ , this leads to a “Larmor precession”—the spin rotates at constant rate about the field direction. This well-known spin effect has a simple incarnation for pseudospins where it further implies a nontrivial time evolution of electronic orbitals (Nussinov and Ortiz, 2008) or any other degree of freedom that the pseudospin represents.

From Eq. (40), we see that for uniform ferromagnetic variants of the compass models (with a single constant  $J$ ), the equation of motion is

$$\frac{\partial \mathbf{T}_i}{\partial t} = J \mathbf{T}_i \times \sum_j (\mathbf{T}_j \cdot \mathbf{e}_{\gamma \parallel \langle ij \rangle}) \mathbf{e}_{\gamma \parallel \langle ij \rangle}, \quad (41)$$

which directly follows from Eq. (40). In Eq. (41), the sum is over sites  $j$  that are nearest neighbors of  $i$ . By the designation  $\mathbf{e}_{\gamma \parallel \langle ij \rangle}$ , we make it explicit that the internal pseudospin direction  $\mathbf{e}_\gamma$  is set by that particular value of  $\gamma$  that corresponds to the direction from site  $i$  to site  $j$  on the lattice itself (i.e., by the direction of the lattice link  $\langle ij \rangle$ ). If the effective pseudomagnetic field at site  $i$  is parallel to the pseudospin at that site, i.e., if  $(\sum_j (\mathbf{T}_j \cdot \mathbf{e}_{\gamma \parallel \langle ij \rangle}) \mathbf{e}_{\gamma \parallel \langle ij \rangle}) \parallel \mathbf{T}_i$ , then semiclassically the pseudospin is stationary (i.e.,  $\partial \mathbf{T}_i / \partial t = 0$ ). Such a situation arises, for instance, for any semiclassical uniform pseudospin configuration:  $\mathbf{T}_i = \text{const}$  for all  $i$  and we denote it by  $\mathbf{T}$ . In such a case, for the  $90^\circ$  compass,  $\sum_j (\mathbf{T}_j \cdot \mathbf{e}_{\gamma \parallel \langle ij \rangle}) \mathbf{e}_{\gamma \parallel \langle ij \rangle} = 2\mathbf{T}$ , whereas for the cubic lattice  $120^\circ$  compass,  $\sum_j (\mathbf{T}_j \cdot \mathbf{e}_{\gamma \parallel \langle ij \rangle}) \mathbf{e}_{\gamma \parallel \langle ij \rangle} = 3\mathbf{T}$ .

As, classically,  $\mathbf{T} \times \mathbf{T} = \mathbf{0}$ , all uniform pseudospin states are stationary states (which correspond to classical ground states at strictly zero temperature). Similarly, of course, a staggered uniform configuration in which  $\mathbf{T}_i$  is equal to one constant value ( $\mathbf{T}$ ) on one sublattice and is equal to  $(-\mathbf{T})$  on the other sublattice will also lead to a stationary state (that of highest energy for  $J > 0$ ). Such semiclassical uniform states are also ground states of the usual spin ferromagnets. The interesting twist here is that the effective field  $\mathbf{h}_i$  is not given by  $J \sum_j \mathbf{S}_j$  as for usual spin systems but rather by  $\sum_j (\mathbf{T}_j \cdot \mathbf{e}_{\gamma \parallel \langle ij \rangle}) \mathbf{e}_{\gamma \parallel \langle ij \rangle}$ .

#### V. PHYSICAL MOTIVATIONS AND INCARNATIONS

In this section we review the different physical contexts that motivate compass models and how they can emerge as low-energy effective models of systems with strongly interacting electrons. There are quite a few classes of materials where the microscopic interactions between electrons are described by an extended Hubbard model. Typically such materials contain transition-metal ions. Hubbard-type models incorporate both the hopping of electrons from lattice site to lattice site and the Coulomb interaction  $U$  between electrons that meet on the same site, typically the transition-metal ion. Particularly in the situation in which electron-electron interactions are strong, effective low-energy models can be derived by expanding the Hubbard Hamiltonian in  $1/U$ —the inverse interaction strength. In such a low-energy model the interactions are only between the remaining *spin* and *orbital* degrees of freedom of

the electrons. Compass model Hamiltonians arise when orbital degrees of freedom interact with each other, which we survey in detail (Sec. V.A). But they can also emerge in the description of chiral degrees of freedom in frustrated magnets (Sec. V.C).

In the situation in which both orbital and spin degrees of freedom are present and their interactions are intertwined, the Kugel-Khomskii models (Sec. III.A) arise. We briefly review in Sec. V.A.4 how such models are relevant for strongly correlated electron systems such as TM oxides, when the low-energy electronic behavior is dominated by the presence of very strong electron-electron interactions. The orbital degrees of freedom can be represented via pseudospins.

So-called  $e_g$  and  $t_{2g}$  orbital degrees of freedom that can emerge in transition-metal compounds with electrons in partially filled TM  $d$  shells give rise to two-flavor compass models (for  $e_g$ ) and to three-flavor compass models (for  $t_{2g}$ ) which, as we explain in this section, are conveniently cast in an SU(3) Gell-Mann matrix form. Precisely these types of compass models also emerge in the study of systems of cold atoms in optical traps (Sec. V.B).

### A. Orbital degrees of freedom

Understanding the structure and interplay of orbital degrees of freedom has garnered much attention in various fields. Among many others, these include studies of the colossal-magnetoresistance manganites (Feiner and Oleš, 1999; Tokura and Tomioka, 1999; Dagotto, Hotta, and Moreo, 2001; Weisse and Fehske, 2004; van den Brink, Khaliullin, and Khomskii, 2004; Dagotto, 2005; Tokura, 2006) and pnictide superconductors (Kuroki *et al.*, 2008; Cvetkovic and Tesanovic, 2009; Kruger *et al.*, 2009; Lv, Wu, and Phillips, 2009; Nakayama *et al.*, 2009; Paglione and Greene, 2010; Andersen and Boeri, 2011).

Orbital degrees of freedom are already present in the electronic wave functions of the hydrogen atom. A brief discussion of the hydrogen atoms with just a single electron can thus serve as a first conceptual introduction to orbital physics (Sec. V.A.1). These concepts translate to transition-metal ions, where electrons in partially filled TM  $d$  shells can have so-called  $e_g$  and  $t_{2g}$  orbital degrees of freedom (Griffith, 1971; Fazekas, 1999). These orbital states, which can be represented as spinors (Sec. V.A.2), of ions on neighboring lattice sites can interact via electronic superexchange interactions (Sec. V.A.3), which in the most general situation also depend on the spin orientation of the electrons.

In this section, the relevant Hamiltonians that govern orbital-orbital interactions are derived, and we briefly review how spin-spin interactions affect the interactions between orbitals in Kugel-Khomskii models (Sec. V.A.4). Reviews on this subject are given by Kugel and Khomskii (1982), Tokura and Nagaosa (2000), Khaliullin (2005), and Oleš (2012). The basic concepts relevant to strongly correlated electron systems are found in the books by Goodenough (1963), Griffith (1971), Fazekas (1999), and Khomskii (2010).

We first review orbital systems on cubic and other unfrustrated lattices. The systems are associated with the most prominent realizations of compass models. It is notable that, on frustrated lattices, coupling with the orbital degrees of freedom may lead to rather unconventional states and

corresponding transitions. These include, e.g., on spinel-type geometries, spin-orbital molecules in  $\text{AlV}_2\text{O}_4$  (Horibe *et al.*, 2006), and a cascade of transitions in  $\text{ZnV}_2\text{O}_4$  (Motome and Tsunetsugu, 2004). In a similar vein resonating valence bond states were suggested to occur in the layered triangular compound  $\text{LiNiO}_2$  (Vernay, Penc, and Mila, 2004).

### 1. Atomiclike states in correlated solids

The well-known hydrogen wave functions are the product of a radial part  $R_{nl}$  and an angular part  $Y_l^m$ , with principal quantum number  $n$  and angular quantum numbers  $l$  and  $m$ :

$$\psi_{nlm}(r, \theta, \phi) = R_{nl}(2r/n) \cdot Y_l^m(\theta, \phi), \quad (42)$$

where the radial coordinate  $r$  is measured in Bohr radii,  $\theta$  and  $\phi$  are the angular coordinates, and  $n$  is any positive integer,  $l = 0, \dots, n-1$  and  $m = -l, \dots, l$ . States with  $l = 0, 1, 2, 3$  correspond to  $s, p, d$ , and  $f$  states, respectively. The energy levels of hydrogen are  $E_n = -13.6 \text{ eV}/n^2$  when the small spin-orbit coupling is neglected. The energy therefore does not depend on the angular quantum numbers  $l$  and  $m$ . As is well known, in the hydrogen atom, due to ‘‘accidental reasons,’’ the  $n$ th level has (when spin is included) a degeneracy of size  $2n^2$ . Far more generally, in rotationally invariant systems, the degeneracy factor associated with orbital momentum alone is  $(2l+1)$ . Thus, the orbital degeneracy associated with the  $l = 1$  (or  $p$ ) states is three. Similarly, the  $d$  (or  $l = 2$ ) states are fivefold degenerate and the  $f$  (i.e.,  $l = 3$ ) states are sevenfold degenerate. In explicit terms the angular wave functions for the  $d$  states, the spherical harmonics  $Y_2^m$ , are

$$Y_l^{-m} = (-1)^m (Y_l^m)^*$$

and

$$Y_2^0 = \sqrt{\frac{5}{16\pi}}(3\cos^2\theta - 1),$$

$$Y_2^1 = \sqrt{\frac{15}{8\pi}}\sin\theta\cos\theta e^{i\phi},$$

$$Y_2^2 = \sqrt{\frac{15}{32\pi}}\sin^2\theta e^{i2\phi}.$$

Introducing the radial coordinates  $x = r\sin\theta\cos\phi$ ,  $y = r\sin\theta\sin\phi$ , and  $z = r\cos\theta$  the complex valued angular basis functions (the spherical harmonics  $Y_2^m$ ) can be combined into real wave function basis states, for instance,

$$(Y_2^{-2} + Y_2^2)/\sqrt{2} = \sqrt{\frac{15}{16\pi}}\sqrt{\frac{1}{r^2}}(x^2 - y^2).$$

Apart from an overall normalization constant the resulting  $d$  orbitals are

$$e_g \text{ orbitals} \quad \left\{ \begin{array}{l} Y_2^{-2} + Y_2^2 \\ \sqrt{2}Y_2^0 \end{array} \right\} \begin{array}{l} x^2 - y^2, \\ (3z^2 - r^2)/\sqrt{3}, \end{array}$$

$$t_{2g} \text{ orbitals} \quad \left\{ \begin{array}{l} Y_2^{-2} - Y_2^2 \\ Y_2^{-1} + Y_2^1 \\ Y_2^{-1} - Y_2^1 \end{array} \right\} \begin{array}{l} xy, \\ yz, \\ zx, \end{array}$$

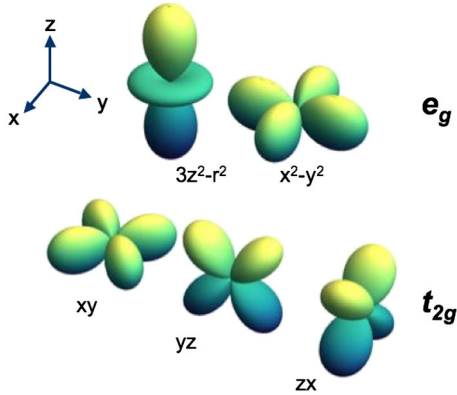


FIG. 9 (color online). The five orthogonal  $d$  orbitals. Crystal field effects lift the fivefold degeneracy of the  $d$  atomic orbitals into an  $e_g$  doublet (top) and a  $t_{2g}$  triplet of states.

where a distinction between so-called  $e_g$  and  $t_{2g}$  orbitals is made, which is based on their different local symmetry properties, as will shortly become clear from crystal field considerations. These orbitals are pictured in Fig. 9. In atoms and ions farther down the periodic table this orbital degree of freedom can persist, depending on the number of electrons filling a particular electronic shell.

In solids,  $p$  wave functions of atoms may tend to be rather delocalized, forming wide bands. When such wide bands form, a material tends to be a metal and the different atomic states mix. Local orbital degeneracies become completely lifted due to the delocalized character of the electrons. However,  $d$  and  $f$  states tend to retain to a certain extent their atomic character and the  $3d$  and  $4f$  states especially are particularly localized— $4d$ ,  $5d$ , and  $5f$  wave functions are again more extended than  $3d$  and  $4f$ , respectively. In the periodic table ions with open  $d$  shells are in the group of transition metals and open  $f$  shells are found in the lanthanides and actinides.

The localized nature of  $3d$  and  $4f$  states has as a consequence the fact that in the solid the interactions between electrons in an open  $3d$  or  $4f$  shell are much like those in the atom (Griffith, 1971). For instance, Hund's first rule (stating that when possible the electrons form high-spin states and maximize their total spin) keeps its relevance for these ions and for the  $3d$  states leads to an energy lowering of  $J_H \sim 0.8$  eV for a pair of electrons having parallel spins. Another large energy scale is the Coulomb interaction  $U$  between electrons in the same localized shell. In a solid  $U$  is substantially screened from its atomic value and its precise value therefore depends critically on the details of the screening processes—it, for instance, reduces the Cu  $d$ - $d$  Coulomb interactions in copper oxides from an atomic value of 16 eV to a solid state value of about 5 eV (van den Brink *et al.*, 1995). But in many cases it is still the dominant energy scale compared to the bandwidth  $W$  of the  $3d$  electrons (Imada, Fujimori, and Tokura, 1998). If  $U$  is strong enough, roughly when  $U > W$ , this causes a collective localization of the electrons and the system becomes a Mott insulator (Mott, 1990; Fazekas, 1999; Khomskii, 2010), or, when a filled oxygen band still lies between the lower and upper Hubbard bands (split by an energy of about  $U$ ), a charge transfer insulator (Zaanen, Sawatsky, and Allen, 1985).

In a strongly correlated Mott insulator electrons in an open  $d$  shell can partially retain their orbital degree of freedom. The full fivefold degeneracy of the hydrogenlike  $d$  states is broken down by the fact that in a solid a positively charged TM ion is surrounded by other ions, which manifestly breaks the rotational invariance that is present in a free atom and on the basis of which the hydrogenlike atomic wave functions were derived. How precisely the fivefold degeneracy is broken depends on the point group symmetry of the lattice (Ballhausen, 1962; Fazekas, 1999).

The simplest, and rather common, case is that of cubic symmetry, in which a TM ion is in the center of a cube, with ligand ions at the center of each of its six faces. The negatively charged ligand ions produce an electrical field at the center of the cube. Expanding this field in its multipoles, the first nonvanishing contribution is quadrupolar. This quadrupole field splits the  $d$  states into the two  $e_g$ 's and the three  $t_{2g}$  states, where the  $t_{2g}$  states are lower in energy because the lobes of their electronic wave functions point away from the negatively charged ligand ions (Ballhausen, 1962; Fazekas, 1999); see Fig. 9. Also, the electronic hybridization of these two classes of states with the ligand states is different, which further adds to the energy splitting between the  $e_g$  and  $t_{2g}$  states. But for a cubic ligand field (also referred to as a crystal field) a twofold orbital degeneracy remains if there is an electron (or a hole) in the  $e_g$  orbitals and a threefold degeneracy for an electron or hole in the  $t_{2g}$  orbitals.

The two  $e_g$  states and the three  $t_{2g}$  states relate, respectively, to two- and three-dimensional vector spaces (or two- and three-component pseudovectors  $\mathbf{T}$ ). This combined with the real space anisotropic directional character of the orbitals leads to Hamiltonians similar to compass models that we introduced in earlier sections.

A further lowering of the lattice point group symmetry, from, for instance, cubic to tetragonal, will cause a further splitting of degeneracies. The existence of degenerate orbital freedom raises the specter of cooperative effects, i.e., orbital ordering. Because of the coupling to the lattice in many of the materials in which they occur, orbital orders appear at high temperatures—often at temperatures far higher than magnetic orders.

## 2. Representations of orbital states

In this section we describe the two- and three-dimensional representations of, respectively, the two  $e_g$  states and three  $t_{2g}$  states.

- $e_g$  orbitals: For the  $e_g$  doublet the orbital pseudospin can be represented by a spinor, where  $\begin{pmatrix} 1 \\ 0 \end{pmatrix}$  corresponds to an electron in the  $x^2 - y^2$  orbital and  $\begin{pmatrix} 0 \\ 1 \end{pmatrix}$  to the electron in the  $(3z^2 - r^2)/\sqrt{3}$  orbital. It is instructive to consider the rotations of this spinor, which are generated by the Pauli matrices  $\sigma_1$ ,  $\sigma_2$ , and  $\sigma_3$ , the generators of the SU(2) algebra; the identity matrix is  $\sigma_0$ . Rotation by an angle  $\phi$  around the 2 axis is denoted by the operator  $\hat{R}_2(\phi)$ , where

$$\hat{R}_2(\phi) = e^{i\sigma_2\phi/2} = \sigma_0 \cos \phi/2 + i\sigma_2 \sin \phi/2. \quad (43)$$

It is easily checked that for  $\phi/2 = \pm 2\pi/3$ , rotation of the spinor corresponding to  $x^2 - y^2$  leads to

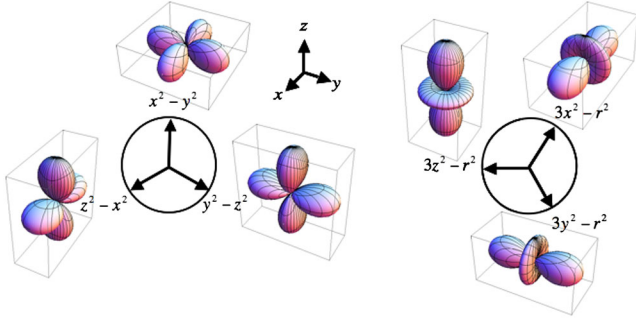


FIG. 10 (color online). Result of the rotations of the  $e_g$  orbital spinor by an angle  $\phi/2 = 2\pi/3$ .

$$\hat{R}_2^\pm \begin{pmatrix} 1 \\ 0 \end{pmatrix} = -\frac{1}{2} \begin{pmatrix} 1 \\ \mp\sqrt{3} \end{pmatrix} = -\frac{1}{2} [x^2 - y^2 \mp (3z^2 - r^2)] = y^2 - z^2,$$

$z^2 - x^2$ , and similarly  $3z^2 - r^2 \rightarrow 3x^2 - r^2, 3y^2 - r^2$ . Rotations of the orbital wave function by  $\phi/2 = 2\pi/3$  thus cause the successive cyclic permutations  $xyz \rightarrow yzx \rightarrow zxy \rightarrow xyz$  in the wave functions, as depicted in Fig. 10.

Next we consider how the pseudospin operator  $\tau$  transforms under these rotations (van den Brink *et al.*, 1999). As

$$\tau = \frac{1}{2} \sum_{\alpha\beta} c_\alpha^\dagger \sigma_{\alpha\beta} c_\beta,$$

where the sum is over the two different orbital states for each  $\alpha$  and  $\beta$ , after the rotation it is

$$\tau = \frac{1}{2} \sum_{\alpha\beta} c_\alpha^\dagger \hat{R}_2^\mp \sigma_{\alpha\beta} \hat{R}_2^\pm c_\beta.$$

For the vector component  $\tau^3$  this implies, for instance, that successive rotations by an angle  $\phi/2 = \pm 2\pi/3$  transform it as

$$\tau^3 \rightarrow -\frac{1}{2}(\tau^3 + \sqrt{3}\tau^1) \rightarrow -\frac{1}{2}(\tau^3 - \sqrt{3}\tau^1) \rightarrow \tau^3.$$

•  $t_{2g}$  orbitals: The same procedure may be applied to the three  $t_{2g}$  states. These states can be represented by three-component spinors

$$xy = \begin{pmatrix} 1 \\ 0 \\ 0 \end{pmatrix},$$

$$yz = \begin{pmatrix} 0 \\ 1 \\ 0 \end{pmatrix},$$

and

$$zx = \begin{pmatrix} 0 \\ 0 \\ 1 \end{pmatrix}.$$

In general, the operators acting on the three-flavor spinors form an SU(3) algebra, which is generated by the eight Gell-Mann matrices  $\lambda^1, \dots, \lambda^8$ ; see Appendix B. This implies that the pseudospin operator for  $t_{2g}$  orbitals

$$\tau = \frac{1}{2} \sum_{\alpha\beta} c_\alpha^\dagger \lambda_{\alpha\beta} c_\beta$$

is an eight-component vector. The operator

$$\hat{R}^+ = \begin{pmatrix} 0 & 0 & 1 \\ 1 & 0 & 0 \\ 0 & 1 & 0 \end{pmatrix}$$

brings about the cyclic permutations  $xyz \rightarrow yzx \rightarrow zxy \rightarrow xyz$  in the  $t_{2g}$  wave functions and  $\hat{R}^- = (\hat{R}^+)^T$ .  $\hat{R}^\pm$  applied to the Gell-Mann matrices transforms the  $t_{2g}$  pseudospin operators accordingly. We wish to highlight this SU(3) character here. Conventionally, SU(3) algebra is not employed.

### 3. Orbital-orbital interactions

Even if in a Mott insulator, the electrons are localized in their atomiclike orbitals, they are not completely confined and can hop between neighboring sites. For electrons in non-degenerate  $s$ -like orbitals, this leads to the magnetic superexchange interactions between the spins of different electrons; see Fig. 11. The competition between the strong Coulomb interaction that electrons experience when they are in the same orbital, which tends to localize electrons, and the hopping, which tends to delocalize them, is captured by the isotropic Hubbard Hamiltonian (Hubbard, 1963)

$$H_{\text{Hub}}^{\text{iso}} = \sum_{\langle ij \rangle, \alpha=\uparrow, \downarrow} t (c_{i\alpha}^\dagger c_{j\alpha} + \text{H.c.}) + U \sum_i n_{i\uparrow} n_{i\downarrow}, \quad (44)$$

where  $c_{i\alpha}^\dagger$  creates an electron with spin  $\alpha = \uparrow, \downarrow$  on site  $i$  and  $c_{j\alpha}$  annihilates it on neighboring site  $j$ ,  $t$  is the hopping amplitude, and the Hubbard  $U$  the energy penalty when two electrons meet on the same site and thus are in the same  $s$ -like orbital (Fazekas, 1999; Khomskii, 2010).

For later purposes it is convenient at this point to introduce a  $2 \times 2$  hopping matrix  $t_{\alpha\beta}^\gamma$ , with  $\alpha = \uparrow, \downarrow$  and  $\beta = \uparrow, \downarrow$ . The hopping matrix determines how an electron changes its spin “polarization” from  $\alpha$  to  $\beta$  when it hops from site  $i$  to  $j$  on the bond  $\langle ij \rangle$  in the direction  $\gamma$ , which connects sites  $\mathbf{r}$  and  $\mathbf{r} + \mathbf{e}_\gamma$ , where  $\mathbf{e}_\gamma$  is the unit lattice vector. Using this notation the first term in the Hubbard Hamiltonian  $H_{\text{Hub}}$  is

$$\sum_{\langle ij \rangle, \alpha} t c_{i\alpha}^\dagger c_{j\alpha} = \sum_{\substack{r, \gamma \\ \alpha, \beta}} t_{\alpha\beta}^\gamma c_{r,\alpha}^\dagger c_{r+\mathbf{e}_\gamma, \beta}, \quad (45)$$

so that

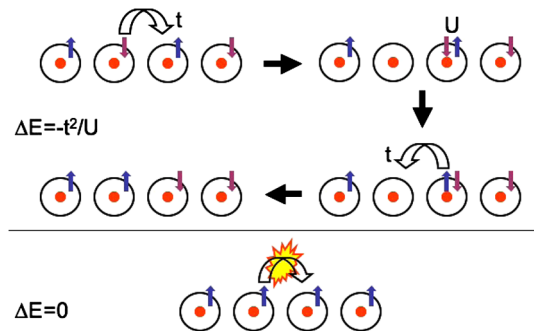


FIG. 11 (color online). Superexchange between spin-1/2 electrons, resulting into the effective antiferromagnetic Heisenberg Hamiltonian  $H = J \sum_{i,j} (\mathbf{S}_i \cdot \mathbf{S}_j - 1/4)$ , with  $J = 4t^2/U$ .

$$H_{\text{Hub}} = \sum_{\substack{r,\gamma \\ \alpha,\beta}} (t_{\alpha\beta}^{\gamma} c_{r,\alpha}^{\dagger} c_{r+e_{\gamma},\beta} + \text{H.c.}) + U \sum_r n_{r\uparrow} n_{r\downarrow}, \quad (46)$$

where for the isotropic Hubbard Hamiltonian  $H_{\text{Hub}}^{\text{iso}}$  of Eq. (46), since hopping does not depend on the direction  $\gamma$  of the bond and spin is conserved during the hopping process, we simply have

$$t_{\alpha\beta}^{\gamma} = t \begin{pmatrix} 1 & 0 \\ 0 & 1 \end{pmatrix}, \quad (47)$$

for all  $\gamma$ . A compass model is the low-energy effective model of a Hubbard Hamiltonian with more involved, bond-direction-dependent, forms of  $t_{\alpha\beta}^{\gamma}$ . Numerous works have investigated direction-dependent hopping for different orbital flavors; note that in some cases these hoppings may lead to an effective dimensional reduction wherein deconfined motion appears along lattice directions (Daghofer *et al.*, 2008).

In the isotropic Hubbard Hamiltonian with  $U \gg t$  and at half filling (i.e., when the number of electrons equal to the number of sites in the system) the resulting Heisenberg-type interaction between spins is

$$H = J \sum_{i,j} \left( \mathbf{S}_i \cdot \mathbf{S}_j - \frac{1}{4} \right).$$

This interaction is antiferromagnetic:  $J = 4t^2/U > 0$ . The high symmetry of the Heisenberg Hamiltonian (the interaction  $\mathbf{S}_i \cdot \mathbf{S}_j$  is rotationally invariant) is rooted in the fact that the hopping amplitude  $t$  is equal for spin-up and spin-down electrons. This is again reflected by the hopping matrix of an electron on site  $i$  and spin  $\alpha$  to site  $j$  and spin  $\beta$  being diagonal:

$$t_{\alpha\beta} = t \begin{pmatrix} 1 & 0 \\ 0 & 1 \end{pmatrix}.$$

For the orbital degrees of freedom the situation is very different from that of the spin. This is so as the hopping amplitudes strongly depend on the type of orbitals involved and thus on the orbital pseudospin. This anisotropy is rather extreme as it depends not only on the local symmetry of the two orbitals involved, but also on their relative position in the lattice: for instance, the hopping amplitude between two  $3z^2 - r^2$  orbitals is very different when the two sites are positioned above each other, along the  $z$  axis, or next to each other, e.g., on the  $x$  axis; see Fig. 12.

#### a. $e_g$ -orbital-only Hamiltonians

As in our discussion of the representations (Sec. V.A.2), because there are two independent  $e_g$  orbitals, in the  $e_g$  sector the pseudospin  $\tau$  has two independent components. Thus, the orbital-orbital interactions in  $e_g$  systems may be represented by  $2 \times 2$  matrices as we detail below. For the  $e_g$  orbitals the hopping matrix between sites  $i$  and  $j$  along the  $\hat{z}$  direction is

$$t_{\alpha\beta}^{\hat{z}} = t \delta_{\alpha,2} \delta_{\beta,2} = t \begin{pmatrix} 0 & 0 \\ 0 & 1 \end{pmatrix}$$

in the basis  $x^2 - y^2, 3z^2 - r^2$ ; see Fig. 12: due to the symmetry of the orbitals only hopping from one  $3z^2 - r^2$  orbital to another  $3z^2 - r^2$  one is allowed along the  $\hat{z}$  direction. This fully specifies the hopping between orbitals on a cubic lattice,

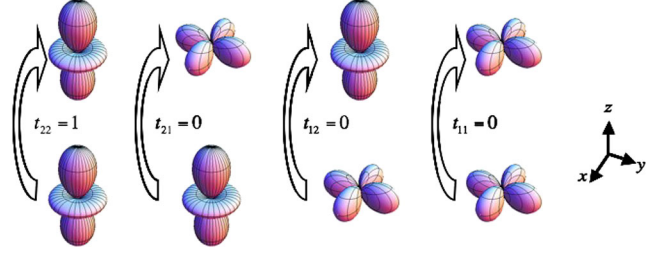


FIG. 12 (color online). Hopping amplitudes between  $e_g$  orbitals along the  $\hat{z}$  axis: the hopping matrix is  $t_{\alpha\beta}^{\hat{z}} = t \delta_{\alpha,2} \delta_{\beta,2}$ . Three matrix elements vanish because of the symmetry of the  $x^2 - y^2$  orbitals, with a wave function on adjacent lobes that has opposite sign.

as the hopping along  $\hat{x}$  and  $\hat{y}$  is dictated by symmetry. The corresponding hopping matrices can be determined with the help of the rotations introduced in Sec. V.A.2. The hopping matrix along the  $x$  direction,  $t_{\alpha\beta}^{\hat{x}}$  is obtained by first rotating the full coordinate system by  $\pi/2$  around the  $y$  axis, so that  $t_{\alpha\beta}^{\hat{z}} \rightarrow t_{\alpha\beta}^{\hat{x}} = t \delta_{\alpha,2} \delta_{\beta,2}$ , now with basis states  $z^2 - y^2, 3x^2 - r^2$ . A subsequent rotation of the orbital spinors by  $\phi/2 = -2\pi/3$  around the  $z$  (i.e., the internal pseudospin  $y$ ) direction brings the matrix back into the original  $x^2 - y^2, 3z^2 - r^2$  basis and transforms  $t_{\alpha\beta}^{\hat{x}} \rightarrow R_2^+ t_{\alpha\beta}^{\hat{x}} R_2^-$ . After the rotations one finds

$$t_{\alpha\beta}^{\hat{x}} = \frac{t}{4} \begin{pmatrix} 3 & \sqrt{3} \\ \sqrt{3} & 1 \end{pmatrix}.$$

Similarly first rotating around the  $\hat{y}$  axis and transforming  $t_{\alpha\beta}^{\hat{z}} \rightarrow R_2^- t_{\alpha\beta}^{\hat{z}} R_2^+$  leads to

$$t_{\alpha\beta}^{\hat{y}} = \frac{t}{4} \begin{pmatrix} 3 & -\sqrt{3} \\ -\sqrt{3} & 1 \end{pmatrix},$$

a well-known result (Kugel and Khomskii, 1982; van den Brink and Khomskii, 1999; Ederer, Lin, and Millis, 2007) that is in accordance with microscopic tight-binding considerations (Harrison, 2004).

Orbital-orbital interactions are generated by superexchange processes between electrons in  $e_g$  orbitals. When the electron spin is disregarded, the most basic form of the orbital-orbital interaction Hamiltonian is obtained. Superexchange with spin-full electrons leads to Kugel-Khomskii Hamiltonians which will be derived and discussed in Sec. V.A.4. For spinless fermions the exchange interactions along the  $\hat{z}$  axis take a particularly simple form. If the electron on site  $i$  is in an  $x^2 - y^2$  orbital, corresponding to  $\tau_i^3 = -1/2$ , and the one on site  $j$  is in a  $3z^2 - r^2$  orbital ( $\tau_j^3 = 1/2$ ), a virtual hopping process is possible, giving rise to an energy gain of  $-t^2/U$  in second-order perturbation theory, where  $U$  is the energy penalty of having spinless fermions on the same site (which are by definition in different orbitals). The only other configuration with nonzero energy gain is the one with  $i$  and  $j$  interchanged. The Hamiltonian on the bond  $ij$  is therefore

$$\begin{aligned} H_{ij}^{\hat{z}} &= -\frac{t^2}{U} \left[ \left( \frac{1}{2} - \tau_i^3 \right) \left( \frac{1}{2} + \tau_j^3 \right) + \left( \frac{1}{2} - \tau_j^3 \right) \left( \frac{1}{2} + \tau_i^3 \right) \right] \\ &= \frac{J}{2} \left( \tau_i^3 \tau_j^3 - \frac{1}{4} \right). \end{aligned}$$

With the same rotations as above, but now acting on the operator  $\tau^z$ , the Hamiltonian on the bonds in the other two directions can be determined: along the  $\hat{x}$  and  $\hat{y}$  axes, respectively,

$$\begin{aligned}\tau^z &\rightarrow R_2^+ \tau^z R_2^- \quad \text{along } \hat{x}, \\ \tau^z &\rightarrow R_2^- \tau^z R_2^+ \quad \text{along } \hat{y},\end{aligned}\quad (48)$$

so that

$$H_{ij}^{\hat{x}} = \frac{J}{8} \left[ (\tau_i^z + \sqrt{3}\tau_i^x)(\tau_j^z + \sqrt{3}\tau_j^x) - 1 \right] = \frac{J}{4} \pi_i^x \pi_j^x,$$

where the last step defines  $\pi^\gamma$  [see Eq. (49)] as in Eq. (10), and along  $\hat{y}$  one obtains

$$H_{ij}^{\hat{y}} = \frac{J}{8} \left[ (\tau_i^z - \sqrt{3}\tau_i^x)(\tau_j^z - \sqrt{3}\tau_j^x) - 1 \right] = \frac{J}{4} \pi_i^y \pi_j^y.$$

The orbital-only Hamiltonian for  $e_g$  orbital pseudospins therefore is exactly the  $120^\circ$  compass model of Eqs. (9) and (10) (van den Brink *et al.*, 1999) on the cubic lattice

$$H_{3\Box}^{e_g} = \frac{J}{2} \sum_{r,\gamma} \left( \pi_r^\gamma \pi_{r+e_\gamma}^\gamma - \frac{1}{4} \right),$$

with

$$\begin{aligned}\pi^\gamma &= \tau^z \cos \theta_\gamma + \tau^1 \sin \theta_\gamma, \\ \{e_\gamma\} &= \{e_x, e_y, e_z\}, \\ \{\theta_\gamma\} &= \{0, 2\pi/3, 4\pi/3\}.\end{aligned}\quad (49)$$

The exchange  $J = 4t^2/U > 0$  is antiferromagnetic. These antiferromagnetic orbital-orbital interactions drive a tendency toward the formation of staggered orbital patterns.

Similar analysis leads to the  $120^\circ$  model on other lattices. The  $120^\circ$  model on the honeycomb lattice,  $H_{\square}^{120^\circ}$ , Eq. (12), was motivated by Nasu *et al.* (2008) in a study of the layered iron oxides  $R\text{Fe}_2\text{O}_4$  ( $R = \text{Lu}, \text{Y}, \text{Yb}$ ); see Fig. 13. These oxides are multiferroic systems in which both the magnetic and electric responses are dominated by Fe  $3d$  electrons. The nominal valence of the Fe ions is  $2.5+$  and thus an equal number of  $\text{Fe}^{2+}$  and  $\text{Fe}^{3+}$  are present. One of the  $e_g$  levels in the  $\text{Fe}^{2+}$  ions is doubly occupied, where all of the five  $3d$  orbitals in the  $\text{Fe}^{3+}$  ions are singly occupied. The system assumes the form of a stack of pairs of triangular lattice planes along the  $c$  axis of the form  $\text{Fe}^{2+}\text{-}2\text{Fe}^{3+}$  and  $2\text{Fe}^{2+}\text{-}\text{Fe}^{3+}$ . In the  $2\text{Fe}^{2+}\text{-}\text{Fe}^{3+}$  member of this pair,  $\text{Fe}^{2+}$  ions (with a doubly degenerate  $e_g$  orbital degree of freedom) form a honeycomb lattice. Superexchange with the  $\text{Fe}^{3+}$  ions leads directly to the Hamiltonian of Eq. (12).

The  $120^\circ$  model has been proposed to account for the physics of materials such as  $\text{NaNiO}_2$  in which the transition-metal ions (with doubly degenerate  $e_g$  orbitals occupied by a single electron or hole) lie on weakly coupled triangular layers (Mostovoy and Khomskii, 2002). In  $\text{NaNiO}_2$ , Na and Ni ions occupy alternate [111] planes as seen in Fig. 14 and consecutive low-spin  $\text{Ni}^{3+}$  triangular layers are weakly coupled to each other. Within each such layer the dominant interactions

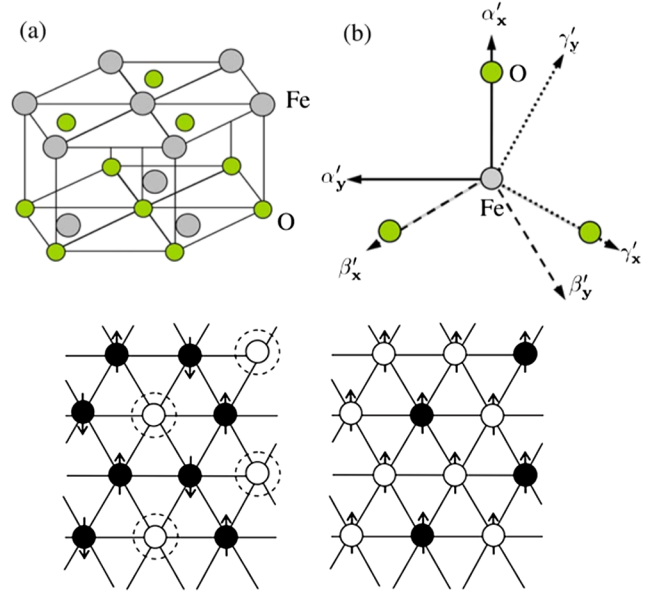


FIG. 13 (color online). Top:  $H_{\square}^{120^\circ}$  models orbital-orbital interactions in  $R\text{Fe}_2\text{O}_4$  (a) A pair of triangular planes and (b) three Fe-O bond directions in a triangular lattice in  $R\text{Fe}_2\text{O}_4$ . Below: Schematic of the charge and spin structures in the  $2\text{Fe}^{2+}\text{-}\text{Fe}^{3+}$  plane (right) and in the  $\text{Fe}^{2+}\text{-}2\text{Fe}^{3+}$  plane (left) for  $R\text{Fe}_2\text{O}_4$ . Filled and open circles represent  $\text{Fe}^{3+}$  and  $\text{Fe}^{2+}$ , respectively. At sites surrounded by dotted circles, spin directions are not uniquely determined due to frustration. From Nasu *et al.*, 2008.

between Ni ions involve exchange paths via intermediate oxygen ions (Reitsma, Feiner, and Oleš, 2005). The bonds between neighboring Ni and oxygen ions form a  $90^\circ$  angle. Direct calculations lead to the triangular lattice  $120^\circ$  Hamiltonian of Eq. (14). In Sec. V.A.7, we further review charge transfer via intermediate ligand (e.g., oxygen) sites and how they may lead to orbital interactions. Augmenting the orbital-only interactions of the  $120^\circ$  compass type, an additional orbital-dependent ferromagnetic spin exchange can become active (Mostovoy and Khomskii, 2002). The dominant interactions are those of the orbital-orbital type.

### b. Compass and Kitaev Hamiltonians

Compass and Kitaev Hamiltonians are the low-energy effective description of certain two-flavor Hubbard Hamiltonians of the type  $H_{\text{Hub}}$  given by Eq. (46). When the two flavors are spin up and down, the hopping matrix corresponds to that of the simple isotropic Hubbard model  $H_{\text{Hub}}^{\text{iso}}$  [see Eqs. (45) and (47)] and the low-energy effective spin Hamiltonian is the spin-1/2 Heisenberg model. Instead,

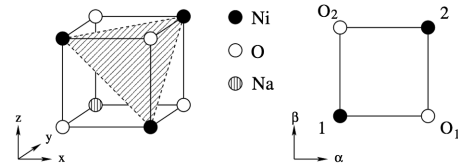


FIG. 14. Left: The crystal structure of  $\text{NaNiO}_2$ . Right: A plaquette in the  $\alpha\beta$  plane ( $\alpha, \beta = x, y, z$ ) formed by two nearest-neighbor Ni ions, 1 and 2, and two oxygen ions,  $O_1$  and  $O_2$ . From Mostovoy and Khomskii, 2002.

in compass models in which we, e.g., consider orbital pseudospins instead of spins, the hopping matrix along the  $\hat{z}$  lattice direction is given by

$$t_{\alpha\beta}^{\hat{z}} = \begin{pmatrix} 0 & 0 \\ 0 & 1 \end{pmatrix}.$$

That is, for  $e_g$  orbitals along  $\hat{z}$ , this gives rise to an Ising type of interaction  $\tau_i^3 \tau_j^3$  between pseudospins on the bond  $\langle ij \rangle$  parallel to  $\hat{z}$ . Such a hopping matrix is realized in the original Hubbard model [Eq. (46)], if only spin- $\downarrow$  electrons are permitted to hop between the sites  $i$  and  $j$  (and spin- $\uparrow$  electrons cannot hop).

When the hopping matrix has a different form along different bonds a compass model arises. The  $90^\circ$  compass model, for instance, has an Ising-type interaction  $\tau_i^3 \tau_j^3$  along  $\hat{z}$ , corresponding to the matrix  $t_{\alpha\beta}^{\hat{z}}$  above.

Next, we come to a very central idea—hoppings along different cubic lattice directions are related by rotations of the components of the orbital pseudospins. Specifically, along the bond parallel to the  $x$  axis, the term  $\tau_i^1 \tau_j^1$  has to be active. A rotation of the pseudospin by an angle of  $\phi = \pi/2$  around the  $2$  axis transforms  $\tau^z$  into  $\tau^x$ . Thus, in such a rotated basis the hopping matrix must again take the form

$$\begin{pmatrix} 0 & 0 \\ 0 & 1 \end{pmatrix}.$$

Let us now see what effective interactions this implies in the original unrotated pseudospin basis. The above operator requires a specific hopping  $t_{\alpha\beta}$  along  $\hat{x}$ . It is easy to check by performing these rotations that for

$$t_{\alpha\beta}^{\hat{x}} = \frac{1}{2} \begin{pmatrix} 1 & -1 \\ -1 & 1 \end{pmatrix}.$$

Similarly, by symmetry, for hopping along the  $\hat{y}$  direction,

$$t_{\alpha\beta}^{\hat{y}} = \frac{1}{2} \begin{pmatrix} 1 & -i \\ i & 1 \end{pmatrix}.$$

Summing the three terms associated with the hopping along the  $\hat{x}$ ,  $\hat{y}$ , and  $\hat{z}$  directions, the cubic  $90^\circ$  compass model  $H_{3\Box}^{90^\circ}$  [Eq. (6)] is seen to arise. Thus for hopping matrices in the Hubbard Hamiltonian [Eq. (46)] that have the form

$$t_{\alpha,\beta}^{\hat{x}} = \frac{1-\sigma^x}{2}, \quad t_{\alpha,\beta}^{\hat{y}} = \frac{1-\sigma^y}{2}, \quad \text{and} \quad t_{\alpha,\beta}^{\hat{z}} = \frac{1-\sigma^z}{2} \quad (50)$$

on a cubic lattice in the large- $U$  limit and at half filling, the low-energy effective Hamiltonian is the  $90^\circ$  compass model  $H_{3\Box}^{90^\circ}$  [Eq. (6)]. A hopping matrix of this type can be realized physically for electrons in the  $5d$  states of iridium ions, where a strong relativistic spin-orbit coupling locks the spin to the orbital degree of freedom (Jackeli and Khaliullin, 2009). Controlling the (pseudo)spin dependence of the hopping amplitudes on different bonds thus suffices to generate any type of compass Hamiltonian as the effective low-energy (pseudo)spin model of the Hubbard Hamiltonian.

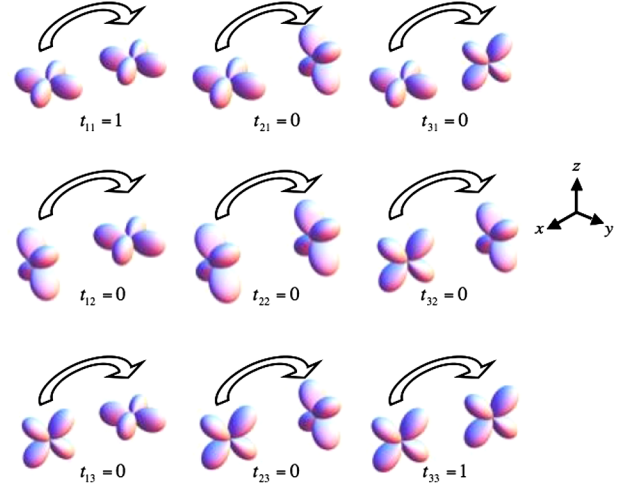


FIG. 15 (color online). Hopping amplitudes between  $t_{2g}$  orbitals along the  $\hat{x}$  axis, assuming that the hopping is via a ligand intermediate  $p$  state (not shown here), for instance, of an oxygen atom between two TM ions; see Fig. 24.

### c. $t_{2g}$ orbital-only Hamiltonian

The three flavors of  $t_{2g}$  orbitals  $xy$ ,  $yz$ , and  $zx$  are most naturally represented by a three-component spinor so that the hopping  $t_{\alpha\beta}$  is a  $3 \times 3$  matrix. The structure of the hopping matrix is rather simple (Fig. 15), as between sites  $i$  and  $j$  electrons can hop only between orbitals of the same symmetry, so that orbital flavor is conserved in the hopping process, which renders  $t_{\alpha\beta}$  diagonal. Moreover, along the  $\hat{x}$  axis the hopping between  $yz$  orbitals vanishes. This determines the hopping matrices in all three directions, which can be constructed via rotations, as for the  $e_g$  orbitals (see Appendix B):

$$t^{\hat{x}} = \begin{pmatrix} 1 & 0 & 0 \\ 0 & 0 & 0 \\ 0 & 0 & 1 \end{pmatrix}, \quad t^{\hat{y}} = \begin{pmatrix} 1 & 0 & 0 \\ 0 & 1 & 0 \\ 0 & 0 & 0 \end{pmatrix}, \quad t^{\hat{z}} = \begin{pmatrix} 0 & 0 & 0 \\ 0 & 1 & 0 \\ 0 & 0 & 1 \end{pmatrix}. \quad (51)$$

As along the  $\hat{y}$  direction, for instance, the hopping matrix is diagonal for the two orbitals involved, the exchange interaction for two (spinless) fermions in these two active orbitals on sites  $i$  and  $j$  is of Heisenberg type. In terms of Gell-Mann matrices it is  $(J/4)(\lambda_{1,i}\lambda_{1,j} + \lambda_{2,i}\lambda_{2,j} + \lambda_{3,i}\lambda_{3,j} - 1)$ , which is SU(2) invariant. Because both fermions need not be in the two active orbitals, an additional diagonal term  $\rho_{1,i}\rho_{1,j}$  is present, where  $\rho_1 = (1/3)(\lambda_0 - \sqrt{3}\lambda_8)$ . As  $\rho_1$  commutes with  $\lambda_{1,\dots,3}$ , it does not break the SU(2) invariance. Defining the vector  $\boldsymbol{\mu}^1 = (\lambda_1, \lambda_2, \lambda_3, \rho_1)$  along the  $\hat{x}$  direction,  $H_{r,r+e_x} = (J/4)(\boldsymbol{\mu}_r^1 \cdot \boldsymbol{\mu}_{r+e_x}^1 - 1)$ . Rotation of the coordinate system and subsequently of the orbital basis produces the interactions along the other two directions,  $\boldsymbol{\mu}_r^2 \cdot \boldsymbol{\mu}_{r+e_y}^2 - 1$  along  $\hat{y}$  and  $\boldsymbol{\mu}_r^3 \cdot \boldsymbol{\mu}_{r+e_z}^3 - 1$  along  $\hat{z}$ , so that

$$H_{3\Box}^{t_{2g}} = \frac{J}{4} \sum_{r,\gamma} (\boldsymbol{\mu}_r^\gamma \cdot \boldsymbol{\mu}_{r+e_\gamma}^\gamma - 1), \quad (52)$$

with  $\{\mathbf{e}_\gamma\} = \{\mathbf{e}_x, \mathbf{e}_y, \mathbf{e}_z\}$ . Along each of the bonds one of the SU(2) subgroups corresponding to the elements of  $\mu^\gamma$  is active and the Hamiltonian is rotationally invariant in terms of that subgroup. This aspect emphasizes the compass character of the ensuing Hamiltonian. The situation is complicated by the fact that all three  $\mu^\gamma$  belong to the same SU(3) algebra, so that the elements of  $\mu^\gamma$  and  $\mu^{\gamma'}$  in general do not commute.

As the three-flavor exchange Hamiltonian is represented by Gell-Mann matrices, it is natural to refer to it as a *Gell-Mann matrix model*. This approach allows for a representation of the interactions between  $t_{2g}$  orbitals that goes beyond the current well-studied orbital Hamiltonians in which SU(2) representations are used. In the context of ultracold gas systems a number of this type of model has been proposed. Of course, the Gell-Mann representation is not unique. Gell-Mann matrices can, for example, be expressed in polynomials of the three  $L = 1$  angular momentum matrices  $L_x$ ,  $L_y$ , and  $L_z$ , which thus also can be used to represent  $H_{3\Box}^{t_{2g}}$  (Kugel and Khomskii, 1982).

#### 4. Spin-spin and orbital-orbital interactions

Going beyond the case of spinless fermions requires considering the local Coulomb and exchange interactions between electrons in various orbital configurations, via a multiorbital Hubbard Hamiltonian. This opens an entire field, of which reviews can be found by Kugel and Khomskii (1982), Tokura and Nagaosa (2000), and Khaliullin (2005). Here we restrict ourselves to indicating how compass models are decorated with spin-spin interactions, with a particular focus on the  $120^\circ$  compass model for  $e_g$  electrons.

The considerations concerning the hopping amplitudes of  $e_g$  electrons directly enter into the kinetic part of the  $e_g$ -orbital Hamiltonian

$$H_{\text{Hub}}^{\text{multi}} = \sum_{\substack{r,\gamma \\ \alpha,\beta,\sigma}} t_{\alpha\beta}^\gamma (c_{r,\alpha\sigma}^\dagger c_{r+e_\gamma,\beta\sigma} + \text{H.c.}) + H_C,$$

with

$$t_{\alpha\beta}^\gamma = \frac{t}{2} \begin{pmatrix} 1 - \cos 2\theta_\gamma & \sin 2\theta_\gamma \\ \sin 2\theta_\gamma & 1 + \cos 2\theta_\gamma \end{pmatrix}, \quad \{\theta_\gamma\} = \{0, 2\pi/3, 4\pi/3\}, \quad (53)$$

where the on-site electron-electron interaction terms are (Kugel and Khomskii, 1982; Oleś, 1983)

$$\begin{aligned} H_C &= (U + 2J_H) \sum_{r,\alpha} n_{r,\alpha\uparrow} n_{r,\alpha\downarrow} - 2J_H \sum_{r,\alpha<\beta} \mathbf{S}_{r,\alpha} \cdot \mathbf{S}_{r,\beta} \\ &+ (U - J_H/2) \sum_{r,\sigma,\sigma',\alpha<\beta} n_{r,\alpha\sigma} n_{r,\beta\sigma'} \\ &+ J_H \sum_{r,\alpha,\beta} c_{r,\alpha\uparrow}^\dagger c_{r,\alpha\downarrow}^\dagger c_{r,\beta\downarrow} c_{r,\beta\uparrow}. \end{aligned} \quad (54)$$

Here not only the Hubbard  $U$ , but also Hund's rule  $J_H$  enters, and in such a form that  $H_C$  does not break the local rotational symmetry in the spin-orbital basis. Normally the regime  $U \gg J_H$  is considered, which is considered the most physical, in particular, for  $3d$  transition-metal oxides where the on-site Coulomb interactions are typically around 4–6 eV and the

Hund's rule exchange around 0.8 eV. It should however be noted that  $U$ , which is the monopole part of the Coulomb interaction, is strongly screened in a solid and depends on the polarizability of the anions and the anion coordination in a material. The magnetic interaction strength  $J_H$  instead is little screened. A similar trend is observed ongoing to  $4d$  and  $5d$  systems, where due to the larger spatial extent of the wave function, in particular, the effective value of  $U$  is substantially smaller.

A second-order perturbation expansion of  $H_{\text{Hub}}^{\text{multi}}$  in powers of  $(t/U)$  directly leads to exchange interactions between spin and  $e_g$ -orbital degrees of freedom, resulting in an effective low-energy KK Hamiltonian (Kugel and Khomskii, 1972, 1973, 1982). The KK Hamiltonian can also be derived from symmetry arguments. In doing so, first the case  $J_H = 0$  is considered. For spin-full  $e_g$  systems, superexchange is possible along the  $\hat{z}$  direction if both electrons are in  $3z^2 - r^2$  orbitals ( $\tau_j^3 = 1/2$ ). This leads to

$$J(\mathbf{S}_r \cdot \mathbf{S}_{r+e_z} - \frac{1}{4})(\frac{1}{2} - \tau_r^3)(\frac{1}{2} - \tau_{r+e_z}^3).$$

This contribution to the Hamiltonian has to be added to the orbital only term

$$\frac{J}{2} \left( \tau_r^3 \tau_{r+e_z}^3 - \frac{1}{4} \right)$$

from  $H_{3\Box}^{e_g}$  in the  $\hat{z}$  direction [see Eq. (49)]. Thus, the total contribution associated with interactions along the  $z$  direction is

$$\begin{aligned} H_{r,r+e_z} &= J(\mathbf{S}_r \cdot \mathbf{S}_{r+e_z} + \frac{1}{4})(\frac{1}{2} - \tau_r^3)(\frac{1}{2} - \tau_{r+e_z}^3) \\ &+ (J/4)(\tau_r^3 + \tau_{r+e_z}^3 - 1). \end{aligned} \quad (55)$$

The Hamiltonian along the other two axes is generated by the rotations of the orbital basis specified in Eqs. (43) and (48). The result, up to an innocuous constant, is the celebrated Kugel-Khomskii Hamiltonian [cf. Eq. (16)]

$$H_U^{\text{KK}} = J \sum_{r,\gamma} H_{r,r+e_\gamma}^{U,\text{orb}} H_{r,r+e_\gamma}^{U,\text{spin}}.$$

Here

$$H_{r,r+e_\gamma}^{U,\text{spin}} = \mathbf{S}_r \cdot \mathbf{S}_{r+e_\gamma} + \frac{1}{4}, \quad H_{r,r+e_\gamma}^{U,\text{orb}} = (\frac{1}{2} - \pi_r^\gamma)(\frac{1}{2} - \pi_{r+e_\gamma}^\gamma), \quad (56)$$

where the operators  $\pi^\gamma$  are defined in Eq. (10). Interestingly, the energy of the classical antiferromagnetic Néel state, where  $\mathbf{S}_i \cdot \mathbf{S}_j = -1/4$  is identically zero independent of any orbital configuration and therefore macroscopically degenerate. This opens the possibility of stabilizing spin-orbital liquid states (Feiner, Oleś, and Zaanen, 1997; Oleś, Feiner, and Zaanen, 2000) or driving the formation of quasi-one-dimensional spin states (Khaliullin and Oudovenko, 1997). However, the presence of a finite Hund's coupling  $J_H$  [Eq. (54)] lifts this degeneracy of the Néel-ordered spin state. To leading order in  $\eta = J_H/U$ , this generates the spin-orbital Hamiltonian

$$H_{J_H}^{\text{KK}} = \eta J \sum_{r,\gamma} H_{r,r+e_\gamma}^{J_H,\text{orb}} H_{r,r+e_\gamma}^{J_H,\text{spin}},$$

with

$$H_{r,r+e_\gamma}^{J_H,\text{spin}} = \mathbf{S}_r \cdot \mathbf{S}_{r+e_\gamma} + \frac{3}{4}, \quad H_{r,r+e_\gamma}^{J_H,\text{orb}} = \pi_r^\gamma \pi_{r+e_\gamma}^\gamma - \frac{1}{4}, \quad (57)$$

and the full Kugel-Khomskii (Kugel and Khomskii, 1982) model for electrons in  $e_g$  orbitals on a cubic lattice, given by

$$H^{\text{KK}} = H_U^{\text{KK}} + H_H^{\text{KK}}. \quad (58)$$

It is interesting to note that when, on two neighboring sites, different orbitals are occupied, i.e.,  $\langle \pi_i^\gamma \pi_{i+e_\gamma}^\gamma \rangle < 0$ , the resulting spin-spin interaction according to Eq. (58) is ferromagnetic. If instead different orbitals are occupied and  $\langle \pi_i^\gamma \pi_{i+e_\gamma}^\gamma \rangle > 1/4$ , the magnetic exchange is antiferromagnetic. This correlation between orbital occupation and magnetic exchange interactions reflects the well-known Goodenough-Kanamori-Anderson rules for superexchange (Anderson, 1959; Kanamori, 1959; Goodenough, 1963).

Similar models describe magnetic systems with  $e_g$ -orbital degrees of freedom on different lattices, for instance, the checkerboard lattice (Nasu and Ishihara, 2012), and with different types of bonds between the ions, for instance, 90° bonds (Mostovoy and Khomskii, 2002), and have been extended to systems with  $t_{2g}$ -orbital degrees of freedom (Kugel and Khomskii, 1982; Khaliullin, 2001, 2005).

### 5. Compass Hubbard models

Compass-type hopping amplitudes lead to more complex variants of the standard Hubbard model (Hubbard, 1963) and give further impetus to the study of compass systems. In this section, we describe an extended compass Hubbard model on the square lattice that contains both standard kinetic hopping terms (as in the Hubbard model) and pairing terms. As will be elaborated in Sec. IX.K, this system has the virtue of being exactly reducible to well-studied quantum gauge systems at a point of symmetry. At this point of symmetry, the ‘‘symmetric extended compass Hubbard model’’ (SECHM) is given by

$$H_{\text{SECHM}} = - \sum_{r,\gamma=x,y} t_{r,r+e_\gamma} (c_{r,s_\gamma}^\dagger + c_{r,s_\gamma}) (c_{r+e_\gamma,s_\gamma}^\dagger - c_{r+e_\gamma,s_\gamma}) + \sum_r U_r (n_{r,\uparrow} n_{r,\downarrow} - n_r). \quad (59)$$

Here both the Coulomb penalty  $U_r$  and the hopping amplitudes ( $t$ ) linking sites  $\mathbf{r}$  and  $\mathbf{r} + \hat{e}_\gamma$  are allowed to vary spatially with the site  $i$  and direction  $\gamma$ . Somewhat similar to earlier sections, the operators  $c_{r,s_\gamma}$  ( $c_{r,s_\gamma}^\dagger$ ) denote the annihilation (creation) of an electron of spin polarization  $s_\gamma$  at site  $i$ . The shorthand  $s_\gamma$  (with  $\gamma = x, y$ ) is, in this case, defined via  $s_x = \uparrow$  and  $s_y = \downarrow$ . The dependence of a hopping amplitude for an electron of spin polarization  $\sigma$  on the lattice direction  $\gamma$  along which the electron may hop embodies a compass-type feature. In Secs. V.A.3 and V.A.4 we review how such hopping amplitudes precisely appear for the pseudospin orbital degrees of freedom. The number operators  $n_{r\sigma}$  with the spin polarization  $\sigma = \uparrow, \downarrow$  are, as usual, given by  $n_{r\sigma} = c_{r,s_\gamma}^\dagger c_{r,s_\gamma}$ . The total number operator at site  $\mathbf{r}$  is  $n_r = n_{r,\uparrow} + n_{r,\downarrow}$ . The Hamiltonian of Eq. (59) is symmetric inasmuch as the pairing and hopping terms are of equal magnitudes. Reminiscent to the situation for  $H_{\text{SECHM}}$ , equal-strength pairing and hopping terms appear in soluble

antiferromagnetic spin chains (Lieb, Schultz, and Mattis, 1961) and related fermionic representations of the two-dimensional Ising model (Schultz, Mattis, and Lieb, 1964). An extended compass Hubbard model arises away from the particular point of symmetry in Eq. (59); such a system allows for differing ratios of the pairing and hopping terms as well as a general chemical potential term  $\sum_r \mu_r n_r$  where  $\mu_r \neq U_r$ . Further extensions to other lattices are possible as well.

### 6. Lattice-mediated interactions

Orbital degrees of freedom couple strongly to the lattice via the Jahn-Teller effect (Jahn and Teller, 1937; Kugel and Khomskii, 1982). A convenient mathematical way to derive the effective Hamiltonian for  $e_g$  electrons on a cubic lattice interacting via Jahn-Teller distortions is to consider first an elongated  $3z^2 - r^2$  orbital that is occupied on site  $i$ , so that the octahedron elongates with a so-called  $Q_3$  distortion; see Fig. 16. We denote the crystallographic axes of the solid by  $a$ ,  $b$ , and  $c$  and now consider how the Jahn-Teller distortions of neighboring octahedra interact. If site  $i$  has a  $Q_3$  distortion, the octahedron connected to it along the  $c$  axis is automatically compressed; see Fig. 16. Thus a distortion  $-Q_3$  is induced on  $j$ , the neighboring site of  $i$  along the  $c$  axis. Therefore the interaction between the distortions of these nearest neighbors  $\langle ij \rangle$  is  $Q_{3,i} Q_{3,j}$ . One can, however, rotate the orbitals in any direction: by choosing  $\theta = 2\pi/3$  one obtains an orbital that is elongated along the  $a$  axis, the  $3x^2 - r^2$  orbital. As discussed earlier, a  $3x^2 - r^2$  orbital corresponds to the linear combination  $(1/2)(-|3z^2 - r^2\rangle + \sqrt{3}|x^2 - y^2\rangle)$ . The distortion that goes along with it is  $(1/2)(-Q_3 + \sqrt{3}Q_2)$ ; see Fig. 16. Therefore it is this linear combination of distortions that determines the interaction along the  $a$  axis. Along the  $b$  axis the situation is analogous with  $\theta = -2\pi/3$ . One arrives at the Hamiltonian for  $e_g$  orbitals on a cubic lattice with corner-sharing octahedra (Kanamori, 1960; Kugel and Khomskii, 1982; van den Brink, 2004)

$$H_{120} = \sum_{r,\gamma} Q_r^\gamma Q_{r+e_\gamma}^\gamma, \quad (60)$$

where  $\gamma = a, b, c$  and  $Q^a = (1/2)(Q_3 - \sqrt{3}Q_2)$ ,  $Q^b = (1/2)(Q_3 + \sqrt{3}Q_2)$ , and  $Q^c = Q_3$ ; see Fig. 16. This model is that of the 120° model of Eqs. (9) and (10). Note that unlike

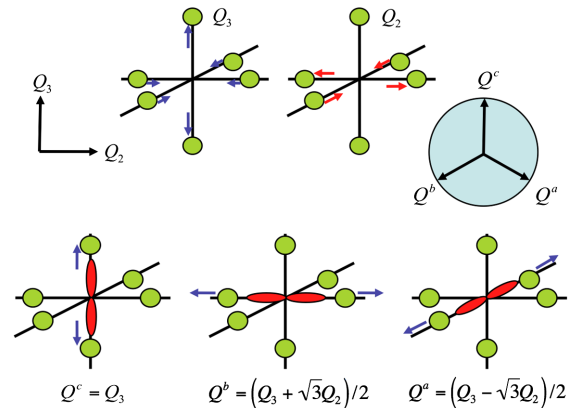


FIG. 16 (color online). Jahn-Teller distortions of  $e_g$  symmetry,  $Q_2$  and  $Q_3$ , of a transition metal–oxygen octahedron. The electronic orbital degree of freedom is locked to the distortion ( $Q_3, Q_2$ ).

the realization of Eq. (49), the  $120^\circ$  model of Eq. (60) derived from Jahn-Teller distortions is essentially classical: the zero-point quantum oscillations of the heavy oxygen ions that mediate the orbital-orbital interactions (or, equivalently, the interactions between Jahn-Teller centers) are negligible. Similar  $90^\circ$ -type compass models describe Jahn-Teller effects in  $t_{2g}$  systems [see, e.g., Eq. (8) of van den Brink (2004)].

### 7. Charge transfer effects through ligand sites

The electronic hopping can occur directly from a  $d$  orbital on one site to a  $d$  orbital on a neighboring one, but as stated previously, in many oxides such hoppings from  $d$  to  $d$  state occur via an oxygen  $p$  orbital of an oxygen ion that is bridging two transition-metal ions. This is particularly relevant for oxides that are charge transfer isolators (Zaanen, Sawatsky, and Allen, 1985). In these materials the charge transfer through ligand sites is dominant when the energy for an electron transfer  $\Delta$  between the ligand and the TM ion is smaller than the energy penalty  $U$  for direct charge transfer between one TM ion and another.

However, it can be easily shown that the effective hopping integrals between  $e_g$  and  $t_{2g}$  states do not change their symmetry if the hopping occurs via an oxygen ligand bridging the two transition-metal sites. In these circumstances, emerging Kugel-Khomskii, and compass models for the orbital and/or spin degrees of freedom in the strong-coupling limit of large  $U$  basically remain unaltered. This situation changes fundamentally when the TM-oxygen-TM bond is not  $180^\circ$ , which is, in particular, the case for edge-sharing octahedra, where this bond is (close to)  $90^\circ$  (Mostovoy and Khomskii, 2002).

The effective orbital-only and orbital-dependent spin exchange Hamiltonians that result when charge transfer through ligand sites is the dominant conduit for charge excitations lead to compass-type Hamiltonians different from those we have discussed thus far (Mostovoy and Khomskii, 2004). Most notably, an orbital-only Hamiltonian appears which remains finite in the limit of  $U \rightarrow \infty$  and is asymmetric between  $e_g$  orbitals partially filled by holes and by electrons. When pairs of transition-metal ions with a single hole ( $h$ ) on the doubly degenerate  $e_g$  orbitals (e.g.,  $\text{Cu}^{2+}$  ions that have an outer-shell structure of  $t_{2g}^6 e_g^3$ ) interact with one another through ligand sites, in the limit  $U \rightarrow \infty$  (leaving the charge transfer  $\Delta$  as the only remaining finite energy scale), the effective resultant charge transfer orbital-only Hamiltonian assumes the form

$$H_{\text{CT}}^{(h)} = \frac{2t^2}{\Delta^3} \sum_{r,\gamma} \left( \frac{1}{2} + \pi_r^\gamma \right) \left( \frac{1}{2} + \pi_{r+e_\gamma}^\gamma \right). \quad (61)$$

Here  $t$  denotes the hopping amplitude between the transition-metal ion and the ligand site. The operators  $\pi_r^\gamma$  are of the same form as in Eqs. (10) and (49). Similarly, for transition-metal ions that have one electron ( $e$ ) in the doubly degenerate  $e_g$  states, the effective interaction that remains in the large- $U$  limit is of the form

$$H_{\text{CT}}^{(e)} = \frac{2t^2}{\Delta^3} \sum_{r,\gamma} \left( \frac{3}{2} - \pi_r^\gamma \right) \left( \frac{3}{2} - \pi_{r+e_\gamma}^\gamma \right). \quad (62)$$

The situation of a single electron in the  $e_g$  orbitals is encountered in ions such as  $\text{Mn}^{3+}$   $\text{Cr}^{2+}$  [both having an  $(t_{2g}^3 e_g^1)$  structure] as well as the low-spin  $\text{Ni}^{3+}$  ( $t_{2g}^6 e_g^1$ ).

The Hamiltonians of Eqs. (61) and (62) capture the effect of common ligand sites which are shared by the transition-metal ions. For finite values of  $U$ , a compass-type coupled spin and orbital Hamiltonian different from the Kugel-Khomskii Hamiltonian appears.

The energetics associated with these orbital-only Hamiltonians favors orbital and spin states which differ from those that would be chosen by the Jahn-Teller or Kugel-Khomskii Hamiltonians. A marked feature of the orbital-only interactions that results is, as clearly seen in Eqs. (61) and (62), the appearance of linear terms in the pseudospins. Such terms are not present in the Jahn-Teller Hamiltonian of Eq. (60). These linear terms effectively act as external effective fields that couple to the pseudospins and may help account for empirically observed orbital structure which is not favored by Jahn-Teller nor Hubbard (and thus also Kugel-Khomskii)-type Hamiltonians (Mostovoy and Khomskii, 2004). We remark that such linear terms may lead to orbital precessions as discussed in Sec. IV.D (Nussinov and Ortiz, 2008).

### B. Cold atom systems

In recent years, the ability to manipulate cold atom (and molecule) systems in standing-wave laser beams has enabled the generation of systems with tunable interactions. In essence, laser beams enable one to generate confining potentials and a *crystal of light* in which the lattice sites are energy minima for the location of dilute atoms or molecules.

Gaining an understanding of electronic and magnetic effects is, in a solid, typically complicated by, for example, the presence of impurities, and the long-range nature of Coulomb interactions and in general the rather limited possibility to change parameters and interactions. Ultracold atoms in optical lattices provide a great advantage in allowing one to probe model Hamiltonians that capture the essential many-body physics of strongly correlated electron systems in a clean experimental setting (Jaksch and Zoller, 2005; Bloch, Dalibard, and Zwerger, 2008). Relevant parameters can be independently controlled, thus allowing quantitative comparisons of the experiment and theory.

In particular, the Hubbard Hamiltonian for both bosonic (Jaksch *et al.*, 1998; Greiner *et al.*, 2002; Stöferle *et al.*, 2004) and fermionic particles (Schneider *et al.*, 2008) on optical lattices has been realized, also in the Mott-insulating regime. This has opened the road to preparation of other effective spinor models with ultracold atoms on the lattice, such as the ones of compass type, which we review in this section.

Proposals for the creation of compass-type models in the ultracold gas setting can be classified into three categories. The first one uses an ensemble of ultracold bosonic or fermionic atoms with two relevant internal states and engineer the hopping amplitudes by additional laser fields (Duan, Demler, and Lukin, 2003). The second category employs atoms that are in  $p$ -like states, the orbital degeneracy of which constitutes the pseudospin degree of freedom, which can be created either by excitation out of  $s$ -like states or by filling a

site with more than one fermionic atom (Browaeys *et al.*, 2005; Isacsson and Girvin, 2005; Köhl *et al.*, 2005; Kuklov, 2006; Liu and Wu, 2006; Wu *et al.*, 2006; Anderlini *et al.*, 2007; Müller *et al.*, 2007; Wu, 2008; Wu and Das Sarma, 2008; Wu and Zhai, 2008; Zhao and Liu, 2008). Finally, by manipulating ultracold dipolar molecules anisotropic spin interactions can be generated (Micheli, Brennen, and Zoller, 2006; Weimer, 2013).

### 1. Engineering tunneling amplitudes

In an ensemble of ultracold bosonic or fermionic atoms confined in an optical lattice with two relevant internal states, a  $T = 1/2$  pseudospin, the pseudospin-dependent tunneling between neighboring atoms in the lattice can be controlled. As will be reviewed in Sec. V.A.3, full control of these hopping amplitudes is in the Mott-insulating regime of the Hubbard model enough to construct any compass-type Hamiltonian. In both Bose and Fermi systems, the anisotropy of the exchange and, in particular, tunneling directions can be engineered by applying blue-detuned standing-wave laser beams along those directions (Duan, Demler, and Lukin, 2003; Kuklov and Svistunov, 2003).

### 2. Bosonic gases with orbital degree of freedom

In the ground state, the atoms in an optical lattice are centered around their local minima provided by the confining potential of the laser beams which in the vicinity of its minima is harmonic. The atomic states in the lowest Bloch band are, essentially, the ground of the harmonic oscillator (more precisely, the product of a single harmonic oscillator centered around each of the minima of the periodic confining potential generated by the laser beams) and those within the first excited Bloch band correspond to the first excited states of a harmonic oscillator.

Several approaches are available for transferring cold atoms to the first excited  $p$ -orbital band, for instance, by applying an appropriate vibrational pulse with frequency on resonance with the  $s$ - $p$  state transition (Liu and Wu, 2006). A theory for the interactions in a dilute system of bosons in which the two lowest Bloch bands of a three-dimensional optical lattice are considered was developed by Isacsson and Girvin (2005).

The central point in all of this is that in the cold atomic gas there are three such excited states corresponding to an “excitation” along each of the three Cartesian directions (which for a single atom around its local confining potential minimum, which for symmetric confining potentials along all three directions, are of the form  $xe^{-(r/a)^2}$ ,  $ye^{-(r/a)^2}$ , and  $ze^{-(r/a)^2}$ , with  $r^2 = x^2 + y^2 + z^2$  and  $a$  the harmonic confining potential length scale). Henceforth these excitations are labeled as  $p = X, Y$ , and  $Z$ . These  $p$  states are rather confined along all Cartesian directions apart from one and in that sense resemble an atomic  $p$  orbital. In the presence of Hubbard-type local interactions between the bosons the resulting system is thus of a compass type, where the pseudospins emerge from bosonic degrees of freedom. The strength of the confining potential along the three Cartesian directions can be tuned by the optical lattice. In the symmetric case, the resulting effective Hubbard-type model, taking into account on-site interactions of strength  $U$  between atoms, is (Isacsson and Girvin, 2005)

$$\begin{aligned}
 H_{\text{IG}} = & \sum_{i,p} \left( E_i(i) n_i^{(p)} + \frac{U_{pp}}{2} n_i^p (n_i^p - 1) \right) \\
 & + \sum_{i,p \neq p'} U_{pp'} \left( n_i^p n_i^{p'} + \frac{1}{2} (p_i^\dagger p_i^\dagger p_i' p_i' + \text{H.c.}) \right) \\
 & - t \sum_{\langle i,i' \rangle_{p,p}} (p_i^\dagger p_{i'} + \text{H.c.}). \tag{63}
 \end{aligned}$$

The operators  $p_i^\dagger$  and  $p_i$  correspond to the creation and annihilation operators for an excited boson of flavor  $p = X, Y, Z$  at site  $i$ . The constants  $U_{pp'}$ ,  $U_{pp}$ , and  $E_i$  are determined by the parameters describing the confining optical potential. In a similar vein, if the confining potential along, say, the  $z$  direction is much larger than along the  $x$  and  $y$  directions, the system is effectively two dimensional [ $p = X, Y$  in Eq. (63)]. Physically, the Hamiltonian then describes two boson species (of types  $X$  and  $Y$ ) each of which may propagate along only one direction. The interaction terms enable two bosons of type  $X$  to fuse and generate two bosons of type  $Y$  (and vice versa).

There is a formal connection between a system of *hard-core bosons* where the on-site repulsion  $U \rightarrow \infty$  (for which no two bosons can occupy the same site) and the pseudospin variants of the compass models. Toward this end, one can employ the Matsubara-Matsuda transformation (Matsubara and Matsuda, 1956) relating a two-flavor system of hard-core bosons (e.g., bosons of type  $X$  and  $Y$ ) and the two states of a pseudospin  $T = 1/2$  particle.

### 3. Fermionic gases with orbital degree of freedom

Fermionic realizations of compass-type systems have also been considered in optical lattices (Wu, 2008; Zhao and Liu, 2008). A situation with a strong confining potential along, e.g., the spatial  $z$  direction will again lead to a two-dimensional system. Wu (2008) focused on atomic orbitals and considered a situation in which there are two fermions per site with one of the fermions in an inert  $s$  shell and the other occupying the  $p$  bands [which in the case of strong optical confinement along the vertical ( $z$ ) direction is restricted to one of the two  $p$  states (i.e.,  $p_x$  and  $p_y$  orbitals)]. One possibility for hopping within the  $p$ -band states is via the so-called  $\sigma$  overlap integral ( $t_{\parallel}$ ), the head-on overlap of one electronic lobe of one site with another (parallel) single electronic  $p$  lobe on a neighbor site. The other possibility is a  $\pi$  overlap ( $t_{\perp}$ ) between  $p$  wave functions on two neighboring sites that are orthogonal to the axis that links these two sites. Notwithstanding our earlier focus on  $d$ -orbital physics in transition-metal solids, we remark that  $p$  orbitals with a subtle interplay of  $t_{\parallel}$ ,  $t_{\perp}$ , and  $p$ -wave orbital orders not only appear in optical lattices but can also arise in some solids such as the hyperoxides; see, e.g., Wohlfeld, Daghofer, and Oleś (2011).

Because of the far smaller overlaps involved in  $\pi$  bonding, the  $\sigma$  bonding is typically far stronger ( $t_{\parallel}/t_{\perp} \gg 1$ ). In what follows  $\pi$  effects will be neglected. The directional character of the  $\sigma$  bonding underlies the compass-type interactions in this system. Orbitals in the  $p_x$  state have a high tunneling amplitude in only the  $x$  direction, and similarly orbitals in the  $p_y$  state have a high tunneling and lead to consequent effective

interactions only along the  $y$  direction. Scattering in the  $p$ -wave channel as well as enhancements by magnetic effects and proximity to the Feshbach resonance can lead to a substantial Hubbard-like interaction

$$H_I = I \sum_i n_{i,x} n_{i,y}. \quad (64)$$

In Eq. (64), the operators  $n_{i,x} = p_{i,x}^\dagger p_{i,x}$  and  $n_{i,y} = p_{i,y}^\dagger p_{i,y}$  are, respectively, the number operators for states of the  $p_x$  and  $p_y$  type on lattice site  $i$ . Here  $p_{i,x}^\dagger$  and  $p_{i,x}$  denote the creation and annihilation operators for an electron, in this case a spinless fermion, in the  $p_x$  orbital at site  $i$ , the operators  $n_{i,x} = p_{i,x}^\dagger p_{i,x}$  and  $n_{i,y} = p_{i,y}^\dagger p_{i,y}$  are the number operators for states of the  $p_x$  and  $p_y$  type, respectively, on the lattice site  $i$ . The interaction strength is given by  $I$ . Precisely such interactions appear in certain Hubbard models of transition-metal oxides with  $t_{2g}$  orbitals; see, e.g., [Daghofer \*et al.\* \(2008\)](#).

We can define  $T = 1/2$  pseudospin operators to be ([Wu, 2008](#); [Zhao and Liu, 2008](#))  $\tau^1 = (1/2)(n_x - n_y)$ ,  $\tau^2 = (1/2)(p_x^\dagger p_y + \text{H.c.})$ , and  $\tau^3 = -(i/2)(p_x^\dagger p_y - \text{H.c.})$ . The  $p_{x,y}$  states are eigenstates of  $\tau^1$  with eigenvalues  $\pm 1/2$ , respectively. The compass-type character emerges naturally from the  $\sigma$ -bonding exchange between two sites separated along, say, the Cartesian  $x$  lattice direction. In that case, for large  $U$ , a perturbative expansion in  $t_{\parallel}/U$  about the degenerate ground state of Eq. (64) (that of a single  $p_x$  or  $p_y$  state per site) is possible. Second-order perturbation theory in the kinetic  $t_{\parallel}$  term gives rise to an effective Ising-type exchange  $H_{\text{ex}} = J_{\parallel} \tau_i^x \tau_{i+\mathbf{e}_x}^x$  with  $J_{\parallel} = 2t_{\parallel}^2/U$  ([Wu, 2008](#); [Zhao and Liu, 2008](#)). We now consider the case of a general quantization axis and arbitrary separation between neighboring sites on the lattice. Similar to compass models in other arenas (in particular, in orbital physics of the transition-metal oxides), a simple but important feature of the underlying quintessential physics is that the Ising quantization axis will change with different orientations of the link connecting neighboring lattice sites. For a lattice link of general spatial direction  $\mathbf{e}_\theta = \mathbf{e}_x \cos \theta + \mathbf{e}_y \sin \theta$ , it is possible to rotate the  $p_{x,y}$  orbitals by  $\theta$  to restore the situation above (i.e., with the new  $p'_x, p'_y$  states having large hopping amplitudes along the  $x'$  and  $y'$  (or  $\hat{\mathbf{e}}_\theta$  and  $\hat{\mathbf{e}}_{\theta+\pi/2}$ ) directions of the lattice. This change of basis effects  $p'_x = p_x \cos \theta + p_y \sin \theta$  and  $p'_y = p_y \cos \theta - p_x \sin \theta$ . These two states  $p'_{x,y}$  are eigenstates of the operator  $\tau'_1 = \tau_1 \cos 2\theta + \tau_2 \sin 2\theta$ . The exchange interaction for general orientation of a link between nearest-neighbor sites is thus ([Wu, 2008](#); [Zhao and Liu, 2008](#))

$$H_{\text{ex}}(i, i + \mathbf{e}_\theta) = J_{\parallel} [\boldsymbol{\tau}_i \cdot \mathbf{e}_{2\theta}] [\boldsymbol{\tau}_{i+\mathbf{e}_\theta} \cdot \mathbf{e}_{2\theta}]. \quad (65)$$

As in other orbital systems, once the interaction along one link [Eq. (65)] is known, the Hamiltonian for the entire lattice can be pieced together by summing over all links in the lattice (taking into account their different spatial orientations  $\mathbf{e}_\theta$ ).

#### 4. Fermions in an optical lattice

In 3D, similar considerations recently led to the introduction of the *Gell-Mann compass models* of [Chern and Wu \(2011\)](#) on the cubic and diamond [Eqs. (67) and (68)] and

more general lattices as we now review. As in the two-dimensional case, each site of the lattice hosts two fermions with one electron filling the inert  $s$  orbital. In three dimensions, the remaining electron can be in any one of the three  $p$  orbitals ( $p_x, p_y$ , or  $p_z$ ). Replicating the arguments presented above for two dimensions ([Chern and Wu, 2011](#)), in the limit  $U \gg t_{\parallel} \gg t_{\perp}$ , Chern and Wu arrived at the following Hamiltonian ([Chern and Wu, 2011](#)):

$$H_{\text{CW}} = -J \sum_{\langle ij \rangle} [P_i^{e_{ij}} (1 - P_j^{e_{ij}}) + (1 - P_i^{e_{ij}}) P_j^{e_{ij}}]. \quad (66)$$

In Eq. (66),  $\mathbf{e}_{ij} = (e_{ij}^x, e_{ij}^y, e_{ij}^z)$  is the bond direction [along which  $t_{\parallel}$  dominates for the orbital  $|e_{ij}\rangle = e_{ij}^x |p_x\rangle + e_{ij}^y |p_y\rangle + e_{ij}^z |p_z\rangle$  (over the transverse hopping  $t_{\perp}$ )]. The projection operator  $P^{e_{ij}} = |e_{ij}\rangle \langle e_{ij}|$ . The Hamiltonian of Eq. (66) embodies the ability of an electron in state  $|e_{ij}\rangle$  on site  $i$  to hop in a direction parallel to  $\mathbf{e}_{ij}$  to site  $j$  if that site is unoccupied in that state (and vice versa). As in the standard Hubbard model, and the two-dimensional Hubbard-type model discussed previously, this kinetic hopping leads, for large  $U$ , to an effective exchange Hamiltonian in the presence of one relevant electronic degree of freedom per site.

When applied to the cubic and diamond lattices, this Hamiltonian reduces to the form provided in Eqs. (67) and (68) ([Chern and Wu, 2011](#)). Expressing, in the case of the cubic lattice model, the projection operators along the three crystalline directions ( $\gamma = x, y, z$ ) as  $P^\gamma = (1/3)(1 + 2\boldsymbol{\lambda} \cdot \mathbf{e}_\gamma)$  and inserting this form into Eq. (66) leads, up to an innocuous additive constant, to Eq. (67). Similarly, in the case of the diamond lattice, the projection operators may be written as  $P = (1/3)(1 + \sqrt{3}\boldsymbol{\lambda} \cdot \mathbf{n}_\gamma)$  which reduces Eq. (66) to Eq. (68).

#### 5. Spin interactions on a lattice

[Micheli, Brennen, and Zoller \(2006\)](#) discussed how to design general lattice spin systems using cold systems of polar molecules. In cold gases of polar molecules, the spin degree of freedom originates in the spin of an electron outside a closed shell of a heteronuclear molecule in its rotational ground state. The complete energy of the system is given by the sum of the translational kinetic and potential energies representing the confining potential of the laser system and two contributions which are of paramount importance in this setup—the individual rotational excitation energies of each molecule [which contains the nuclear angular momentum energy  $BN^2$  (with  $N$  the nuclear orbital angular momentum) and spin-rotation coupling ( $\mathbf{S} \cdot \mathbf{N}$ )], and the dipole-dipole interactions between two molecules with the dipoles induced by the (nuclear) orbital angular momentum of each molecule. A key point is that large dipole-dipole interactions may be induced by a microwave field when the frequency is near resonance with the transition  $N = 0 \rightarrow N = 1$ . An effective second-order Hamiltonian in the ground-state basis was obtained ([Micheli, Brennen, and Zoller, 2006](#)) which when averaged over the intermolecular relative distance between members of a pair of molecules leads to an effective spin-only interaction. The final effective Hamiltonian enables rather general interactions. The effective spin interactions are due to the dipolar interactions induced by the microwave field. The

interactions depend on the orientation of intermolecular separations relative to the microwave field direction. In this setup spin-orientation-dependent compass-type interactions appear very naturally.

### 6. Three-flavor compass models

One can define models in which there are several fermionic species—each of which has “compass-type” hopping amplitudes and may, e.g., propagate along only one direction or more generally have anisotropic hopping amplitudes that differ from one species to another. Different types of such systems have been investigated (Chern and Wu, 2011). Here the concept is illustrated by specifically considering the incarnation of such a system recently introduced by Chern and Wu (2011). It leads to compass-type systems referred to as Gell-Mann matrix compass models. Unlike the SU(2) isospins that formed the focus of most of our discussion thus far, the basic degrees of freedom in these systems are Gell-Mann operators.

Specifically, on the cubic lattice, these take the form (Chern and Wu, 2011)

$$H_{3\Box}^{\text{Gell-Mann}} = \frac{8J}{9} \sum_{a=x,y,z} \sum_{\langle ij \rangle \| \gamma} (\lambda_i \cdot \mathbf{e}_\gamma)(\lambda_j \cdot \mathbf{e}_\gamma). \quad (67)$$

In Eq. (67),  $\lambda_i$  are two component operator vectors,  $\lambda = \sqrt{3}/2(\lambda^{(3)}, \lambda^{(8)})$ , where the standard Gell-Mann matrices  $\lambda^{(3)}$  and  $\lambda^{(8)}$  are diagonal and given by  $\lambda^{(3)} = \text{diag}(1, -1, 0)$  and  $\lambda^{(8)} = \text{diag}(1, 1, -2)/\sqrt{3}$ . As in the earlier compass model that we introduced,  $\gamma$  denotes the direction of the link between the nearest-neighbor sites  $i$  and  $j$ . Similar to the 120° model, the three unit vectors in Eq. (67) are equidistant on a disk,  $\mathbf{e}_{x,y} = (\pm\sqrt{3}, 1)/2$  and  $\mathbf{e}_z = (0, -1)$ .

On the diamond lattice (Chern and Wu, 2011),

$$H_{3\Diamond}^{\text{Gell-Mann}} = \frac{2J}{3} \sum_{\gamma=0}^3 \sum_{\langle ij \rangle \| \gamma} (\lambda_i \cdot \mathbf{n}_\gamma)(\lambda_j \cdot \mathbf{n}_\gamma). \quad (68)$$

In this case, in Eq. (68), the vector  $\lambda = (\lambda^{(6)}, \lambda^{(4)}, \lambda^{(1)})$ . The Gell-Mann matrices  $\lambda^{(1)}, \lambda^{(4)}$ , and  $\lambda^{(6)}$  are nondiagonal (and do not commute among themselves). The index  $\gamma = 0, 1, 2, 3$  denotes the four nearest-neighbor directions on the diamond lattice with correspondingly  $\{\mathbf{n}_\gamma\}$  denoting the unit vectors from a given lattice site to its nearest neighbors. Specifically, when expressed in the Cartesian coordinate system,  $\mathbf{n}_0 = (\mathbf{e}_x + \mathbf{e}_y + \mathbf{e}_z)/\sqrt{3}$ ,  $\mathbf{n}_1 = (\mathbf{e}_x - \mathbf{e}_y - \mathbf{e}_z)/\sqrt{3}$ ,  $\mathbf{n}_2 = (-\mathbf{e}_x + \mathbf{e}_y - \mathbf{e}_z)/\sqrt{3}$ , and  $\mathbf{n}_3 = (-\mathbf{e}_x - \mathbf{e}_y + \mathbf{e}_z)/\sqrt{3}$ . The motivation and properties of these models are reviewed in Secs. V.B.4 and IX.J.

### C. Chiral degrees of freedom in frustrated magnets

It is interesting to note that compass models can emerge by focusing on the low-energy subspace of certain spin models. In particular, compass models appear in an effective low-energy description of quantum magnets that have a chiral degree of freedom (Ferrero, Becca, and Mila, 2003; Budnik and Auerbach, 2004; Capponi, Laeuchli, and Mambrini, 2004;

Mila *et al.*, 2007). In these systems, the low-energy chiral degrees of freedom play the role of the pseudospin with nontrivial directional dependence of the coupling.

In orbital systems, the pseudospin tracks the different degenerate orbital states belonging to, e.g., the  $e_g$  and  $t_{2g}$  sectors in transition-metal systems. A similar situation appears here. In magnets with basic building blocks (e.g., triangles or others) having frustrated interactions, a multitude of degenerate ground states can appear. The chirality tracks the extra degeneracy in these systems. In the quantum magnets that we detail later, there are, within each building block, several degenerate ground states that are labeled by different values of the chirality. This degeneracy is lifted by interactions between the different building blocks (e.g., interactions between different triangular units in a kagome lattice) that rise to effective interactions involving chiralities on different basic units (triangles) which are precisely of the compass type. To date, two variants of the kagome lattice antiferromagnet have been investigated in their low-energy sector. These are the *trimerized kagome lattice antiferromagnet* (Ferrero, Becca, and Mila, 2003) and the *uniform kagome antiferromagnet* (Budnik and Auerbach, 2004). Both of these systems were investigated for a spin  $S = 1/2$  rendition of the original antiferromagnet. One way to describe the kagome lattice, which was made use of for both the trimerized and uniform systems, is, indeed, as a triangular lattice of triangles; see Fig. 17.

The kagome lattice has a very low coordination number. This feature along with the frustrated nature of the antiferromagnetic interactions around individual triangular loops leads the system to have a richness of low-energy states and an extremely high degeneracy of classical ground states. Next we elaborate on the effective low-energy description and consequent origin of the compass-type interactions in both systems.

#### 1. Nonuniform trimerized kagome lattice antiferromagnet

In systems such as the spin  $S = 3/2$  antiferromagnet  $\text{SrCr}_{8-x}\text{Ga}_{4+x}\text{O}_{19}$ , the existence of triangular layers between the kagome lattice planes generates two types of effective

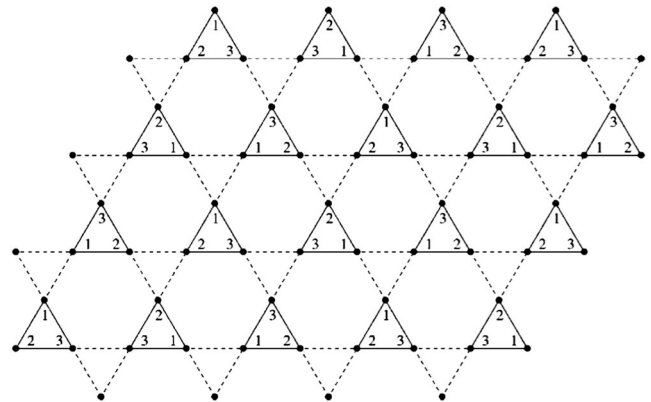


FIG. 17. The trimerized kagome lattice. The solid and dashed lines indicate the antiferromagnetic coupling  $J$  and  $J'$ , respectively. The numbers 1, 2, and 3 indicate the site indexing inside the elementary triangles which defines the gauge. From Ferrero, Becca, and Mila, 2003.

bond strengths inside the kagome lattice plane. The resulting effective planar system (the trimerized kagome lattice antiferromagnet) highlights the geometry of the kagome lattice as a triangular lattice of triangles. Focusing on the upward-facing triangles (see Fig. 17), we observe that they form a triangular lattice. Ferrero, Becca, and Mila (2003) and Capponi, Laeuchli, and Mambrini (2004) considered a spin  $S = 1/2$  model in which the nearest-neighbor couplings inside the triangles ( $J$ ) were far larger than the nearest-neighbor couplings between sites on different triangles ( $J'$ ). In the limit  $J'/J \ll 1$ , the trimerized kagome lattice antiferromagnet becomes a set of decoupled triangular units (with an antiferromagnetic exchange constant of  $J$  within each triangular unit). The idea is then to employ perturbation theory in  $J'/J$  about this limit of decoupled antiferromagnetic triangular units.

Now the problem of a three-spin  $S = 1/2$  on an antiferromagnetic ring (i.e., a basic triangular unit of the kagome lattice) spans  $2^3 = 8$  states. In the total spin basis it can be decomposed into a Hilbert space sector that has a total spin  $S_{\text{tot}} = 3/2$  (a sector spanning four states) as well as two sectors with total spin  $S_{\text{tot}} = 1/2$  (with each of these latter sectors, of course, spanning two states). Formally, that is, the direct product basis can be decomposed in the total spin basis as  $1/2 \otimes 1/2 \otimes 1/2 = 3/2 \oplus 1/2 \oplus 1/2$ . In the antiferromagnetic problem, the tendency is to minimize the spin as much as possible. Indeed an immediate calculation that we perform now shows that at low energies we can confine our attention to the four lower-lying  $S_{\text{tot}} = 1/2$  ground states. Toward that end, we explicitly note that for a three-site antiferromagnetic problem on a triangle,

$$J(\mathbf{S}_1 \cdot \mathbf{S}_2 + \mathbf{S}_1 \cdot \mathbf{S}_3 + \mathbf{S}_2 \cdot \mathbf{S}_3) = \frac{J}{2} S_{\text{tot}}^2 - \frac{9J}{8}, \quad (69)$$

with  $\mathbf{S}_{\text{tot}} = \mathbf{S}_1 + \mathbf{S}_2 + \mathbf{S}_3$  and  $S_{\text{tot}}^2 = S_{\text{tot}}(S_{\text{tot}} + 1)$ . Thus, given the simple identity of Eq. (69), in the ground states we minimize the total spin  $S_{\text{tot}}$ . For the three spins that we consider, the minimal value of  $S_{\text{tot}}$  is  $1/2$ . Physically, these states in which the total spin is smaller than the maximal one (i.e.,  $S_{\text{tot}} < 3/2$ ) are superpositions of states in which two of the three spins combine to form a singlet. This is a particular instance of a more general result that when the total spin is smaller than the maximal possible in a plaquette (such as the three site triangles here), all ground states are superpositions of states that, in any plaquette, contain (at least) one singlet connecting two sites (Nussinov, 2006). The four ground states that are spanned by the two  $S_{\text{tot}} = 1/2$  sectors can be parametrized in terms of an eigenvalue of a spin and a chirality pseudospin each of size  $S = T = 1/2$ . These are defined via (Mila, 1998; Capponi, Laeuchli, and Mambrini, 2004)

$$\begin{aligned} \sigma^z |\alpha R\rangle &= \alpha |\alpha R\rangle, & \sigma^z |\alpha L\rangle &= \alpha |\alpha L\rangle, \\ \tau^z |\alpha R\rangle &= |\alpha R\rangle, & \tau^z |\alpha L\rangle &= -|\alpha L\rangle. \end{aligned} \quad (70)$$

That is,  $\alpha$  and  $R/L$  denote the eigenvalues of the two operators  $S_z$  and  $T_z$ . Written in terms of the original degrees of freedom of the three spins on a triangular unit ( $|\alpha_1, \alpha_2, \alpha_3\rangle$ ), with, e.g.,  $\alpha_1$  corresponding to the “topmost” spin of the upward-facing triangles, we have (Mila, 1998)

$$\begin{aligned} |\alpha R\rangle &= \frac{1}{\sqrt{3}} (|-\alpha\alpha\alpha\rangle + \omega|\alpha-\alpha\alpha\rangle + \omega^2|\alpha\alpha-\alpha\rangle), \\ |\alpha L\rangle &= \frac{1}{\sqrt{3}} (|-\alpha\alpha\alpha\rangle + \omega^2|\alpha-\alpha\alpha\rangle + \omega|\alpha\alpha-\alpha\rangle), \end{aligned}$$

with  $\omega \equiv \exp(2\pi i/3)$ . When  $J' = 0$ , the system exhibits a ground-state degeneracy exponential in size. That is, the degeneracy is equal to  $4^{N_\Delta}$  with  $N_\Delta$  equal to the number of triangular units. This degeneracy is lifted once  $J'$  is no longer zero. For small  $J'/J$ , we can work in the ground-state basis of the  $J' = 0$  problem and employ perturbation theory to write down an effective Hamiltonian in that basis. The resulting effective low-energy Hamiltonian is of a compass type (more precisely, of a form akin to the Kugel-Khomskii Hamiltonian augmenting the usual uniform spin exchange) that is defined on a triangular lattice in which each site represents a triangle of the original kagome lattice. Unlike the definition of  $\mathbf{e}_\gamma$  in the compass models that we considered earlier, now  $\mathbf{e}_\gamma$  depends not only on the orientation of the link connecting two sites, but it differs from bond to bond depending on its physical location on the lattice. A certain “gauge” for  $\mathbf{e}_\gamma$  is to be chosen. Such a gauge is shown in Fig. 18. Explicitly, the effective low-energy Hamiltonian reads (Ferrero, Becca, and Mila, 2003; Capponi, Laeuchli, and Mambrini, 2004)

$$H = \frac{J'}{9} \sum_{\langle ij \rangle} \boldsymbol{\sigma}_i \cdot \boldsymbol{\sigma}_j (1 - 4\mathbf{e}_{ij} \cdot \boldsymbol{\tau}_i)(1 - 4\mathbf{e}_{ij} \cdot \boldsymbol{\tau}_j). \quad (71)$$

## 2. Uniform kagome antiferromagnet

Several research groups (Budnik and Auerbach, 2004; Capponi, Laeuchli, and Mambrini, 2004) employed the “contractor renormalization method” (CORE) to investigate kagome antiferromagnets. This method has been invoked to find an effective low-energy Hamiltonian for the uniform kagome antiferromagnet wherein all exchange couplings are the same. In a spirit similar to the earlier discussion, the individual triangular units are examined and, to lowest order in the CORE, an effective low-energy Hamiltonian is constructed that embodies interactions between different triangular units. A notable difference from the earlier approach is that perturbation theory was not invoked. Rather the system is solved on larger-size units and effective Hamiltonians involving the more primitive basic units are constructed. Budnik and Auerbach (2004) developed a related, yet, by comparison to

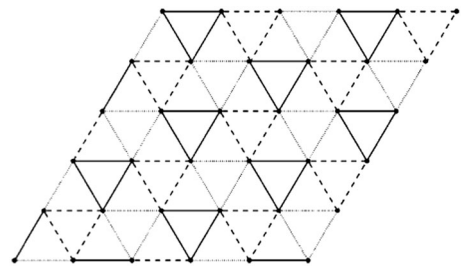


FIG. 18. Triangular lattice on which the effective Hamiltonian is defined. The unit vector for the bond is indicated by solid lines ( $\mathbf{e}_{ij} = \mathbf{e}_1$ ), dashed lines ( $\mathbf{e}_{ij} = \mathbf{e}_2$ ), and dotted lines ( $\mathbf{e}_{ij} = \mathbf{e}_3$ ). From Ferrero, Becca, and Mila, 2003.

the work of Ferrero, Becca, and Mila (2003) and Capponi, Laeuchli, and Mambrini (2004), different definitions of the spin and chiral degrees of freedom are employed. Rather explicitly, with  $s$  an  $S_z$  eigenvalue of a spin operator  $\mathbf{S}$  and  $\uparrow$  and  $\downarrow$  denoting states of eigenvalues  $\pm 1/2$  of a pseudospin operator  $\mathbf{T}$  (Budnik and Auerbach, 2004)

$$\begin{aligned} |s, \uparrow\rangle &= \frac{|s\uparrow\downarrow\rangle - |s\downarrow\uparrow\rangle}{\sqrt{2}}, \\ |s, \downarrow\rangle &= \frac{|s\uparrow\downarrow\rangle + |s\downarrow\uparrow\rangle}{\sqrt{6}} - \sqrt{\frac{2}{3}}|(-s)s\rangle. \end{aligned} \quad (72)$$

As in the perturbative treatment, the resulting effective Hamiltonian (Budnik and Auerbach, 2004) contains effective interactions similar to those of the Kugel-Khomskii model of Secs. III.A and V.A.4. These are further augmented by direct compass-type interactions (i.e., pseudospin interactions uncoupled from spin), similar to those that arise from Jahn-Teller interactions in orbital systems, as well as nontrivial compass-type coupled pseudospin-spin interactions of the form

$$\mathbf{S}_i \cdot \mathbf{S}_j (J_1 \mathbf{T}_i \cdot \mathbf{e}_{ij} + J_2 \mathbf{T}_j \cdot \mathbf{e}_{ji}), \quad (73)$$

with  $J_1$  and  $J_2$  being fixed multiples of the uniform exchange constant  $J$  in the kagome lattice antiferromagnet. The direct pseudospin interactions that couple the chiralities on neighboring triangles favor the formation of aligning singlets parallel to one another along particular directions.

## VI. SYMMETRIES OF COMPASS MODELS

### A. Global, topological, and intermediate symmetries and invariances

In terms of symmetries, compass systems are particularly rich. In what follows, we discuss the invariances that these systems exhibit, but first recall the classification of orders and their relation to symmetry:

- (i) *Global symmetry.* In many condensed matter systems (e.g., ferromagnets, liquids), there is an invariance of the basic interactions with respect to global symmetry operations (e.g., continuous rotations in the case of ferromagnets, uniform translations, and rotations in liquids) that are to be simultaneously performed on all of the constituents of the system. At sufficiently low temperatures (or strong enough interactions), such symmetries might be spontaneously broken.
- (ii) *Topological invariants and orders.* Topological orders have been the object of some fascination in recent years (Wen, 2004). In the condensed matter community, part of the activity in analyzing these types of order is stimulated by the prospects of fault-tolerant-free quantum computation. What lies at the crux of topological order is the observation that even if, in some cases, global symmetry breaking cannot occur, systems may nevertheless still exhibit a robust order of a nonlocal, topological type.

The most prominent examples of topological order, long studied by high-energy theorists, are afforded by gauge theories (Wegner, 1971; Kogut,

1979; Wen, 2004). Some of the current heavily studied quintessential models of topological quantum order in condensed matter and quantum information lattice theories [see, e.g., Kitaev (2003) and Wen (2004)] share much in common with the early pioneering lattice gauge theory concept along with the explicit simplest lattice gauge model first introduced by Wegner (1971).

Gauge theories display local gauge symmetries and indeed, in pure gauge theories (theories that have only gauge bosons yet no matter sources) the only measurable quantities pertain to correlators defined on loops, the so-called *Wilson loops*. Related products pertain to open contours in some cases when matter sources are present (Fradkin and Shenker, 1979; Kogut, 1979; Nussinov, 2005).

- (iii) *Intermediate symmetry.* The crucial point is that many compass systems display symmetries which, generally, lie midway between the above two extremes of global symmetries and local gauge symmetries. These symmetries are sometimes known as “sliding” symmetries, and aside from compass models are also present in numerous other systems. These include, among many others, arrays of Luttinger liquids (Emery *et al.*, 2000; Vishwanath and Carpentier, 2001), quantum Hall smectic phases (Fradkin and Kivelson, 1999; MacDonald and Fisher, 2000), DNA intercalated in lipid bilayers (Golubovic and Golubovic, 1998; O’Hern and Lubensky, 1998; O’Hern, Lubensky, and Toner, 1999), ring-exchange models of frustrated models (Paramekanti, Balents, and Fisher, 2002), and Kondo lattice systems (Venderbos *et al.*, 2011).

To clarify the distinction between these different symmetries, we can rephrase it in a formal way as it applies to general systems (Batista and Nussinov, 2005; Nussinov, Ortiz, and Cobanera, 2012b). Consider a theory with fields  $\{\phi_i\}$  that is characterized by a Hamiltonian  $H$  (or action  $\mathcal{S}$ ).

*Definition:* A  $d$ -dimensional *gaugelike symmetry* of a theory is a group of symmetry transformations such that the minimal nonempty set of fields  $\{\phi_i\}$  changed by the group operations occupies a  $d$ -dimensional subset ( $\mathcal{C}$ ) of the full  $D$ -dimensional region on which the theory is defined. In the following we refer to such symmetries as  *$d$ -dimensional symmetries*.

To exercise this notion it is useful to make contact with known cases. Clearly local gauge symmetries correspond to symmetries of dimension  $d = 0$ . That is, gauge transformations can be applied locally at any point in space—a region of dimension  $d = 0$ . At the opposite extreme, e.g., in a nearest-neighbor ferromagnet on a  $D$ -dimensional lattice, described by the Heisenberg Hamiltonian  $H = -J \sum_{\langle ij \rangle} \mathbf{S}_i \cdot \mathbf{S}_j$ , the system is invariant under a global rotation of all spins. For the Heisenberg model, the volume influenced by the symmetry occupies a  $D$ -dimensional spatial region and thus in this case,  $d = D$ . Sections VI.D, VI.E, VI.F, VI.G, VI.H exemplify how symmetries of intermediate dimension  $0 < d < D$  arise in compass systems.

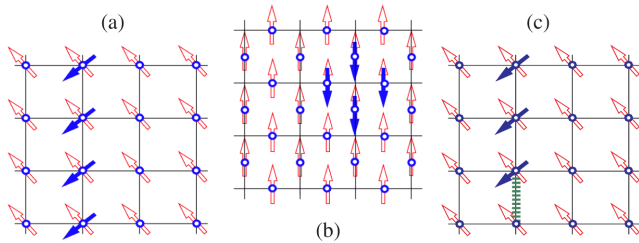


FIG. 19 (color online). (a) The  $90^\circ$  square lattice compass model. The action of the  $d = 1$  symmetry operation of Eq. (84) when the “plane”  $P$  is chosen to lie along the vertical axis. (b) A  $d = 0$  (local) gauge symmetry. Defects within a gauge theory cost a finite amount of energy. Local symmetries such as the one depicted above for an Ising lattice gauge theory cannot be broken. (c) A defect in a semiclassical ground state of the two-dimensional orbital compass model. Defects such as this do not allow for a finite on-site magnetization. The energy penalty for this defect is finite (there is only one bad bond—the dashed line) whereas, precisely as in  $d = 1$  Ising systems, the entropy associated with such defects is monotonically increasing with system size. From Nussinov and Ortiz, 2009c.

In their simplest form, one which typically appears in compass models,  $d$ -dimensional symmetries are of the form

$$\prod_{j \in P} g_j, \quad (74)$$

where  $g_j$  are group elements associated with a site  $j$  and  $P$  is a  $d$ -dimensional spatial region. In many cases, depending on the boundary conditions of the system,  $P$  corresponds to entire open  $d$ -dimensional planes (as in  $90^\circ$  compass models which we review in Sec. VI.D; see, e.g., Fig. 19) or closed contours (when compass models are endowed with periodic boundary conditions). Defect creation operators (those that restore symmetries) and translations of defects are typically products of local group elements that do not span such an entire region  $P$  but rather a fragment of it (see, e.g., the open finite string in Fig. 19 with domain wall boundaries), generally leading to defects at the boundaries where the group element operations are applied (Nussinov and Ortiz, 2009c).

## B. Exact and emergent symmetries

A Hamiltonian  $H$ , and by extension the system it describes, can have two principal kinds of symmetries: exact and emergent ones. These are defined as follows.

- (i) *Exact symmetries*. This refers to the existence operators  $\hat{O}$  that commute with the Hamiltonian,

$$[H, \hat{O}] = 0. \quad (75)$$

Such operators, indicated in this review by a caret, reflect symmetries of the Hamiltonian.

- (ii) *Emergent symmetries*. In many compass (and numerous other) systems, there are operators  $\tilde{O}$  that do not commute with the Hamiltonian,

$$[H, \tilde{O}] \neq 0, \quad (76)$$

i.e., do not satisfy Eq. (75), and are therefore indicated throughout this review by a tilde. Yet

these operators become symmetries when projected to a particular sector—a particular subset of states on which the Hamiltonian acts. That is,

$$[H, \mathcal{P}\tilde{O}\mathcal{P}] = 0, \quad (77)$$

where  $\mathcal{P}$  is the relevant projection operator of that sector. In this case, if one defines  $\mathcal{P}\tilde{O}\mathcal{P} = \hat{O}$ , then  $\hat{O}$  is an exact symmetry satisfying Eq. (75).

The most prominent cases in condensed matter systems, including compass models, in particular [yet also many others, see, e.g., Batista and Trugman (2004), Nussinov *et al.* (2007), Venderbos *et al.* (2011), and Normand and Nussinov (2014)] relate to symmetries that appear in the ground-state sector alone. In such instances, the symmetries are sometimes said to emerge in the low-energy sector of the theory.

Although the formulation above is for quantum Hamiltonians, the same can, of course, be said for classical systems. There are numerous classical systems in which the application of a particular operation on an initial configuration will yield, in general, a new configuration with a differing energy. However, when such an operation is performed on a particular subset of configurations, such as the classical ground states, it will lead to other configurations that have precisely the same energy as the initial state. Similarly, certain quantum systems exhibit such particular symmetries only in their large-pseudospin (or classical) limit, where they may be said to emerge. As reviewed in Secs. VI.D.3, VI.E, and VI.F, particularly in certain compass-type models, symmetries may emerge within a sector of the combined large-pseudospin and/or low-energy (or temperature) limit.

One should note that the emergence of low-energy symmetries is notably different from the far more standard situation of spontaneous symmetry breaking, wherein an invariance of the Hamiltonian (or action) is spontaneously broken in individual low-energy states (which are related to one another by the symmetry operation at hand). In the condensed matter arena, the canonical example is supplied by rotationally symmetric ferromagnets in a spatial dimension larger than 2, in which at sufficiently low temperature a finite magnetization points along a certain direction, thus breaking the rotational symmetry. Another canonical example is the discrete (up  $\leftrightarrow$  down or) time-reversal symmetry which is broken in Ising ferromagnets in dimensions large than 1. Spontaneous symmetry breaking appears in systems that exhibit long-range order of some sort such as the process of crystallization (breaking translational and rotational symmetries), superconductors (local gauge invariance and an Anderson-Higgs mechanism), or superfluid helium. Other examples include the Higgs mechanism of particle physics, chiral symmetry breaking in quantum chromodynamics, nucleon pairing in nuclei, electroweak symmetry breaking at low energies, and related mass generation.

In all of these textbook examples, the system is symmetric at high energies and exhibits low-energy states that do not have that symmetry. However, in low-energy emergent symmetries, the situation is reversed: the system may become more symmetric in the low-energy sector. We discuss explicit examples of exact and emergent symmetries in compass models in Secs. VI.D–VI.H.

### C. Consequences of intermediate symmetry

In this section, we review the consequences of intermediate symmetries. In later sections, we will see how the intermediate symmetries appear in various compass models. Aside from the earlier results reviewed in Sec. VII, we further report on an additional consequence concerning the link between these symmetries and “flat bands” and illustrate how this relation appears throughout the compass models investigated.

#### 1. Degeneracy of spectrum

We now briefly discuss how the presence of a  $d$ -dimensional intermediate symmetry, either classical or quantum, implies an exponential degeneracy of the energy spectrum that corresponds to the Hamiltonian. The application of intermediate symmetries on disparate  $d$ -dimensional planes leads to inequivalent states that all share the same energy. If a symmetry transformation  $\tilde{O}_P$  has its support on a  $d$ -dimensional plane  $P$ , then one can define the composite symmetry operators

$$\tilde{O}_{\text{composite}} = \tilde{O}_{P_1} \tilde{O}_{P_2} \cdots \tilde{O}_{P_R}. \quad (78)$$

For a hypercubic lattice in  $D$  dimensions which is of size  $L \times L \times L \times \cdots \times L$ , the number of independent planes ( $R$ ) in Eq. (78) scales as  $R = \mathcal{O}(L^{d'})$ , where

$$d' = D - d. \quad (79)$$

If each individual  $d$ -dimensional symmetry operation (exact or emergent)  $U_{P_i}$  leads to a degeneracy factor of  $m$  then the composite operation of Eq. (78) can lead to a degeneracy [of any state (for exact symmetries) or of the ground state (for emergent symmetries)] whose logarithm is of magnitude

$$\log_m(\text{degeneracy}) = \mathcal{O}(L^{D-d}). \quad (80)$$

That this is indeed the case is clearer for classical systems with discrete symmetries than for quantum systems. Nevertheless, in the thermodynamic limit and/or on lattices whose boundaries are tilted the degeneracy factor of Eq. (80) associated with the intermediate  $d$ -dimensional symmetries becomes exact (Nussinov and Shtengel, 2015). On hypercubic lattices, such as the square lattice of the planar  $90^\circ$  compass model discussed in Sec. VI.D, whose boundaries are the same along the  $d'$  directions orthogonal to the planes  $P$ , the application of the operators of Eq. (78) does not lead to independent states for finite-size systems. However, in the thermodynamic limit, the application of disparate operators of the form of Eq. (78) on a given initial state may lead to orthogonal states.

#### 2. Dimensional reduction

The existence of intermediate symmetries has important consequences: it implies a dimensional reduction. The corresponding dimensional reduction is only with respect to expectation values of local quantities: the free energies of these systems and the transitions that they exhibit are generally those of systems in high dimensions (Batista and Nussinov, 2005; Nussinov, Ortiz, and Cobanera, 2012b).

#### a. Theorem on dimensional reduction

More precisely, the expectation value of any such quantity  $\langle f \rangle$  in the original system (of dimension  $D$ ) is bounded from above by the expectation value of the same quantity evaluated on a  $d$ -dimensional region:

$$|\langle f \rangle| \leq |\langle f \rangle|_{H_d}. \quad (81)$$

The expectation value  $\langle f \rangle$  refers to that of the original system (or lattice) that resides in  $D$  spatial dimensions. The Hamiltonian  $H_d$  on the right-hand side is defined on a  $d$ -dimensional subregion of the full lattice (system). The dimensionality  $d \leq D$ . The Hamiltonian  $H_d$  preserves the range of the interactions of the original systems. It is formed by pulling out of the full Hamiltonian on the complete ( $D$ -dimensional) lattice, the parts of the Hamiltonian that appear within the  $d$ -dimensional subregion ( $\mathcal{C}$ ) on which the symmetry operates. Fields (spins) external to  $\mathcal{C}$  act as non-symmetry-breaking external fields in  $H_d$ . The bound of Eq. (81) becomes most powerful for quantities that are not symmetry invariant as then the expectation values  $\langle f \rangle_{H_d}$  need to vanish for low spatial dimensions  $d$  (as no spontaneous symmetry breaking can occur). This, together with Eq. (81), then implies that the expectation value of  $\langle f \rangle$  on the full  $D$ -dimensional spatial lattice must vanish. By “noninvariant” we mean that  $f(\phi_i)$  vanishes when summed over all arguments related to each other by a  $d$ -dimensional symmetry operation,  $\sum_k f[\mathbf{g}_{ik}(\phi_i)] = 0$ . For continuous symmetries, noninvariance explicitly translates into an integral over the group elements  $\int f[\mathbf{g}_i(\phi_i)] d\mathbf{g} = 0$ .

We now summarize for completeness general corollaries of such a symmetry-based analysis for general systems.

#### b. Corollaries

By choosing  $f$  to be the order parameter or a two-particle correlator, one arrives at the following general corollaries (Batista and Nussinov, 2005; Nussinov, Batista, and Fradkin, 2006; Nussinov, Ortiz, and Cobanera, 2012b):

*Corollary I:* Any local quantity that is not invariant under local symmetries ( $d = 0$ ) or symmetries that act on one-dimensional regions ( $d = 1$ ) has a vanishing expectation value  $\langle f \rangle_{H_d}$  at any finite temperature. This follows as neither zero- nor one-dimensional systems can exhibit symmetry breaking: in one- and two-dimensional systems, the expectation value of any local quantities not invariant under global symmetries  $\langle f \rangle = 0$ .

Physically, entropy overwhelms energetic penalties and forbids symmetry breaking. Just as in zero- and one-dimensional systems, much more entropy is gained by introducing defects (e.g., domain walls in discrete systems), and the same energy-entropy calculus is replicated when these symmetries are embedded in higher dimensions. An example with  $d = 1$  domain walls in a two-dimensional systems is afforded by the planar  $90^\circ$  compass model (see Fig. 19); even though the planar compass model is two dimensional, the energy cost of these domain walls is identical to that in a  $d = 1$  system. The particular case of local ( $d = 0$ ) symmetry is that of Elitzur’s theorem (Elitzur, 1975), so well known in gauge

theories. We see it more generally as a consequence of dimensional reduction.

A discussion of how, by virtue of this consequence, such symmetries may protect and lead to topological quantum orders in systems at both finite and zero temperature is given by [Nussinov and Ortiz \(2009a, 2009c\)](#).

*Corollary II:* One can push the consequences further by recalling that no symmetry breaking occurs for continuous symmetries in two spatial dimensions. Here again, free-energy penalties are not sufficiently strong to induce order. When embedding continuous two-dimensional symmetries in higher dimensions, the energy-entropy balance is the same and the same result is attained:  $\langle f \rangle = 0$  at all finite temperatures for any quantity  $f$  that is not invariant under continuous  $d \leq 2$  symmetries.

Further noting that order does not exist in continuous two-dimensional systems at zero temperature in the presence of a gap between the ground and the next excited state, one similarly finds that for a ( $d \leq 2$ )-dimensional continuous symmetry the expectation value of any local quantity not invariant under this symmetry strictly vanishes at zero temperature. Although local order cannot appear, multiparticle (including topological) order can exist. In standard gauge ( $d = 0$ ) theories, the product of gauge degrees of freedom along a closed loop (the Wilson loop) can attain a nonzero value as it may be invariant under all  $d = 0$  symmetries. In more general theories with higher  $d$ -dimensional symmetries, similar considerations may lead to loop (or “brane”) type correlators that involve multiple fields and are invariant under all low-dimensional symmetries. Precisely such nonlocal correlation functions appear in Kitaev’s honeycomb model and many other systems with topological orders ([Chen and Nussinov, 2008](#); [Perez-Garcia et al., 2008](#); [Nussinov and Ortiz, 2009a, 2009c](#)).

In [Sec. VIII](#) we review how, when it is indeed allowed by symmetry, symmetry breaking in the highly degenerate compass models often transpires via a fluctuation-driven mechanism (“order by disorder”) ([Villain, 1972](#); [Shender, 1982](#); [Henley, 1989](#)). In this mechanism, entropic contributions to the free energy play a key role.

*Corollary III:* Not only can we make statements about the absence of symmetry breaking, we can also adduce fractionalization of non-symmetry-invariant quantities in high-dimensional systems. That occurs if no (quasiparticle-type) resonant terms appear in the lower-dimensional spectral functions ([Nussinov, Batista, and Fradkin, 2006](#)).

This corollary allows for fractionalization in quantum systems, where  $d = 1, 2$ . It enables symmetry-invariant quasiparticle excitations to coexist with non-symmetry-invariant fractionalized excitations. Fractionalized excitations may propagate in  $(D - d)$ -dimensional regions. Examples are afforded by several frustrated spin models where spinons may drift along lines on the square lattice ([Batista and Trugman, 2004](#)) and in  $D$ -dimensional regions on the pyrochlore lattice ([Nussinov et al., 2007](#); [Normand and Nussinov \(2014\)](#)).

In what follows, we explicitly enumerate the symmetries that appear in various compass models. The physical origin of dimensional reduction in these systems can be seen by examining intermediate symmetry-restoring defects.

## D. Symmetries of the 90° compass model

We now classify symmetries of the 90° compass model in various spatial dimensions, reviewing both quantum and classical versions. To highlight some aspects of the symmetries of this system, it is profitable to discuss the general anisotropic compass model, as given for  $D = 2$  in [Eq. \(1\)](#) with general couplings  $J_x$  and  $J_y$ , and in general spatial dimension  $D$  given by [Eq. \(4\)](#), without field:

$$H_{D\Box}^{90^\circ} = -\sum_{r,\gamma} J_\gamma \tau_r^\gamma \tau_{r+e_\gamma}^\gamma. \quad (82)$$

The equivalent classical Hamiltonian on a  $D$ -dimensional hypercubic lattice is

$$H_{D\Box}^{90^\circ, \text{class}} = -\sum_{r,\gamma} J_\gamma T_r^\gamma T_{r+e_\gamma}^\gamma. \quad (83)$$

In the quantum systems,  $T^\gamma$  are generators of the representations of  $SU(2)$  of size  $(2T + 1)$ . For a pseudospin-1/2 system,  $T^\gamma = \tau^\gamma/2$ . In the classical arena,  $T^\gamma$  are the Cartesian components of the normalized vector  $\mathbf{T}$ , as discussed in [Sec. III.B](#). These classical and quantum Hamiltonian systems exhibit both exact and emergent symmetries.

### 1. Exact discrete intermediate symmetries

Exact symmetries of both the square lattice and cubic lattice 90° compass models in any pseudospin representation are given by [Nussinov et al. \(2004\)](#), [Batista and Nussinov \(2005\)](#), [Biskup, Chayes, and Nussinov \(2005\)](#), [Dorier, Becca, and Mila \(2005\)](#), [Doucot et al. \(2005\)](#), and [Nussinov and Fradkin \(2005\)](#)

$$\hat{O}^{(\gamma)} = \prod_{r \in P_\gamma} e^{i\pi T_r^\gamma}, \quad (84)$$

where, as in [Eq. \(87\)](#),  $P_\gamma$  is any line (in the case of the two-dimensional model) or plane (in the case of the cubic lattice model) which is orthogonal to the external  $e_\gamma$  axis of the lattice. A schematic for the ( $D = 2$ )-dimensional case is provided in [Fig. 19\(a\)](#).

It should be noted that despite appearances, [Eq. \(84\)](#) is, when written longhand, quite different from the emergent symmetries of the 120° model in [Eq. \(87\)](#) that is discussed in [Sec. VI.D.2](#). In that case  $\mathbf{T}$  is a two-component vector that is projected along three different equidistant nonorthogonal planar directions. That is, in [Eq. \(87\)](#), the unit vectors  $e_\gamma$  in the argument of the exponential correspond, with  $\gamma = 1, 2, \text{ and } 3$ , to the equidistant nonorthogonal internal pseudospin directions  $\mathbf{a}$ ,  $\mathbf{b}$ , and  $\mathbf{c}$  that lie in the two-dimensional plane defined of the 120° model. By contrast, in [Eq. \(84\)](#),  $\mathbf{T}$  is a  $D = 2$  (square lattice model) or  $D = 3$  (cubic lattice) vector and  $T^\gamma$  are projections along the orthogonal directions. The two operators appearing in [Eqs. \(84\) and \(87\)](#) differ from one another:  $\mathbf{T} \cdot \mathbf{b} \neq T_2$ , etc. In [Fig. 19](#), we provide a classical schematic of the action of such an operator when it acts on a uniform state. As in the case of the 120° model on the cubic lattice, these operators lead to stratified states.

The exact nature of the symmetries of Eq. (84) is readily seen: the operators of Eq. (84) commute with the general Hamiltonian of Eq. (83),  $[O^{(r)}, H] = 0$ . Thus, rotations of individual planes about an orthogonal axis leave the system invariant. Written generally, for a  $90^\circ$  compass model in  $D$  dimensions, the planes  $P_\gamma$  are objects of spatial dimensionality  $d = D - 1$ . In the ( $D = 3$ )-dimensional system, the symmetries of Eq. (84) are of dimension  $d = 2$  as the planes  $P_\gamma$  are two-dimensional objects. On the square lattice, the symmetries are of dimension  $d = 1$  as  $P_\gamma$  are lines. These symmetries hold for both the quantum system with arbitrary size pseudospin and the classical system of Eq. (20) in a high dimension  $D$ . A consequence of these symmetries is an exponential-in- $L^{D-1}$  degeneracy of each eigenstate of the Hamiltonian (including but not limited to ground states) in systems with “tilted” boundary conditions that emulate the thermodynamic limit (Nussinov and Shtengel, 2015). In pseudospin-1/2 realizations of this system [Eq. (82)], on an  $L \times L$  square lattice, a  $2^L$  degeneracy was numerically adduced for anisotropic systems ( $J_x \neq J_y$ ) in the thermodynamic limit (Dorier, Becca, and Mila, 2005). Correlation functions involving the symmetry operators were examined by Lin and Scarola (2013).

Here is an important point we want to reiterate—that of the physical origin of the dimensional reduction in this system. In a ( $D = 2$ )-dimensional  $90^\circ$  compass model system, the energy cost for creating defects (domain walls) is identical to that in a ( $d = 1$ )-dimensional system (see Fig. 19). With the aid of the bound of Eq. (81), we then see the finite-temperature expectation value  $\langle \sigma_i^z \rangle = 0$  within the  $D = 2$  orbital compass model. The physical mechanism behind the loss of the on-site order of  $\langle \sigma_i^z \rangle$  is the proliferation of solitons; see Fig. 19. Just as in ( $d = 1$ )-dimensional systems, domain walls (solitons) cost only a finite amount of energy while their entropy increases with system size. A schematic is provided in Fig. 19(c). The Hamiltonian  $H_{d=1}$  defined on the vertical chain of Fig. 19 where these operations appear is none other than a one-dimensional Ising Hamiltonian augmented by transverse fields generated by spins outside the vertical chain. Any fixed values of the spins outside the ( $d = 1$ )-dimensional chain lead to transverse fields that act on the chain. Those in the direction of the Ising exchange interactions between neighboring spins along the chain lead in this case to the pertinent  $H_{d=1}$  in Eq. (81): that of a transverse-field Ising model Hamiltonian. By virtue of their location outside the region where the symmetry of Eq. (84) operates, the spins  $\sigma_{i \notin P_x}^x$  do not break the discrete  $d = 1$  symmetry associated with the plane  $P_x$ . These defects do not enable a finite-temperature symmetry breaking.

## 2. Exact discrete global symmetries

When the couplings are not completely anisotropic (e.g.,  $J_x = J_y \neq J_z$  or  $J_x = J_y = J_z$  on the cubic lattice or  $J_x = J_y$  on the square lattice), there are additional discrete symmetries augmenting the  $d = D - 1$  Ising symmetries detailed above. For instance, when  $J_x = J_y \neq J_z$  a global discrete rotation of all pseudospins on the lattice by an angle of  $90^\circ$  about the  $T^z$  direction leaves the Hamiltonian of Eq. (83) invariant. Such a discrete rotation essentially permutes the  $x$ - and  $y$ -oriented bonds, which are all of equal weight in the isotropic case when

they are summed over the entire square lattice. The same, of course, also applies for the square lattice model when  $J_x = J_y$ .

Yet another possible representation of essentially the same symmetry that is pertinent to the exchange of couplings in the compass model is that of a uniform global rotation by  $180^\circ$  about the  $(1/\sqrt{2}, 1/\sqrt{2})$  direction of the pseudospins. Such a representation occurs in Eq. (105). Similarly, when  $J_x = J_y = J_z$ , a uniform global rotation by  $120^\circ$  of all pseudospins about the internal  $(1/\sqrt{3}, 1/\sqrt{3}, 1/\sqrt{3})$  pseudospin direction is also a discrete symmetry; this latter symmetry is of the  $Z_3$  type—if performed 3 times in a row, it gives back the identity operation.

These additional discrete symmetries endow the system with a higher degeneracy. For isotropic systems ( $J_x = J_y$ ), numerically a  $2^{L+1}$ -fold degeneracy is seen in the pseudospin  $T = 1/2$  system (Dorier, Becca, and Mila, 2005); this additional doubling of the degeneracy is related to a global Ising operation of a rotation by  $180^\circ$  about a chosen pseudospin direction that leaves the system invariant. These additional symmetries are global symmetries and thus of a dimension  $d = D$  which is higher than that of the discrete lower-dimensional symmetries that are present in both the anisotropic and isotropic systems ( $d = D - 1$ ). As a result, the isotropic ( $D = 2$ )-dimensional  $90^\circ$  compass model may exhibit a finite-temperature breaking of a discrete global symmetry associated with such a discrete rotation. By contrast, the  $d = 1$  symmetries of the two-dimensional  $90^\circ$  compass model cannot be broken, as discussed in Sec. VI.C.2.

We note that in the classical anisotropic rendition of this system the degeneracy is exactly the same, i.e.,  $2^L$ , aside from continuous emergent symmetries that are discussed in the next section. The classical isotropic case is somewhat richer. There, each uniform pseudospin state (each such state is a ground state as is elaborated in Sec. VII) has an additional degeneracy factor of  $2^{2L}$  associated with the  $2L$  independent classical  $d = 1$  Ising symmetries.

## 3. Emergent intermediate discrete symmetries: Cubic $90^\circ$ model

We now turn to intermediate symmetries that appear in the large-pseudospin (or classical) limit of the  $90^\circ$  compass model in three dimensions. In its classical limit, the classical  $90^\circ$  compass model on the cubic lattice has  $d = 1$  inversion (or reflection) symmetries along lines parallel to each of the three Cartesian axes  $x_a$ . Along these lines, we can set  $\tau_i^a \rightarrow -\tau_i^a$  and not touch the other components. This corresponds to, e.g., a reflection in the internal  $x$ - $y$  pseudospin plane when we invert  $\tau^z$  and do not alter the  $x$  or  $y$  components.

We explicitly note that this transformation is not canonical and does not satisfy the commutation relation and is thus disallowed quantum mechanically; indeed, this appears only as an emergent symmetry in the classical limit of large pseudospin. Instead in the  $90^\circ$  compass model on the cubic lattice, quantum mechanically we have the  $d = 2$  symmetries that we wrote earlier (which, of course, trivially also hold for the classical system). Thus, the quantum system is less symmetric than its classical counterpart.

By contrast to the cubic lattice case, for the square lattice  $90^\circ$  compass model, the intermediate  $d = 1$  symmetries of Eq. (84) are exact quantum (as well as classical) symmetries.

#### 4. Emergent continuous global symmetries

In addition to its exact symmetries, the  $90^\circ$  model also exhibits emergent symmetries in its isotropic version. As mentioned earlier, globally uniform pseudovector configurations are ground states of any classical isotropic ferromagnetic compass model. Thus, following the considerations presented for the  $120^\circ$  compass model, any global rotation of all pseudospins is an emergent symmetry of the  $90^\circ$  models. In the  $D = 2$  system, this corresponds to a global  $U(1)$  rotation of all angles of the planar pseudospins. In the  $D = 3$  cubic lattice system, any  $SO(3)$  rotation of the three-dimensional pseudospins is an emergent symmetry. That a rotation does not change the energy of any uniform configuration is clear in the  $90^\circ$  model. Imagine that all pseudospins in the planar  $90^\circ$  model are oriented at an angle  $\theta$  relative to the  $T^x$  axis. In such a case, the energy associated with the horizontal bonds  $T_r^x T_{r+e_x}^x$  will vary as  $\cos^2 \theta$ , whereas that associated with the vertical bonds varies as  $\sin^2 \theta$ . As  $J_x = J_y = J$  in the isotropic system and as  $\sin^2 \theta + \cos^2 \theta = 1$ , any uniform pseudospin state will have the same energy (which is, in fact, the ground-state energy as discussed in Sec. VII.A) and global rotations will not alter this energy.

#### E. Emergent symmetries: Classical cubic $120^\circ$ compass model

The  $120^\circ$  compass model on a 3D cubic lattice, Eqs. (9) and (10), exhibits nontrivial symmetries which emerge in the ground-state sector in the large-pseudospin  $T$  (classical) limit (Lieb, 1973; Simon, 1980) (see also Sec. III.B). In the classification of Sec. VI.B, all of the symmetries which we next detail correspond to emergent symmetries. Before explicitly describing these symmetries, we briefly recount how to define this classical system from the quantum one, which we alluded to in Sec. V.A.6.

The classical  $120^\circ$  compass model may, following the discussion in Sec. III.B, be specified as follows. At each site we assign a unit length two-component spin denoted by  $\mathbf{T}$ . Let  $\mathbf{a}$ ,  $\mathbf{b}$ , and  $\mathbf{c}$  be evenly spaced vectors on the unit circle that are separated from one another by  $120^\circ$ . To conform with the operators of Eq. (9), one sets  $\mathbf{c}$  to point at  $0^\circ$  and  $\mathbf{a}$  and  $\mathbf{b}$  to be at  $\pm 120^\circ$ , respectively. Next, one defines  $T^{(c)} = \mathbf{T} \cdot \mathbf{c}$ , and similarly for  $T^{(a,b)}$ . These projections onto the above unit vectors  $T^{(a,b,c)}$  are the classical counterpart of the pseudospin  $1/2$  operators of Eq. (9). The classical  $120^\circ$  compass model Hamiltonian is then given by

$$H_{3\Box}^{120,\text{class}} = -\sum_i (T_r^{(a)} T_{r+e_x}^{(a)} + T_r^{(b)} T_{r+e_y}^{(b)} + T_r^{(c)} T_{r+e_z}^{(c)}), \quad (85)$$

where the interaction strength  $J$  is set to unity. The ferromagnetic and antiferromagnetic models are related by symmetry, so that for convenience the interaction strength is chosen as negative, so that low-temperature ordering patterns of pseudospins tend to be uniform. This model exhibits two types of emergent symmetries in its ground-state sector.

#### 1. Emergent continuous global symmetries

All uniform pseudospin configurations, i.e., those with constant pseudospin  $\mathbf{T}_r = \mathbf{T}$  or uniform angular orientation

of the classical two-component pseudospins in the  $XY$  plane, are ground states of  $H_{3\Box}^{120,\text{class}}$  in Eq. (85) (Nussinov *et al.*, 2004). Therefore any configuration for which

$$\mathbf{T}_r^\gamma = T_{r+e_\gamma}^\gamma \quad (86)$$

on all sites  $i$  is also a ground-state configuration. Thus, when the system is restricted to this subspace of uniform configurations, any uniform rotation of all of the pseudospin angles  $\theta_r \rightarrow \theta_r + \delta\theta$  does not change the energy. This global rotation operation [formally a  $U(1)$  symmetry] emerges as a symmetry when the system is restricted to these ground states. It can be readily verified that this emergent symmetry is not an exact symmetry of the system. When a global rotation is applied to any initial pseudospin configuration that is not uniform, it will generally lead to a new state that has energy from that of the initial configuration.

Formally therefore the classical cubic lattice  $120^\circ$  compass model exhibits a global (i.e., a dimension  $d = D = 3$ ) emergent  $U(1)$  symmetry within the ground-state sector. It turns out that on top of this there are additional nonuniform *stratified* classical ground states for which this global rotation is not a symmetry, which is discussed next.

#### 2. Emergent discrete $d = 2$ symmetries

The existence of a global rotational symmetry, as discussed in the previous section, is pervasive in physical systems, although usually these are exact symmetries. Much more specific to the  $120^\circ$  compass and related models is the existence of numerous low-dimensional ( $d < D$ ) symmetries. These symmetries relate to ground states that will be stabilized at finite (yet low) temperatures. An explanation of what these symmetries are is given pictorially. In the top left-hand corner of Fig. 20 a general uniform configuration is shown—a ground state of the classical system. Starting with any such state, it is possible to reflect pseudospins in individual planes to generate myriad other configurations which are also ground states of the classical  $120^\circ$  compass model. For instance, one may take any plane that is orthogonal to the  $e_x$  direction and reflect all of the pseudospins in that plane about the  $\mathbf{a}$  direction. Under such an operation,  $T_r^{(a)}$  is unchanged but the pseudospin component along the direction that is orthogonal to  $\mathbf{a}$  flips its sign. This will lead to a state that has exactly the same energy as that of the uniform state. Similarly, one may reflect all pseudospins in planes orthogonal to the  $e_y$  or  $e_z$

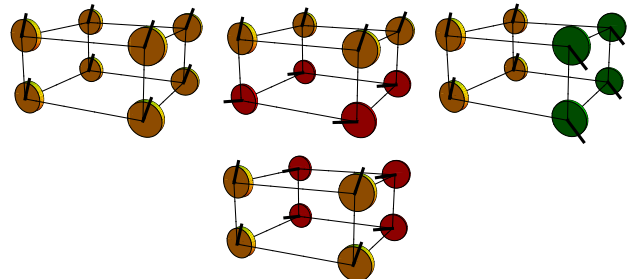


FIG. 20 (color online). The symmetries of Eq. (87) applied to a uniform ground state (top left).

directions by  $\mathbf{b}$  or  $\mathbf{c}$ , respectively. All three cases are depicted in Fig. 20.

These reflections are Ising symmetry operations or, formally,  $Z_2$  symmetries. Any reflection performed twice will lead to the original state and is thus an Ising-type operation. Going beyond the  $2 \times 2 \times 2$  cube shown in Fig. 20, one can consider a cubic lattice of dimension  $L \times L \times L$  with  $L \gg 1$ . On such a lattice, these reflections are emergent ( $d = 2$ )  $[Z_2]^{3L}$  gaugelike symmetry operators (Nussinov *et al.*, 2004; Batista and Nussinov, 2005; Biskup, Chayes, and Nussinov, 2005). The power of  $(3L)$  relates to the number of planes [ $(d = 2)$ -dimensional objects] in which such reflections can be applied: there are  $L$  such planes which are orthogonal to one of the three cubic lattice directions.

Formally, these operations, rotations of all pseudospins by an angle of  $180^\circ$  about the internal  $T^\gamma$  axis, can be written as quantum operators in the limit of large pseudospin size (where they correspond to classical rotations). These operations are

$$\tilde{O}^{(\gamma)} = \prod_{r \in P_\gamma} e^{i\pi T_r \cdot e_\gamma}, \quad (87)$$

where  $P_\gamma$  is any plane orthogonal to the corresponding cubic  $e_\gamma$  axis. It is important to reiterate that these are not bona fide symmetries over the entire spectrum—these are not exact symmetries of the Hamiltonian. That is, these operations are symmetries when restricted to classical ground states and emerge in those combined limits, i.e., the classical limits of (i) high pseudospin and (ii) zero temperature.

It is well known that two-dimensional Ising symmetries can be broken at finite temperatures. Thus, the symmetries of Eq. (87) of the classical  $120^\circ$  model can be broken. And indeed they are, as discussed in Sec. VIII.B.1.

#### F. Emergent symmetries: Classical honeycomb $120^\circ$ compass model

We now review the ground states and associated low-energy emergent symmetries of the classical (or large-pseudospin limit of the)  $120^\circ$  model on the honeycomb lattice (Nasu *et al.*, 2008; Wu, 2008; Zhao and Liu, 2008). This model is given by Eq. (12). In what follows, we invoke a decomposition of the honeycomb lattice into two interpenetrating triangular sublattices, referred to as sublattices A and B. Two neighboring sites of the honeycomb lattices thus belong to different sublattices.

The  $120^\circ$  model on the honeycomb lattice shares a number of similarities with the  $120^\circ$  model on the cubic lattice discussed above and the key elements of the discussion are the same. Nevertheless, in some respects, this system is even richer, largely as a result of the larger number of emergent symmetries in the ground-state sector.

One may generally seek to find all of the ground states of this system using Eq. (86)—a condition for finding all ground states of the classical ferromagnetic compass model. It is instructive, within the framework of symmetries, to compare the consequences of this constraint as they apply to both the cubic lattice  $120^\circ$  model, whose symmetries we enumerated above, and the honeycomb lattice  $120^\circ$  model.

The coordination number of the honeycomb lattice ( $z = 3$ ) is far smaller than that of the cubic lattice ( $z = 6$ ). Thus, the

number of independent conditions of the type of Eq. (86) will be halved. As a result of this simple counting argument, we see that the ground-state manifold might be far richer. This indeed turns out to be the case and emergent local ( $d = 0$ ) symmetries appear.

We first review the ground states of this classical system and stratification procedures that are more similar in nature to those of the  $120^\circ$  model on the cubic lattice (i.e., involve the application of emergent intermediate and global symmetries on a uniform ground state) and then review additional local symmetry operations that appear in this case.

#### 1. Ground states and emergent intermediate symmetries

In the classical limit, the pseudospins in Eq. (12) become two-component ( $XY$ ) variables which may be parametrized by (with some abuse of notation) a continuous angular variable  $\theta_r$  at the different lattice sites  $r$ . Here  $\{\theta_r\}$  denote the orientation of the classical pseudovectors  $T_r$  [the large-pseudospin limit variant of  $\boldsymbol{\tau}_r$  in Eq. (12)].

As in the cubic lattice case reviewed in Sec. VI.E all uniform states ( $T_r = T$ ) are ground states and these may be stratified by the application of low-dimensional emergent symmetry operations. The  $d = 2$  emergent symmetries of Eq. (87) and Fig. 20 have their counterparts in  $d = 1$  symmetries in the  $120^\circ$  model on the honeycomb lattice (Nasu *et al.*, 2008). As shown in Fig. 21 it is possible, starting from a uniform state, to generate other ground states by varying  $\theta_r \rightarrow \theta_r + \delta\theta_r$ . In this case, by considering (the  $d = 1$ ) zigzag chains along one of the three crystalline directions (Nasu *et al.*, 2008), it is possible to generate other ground states by a reflection of all of the spins in these chains as in Fig. 21.

#### 2. Emergent local symmetries

Figure 22 shows particular ground states found by Wu (2008) wherein the pseudospins  $T_r$  are oriented in the plane, at angles of  $(\pm 30^\circ, \pm 90^\circ, \pm 150^\circ)$  such that they are tangential to the basic hexagonal plaquettes. In Fig. 22, the explicitly shown clockwise (or counterclockwise) chirality [correspondingly,  $C_h = 1$  (or  $C_h = -1$ )] for each hexagon  $h$  relates to the tangential direction of the pseudospins which can be flipped with no energy cost. As in our earlier considerations, chiral degrees of freedom adhere to emergent discrete Ising-like gauge symmetries (or  $d = 0$  symmetries in the classification of Sec. VI.A). These particular ground states lie within a larger

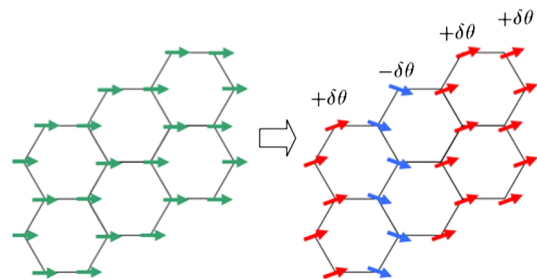


FIG. 21 (color online). Left: Pseudospin configuration for  $\theta^* = 0$ . Right: Configuration obtained by  $\pm\delta\theta$  rotations of pseudospins in each zigzag chain. From Nasu *et al.*, 2008.

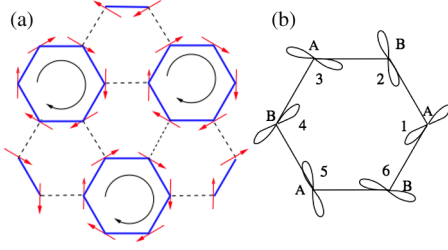


FIG. 22 (color online). The fully packed oriented loop configurations in which  $\tau$  vectors lie in directions of  $\phi = \pm 30^\circ, \pm 90^\circ$ , and  $\pm 150^\circ$ . (a) The closest-packed loop configuration with all the loops in the same chirality. (b) The  $p$ -orbital configuration for one closed loop in (a). The azimuthal angles of the  $p$  orbitals are  $45^\circ, 105^\circ, 165^\circ, 225^\circ, 285^\circ$ , and  $345^\circ$ . From Wu, 2008.

space of classical states that are generated from the chiral tangential patterns as shown in Fig. 22. Generally, a larger set of ground states is generated by an application of a continuous  $d = 2$  symmetry on the ground states of Fig. 22. This set of classical configurations may be obtained as follows: Starting with any tangential state of the pseudospins as in Fig. 22 about the various hexagons, one can apply a global staggered [U(1)] rotation of all of the pseudospins in the plane such that all of the spins that lie on sublattice A are rotated by an angle of  $\delta\theta$  whereas all of the spins lying on sublattice B are rotated by an angle of  $(-\delta\theta)$  (Wu, 2008).

### G. Emergent symmetries of the triangular $120^\circ$ compass model

In its ground-state sector, the classical  $120^\circ$  model of Eq. (14) exhibits ( $d = 1$ )-dimensional emergent symmetries. Similar to those discussed previously, those relate to reflections of the pseudospins ( $T_r^\gamma \rightarrow -T_r^\gamma$ ) for all sites  $r$  that lie along a plane  $P$  (a one-dimensional line in this case) that is parallel to the direction  $e_\gamma$ . This operation leads to stratified states once again. A schematic is shown in Fig. 23.

### H. Three-component Kugel-Khomskii model

In Secs. III.A and V.A.4, we discussed the KK model (Kugel and Khomskii, 1972, 1973, 1982). In particular, we reviewed the underlying physics of this Hamiltonian in

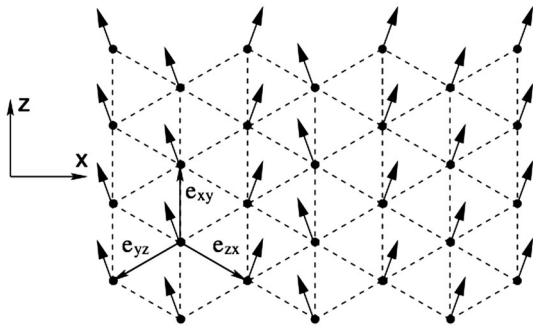


FIG. 23. The triangular lattice formed in the  $[111]$  plane. Shown is a disordered mean-field ground state, in which the isospins form lines parallel to the unit vector  $e_{xy}$ , such that  $\langle T_j^z \rangle$  is the same on all lattice sites, while the sign of  $\langle T_j^z \rangle$  varies arbitrarily from line to line. From Mostovoy and Khomskii, 2002.

Sec. V.A.4. Its most prominent version is that for two-component pseudospins, wherein the KK Hamiltonian describes the two  $e_g$  levels (represented by two-component pseudospins). We now return to the three-component variant of this model that is more pertinent to three- $t_{2g}$ -orbital states. We label these as follows (Khaliullin and Maekawa, 2000; Khaliullin, Horsch, and Oleś, 2001; Harris *et al.*, 2003):

$$|a\rangle \equiv |yz\rangle, \quad |b\rangle \equiv |xz\rangle, \quad |c\rangle \equiv |xy\rangle. \quad (88)$$

To make the discussion self-contained, we write anew the KK Hamiltonian in its general form and focus on its three-component pseudospin version. The KK Hamiltonian is given by

$$H = \sum_{\langle ij \rangle || \gamma} H_{\text{orb}}^{(\gamma)}(ij) \left( \mathbf{S}_i \cdot \mathbf{S}_j + \frac{1}{4} \right). \quad (89)$$

Physically,  $\mathbf{S}_i$  is the spin of the electron at site  $i$  and  $H_{\text{orb}}^{(\gamma)}(ij)$  are operators that act on the orbital degrees of freedom of sites  $i$  and  $j$ . For TM atoms arranged in a cubic lattice, wherein each TM atom is surrounded by an octahedral cage of oxygens, these operators are given by

$$H_{\text{orb}}^{(\gamma)}(ij) = J(4\hat{\pi}_i^\gamma \hat{\pi}_j^\gamma - 2\hat{\pi}_i^\gamma - 2\hat{\pi}_j^\gamma + 1), \quad (90)$$

where  $\hat{\pi}_i^\gamma$  are pseudospin components, and  $\gamma = a, b$ , and  $c$  is the direction of the bond  $\langle ij \rangle$ . In the three-component realization that we discuss now,

$$\hat{\pi}_i^\gamma = \frac{1}{2} \tau_i^\gamma. \quad (91)$$

The KK model in  $t_{2g}$  systems exhibits a continuous exact lower-dimensional symmetry as we now review. In the  $t_{2g}$  compounds, hopping is disallowed via intermediate oxygen  $p$  orbitals between any two electronic states of orbital flavor  $|\gamma\rangle$  ( $\gamma = a, b$ , or  $c$ ) along the  $\gamma$  axis of the cubic lattice (see Fig. 24). As a consequence, as noted by Harris *et al.* (2003), a uniform rotation of all spins, whose electronic orbital state is  $|\gamma\rangle$ , in any plane ( $P$ ) orthogonal to the  $\gamma$  axis  $c_{i\gamma\sigma}^\dagger = \sum_\eta U_{\sigma,\eta}^{(P)} d_{i\eta}^\dagger$  with  $\sigma, \eta$  the spin directions, leaves Eq. (89) invariant. The total spin of electrons of orbital flavor  $|\gamma\rangle$  in any plane orthogonal to the cubic  $\gamma$  axis is conserved. Here we have the  $d = 2$  SU(2) symmetries

$$\hat{O}_{P,\gamma} \equiv [\exp(i\mathbf{S}_P^\gamma \cdot \boldsymbol{\theta}_P^\gamma)/\hbar], \quad [H, \hat{O}_{P,\gamma}] = 0, \quad (92)$$

with  $\mathbf{S}_P^\gamma = \sum_{i \in P} \mathbf{S}_i^\gamma$  being the sum of all the spins  $\mathbf{S}_i^\gamma$  in the orbital state  $\gamma$  in any plane  $P$  orthogonal to the direction  $\gamma$  (see Fig. 24).

We now, once again, turn to the physical origin of dimensional reduction in this system with continuous  $d = 2$  SU(2) symmetries. The bound of Eq. (81) prohibits, at finite temperatures, local on-site order as provided by Eq. (92) for the KK model. Physically, this is due to the proliferation and deleterious effect of ( $d = 2$ )-dimensional defects (i.e., spin waves) in SU(2) continuous pseudospin systems. The energy or entropy balance associated with these defects in the

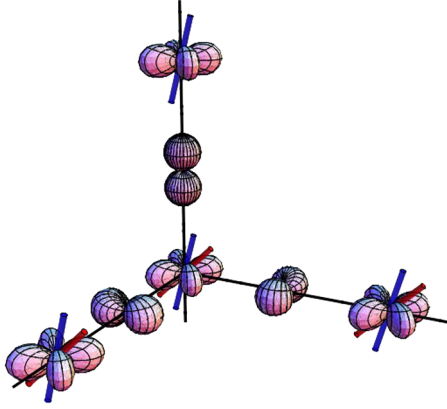


FIG. 24 (color online). The anisotropic hopping amplitudes leading to the KK Hamiltonian after Batista and Nussinov (2005). The spins are indicated by rods. Following Harris *et al.* (2003), the four-lobed states denote the  $3d$  orbitals of a TM ion while the intermediate small  $p$  orbitals are oxygen orbitals through which the superexchange process occurs. Because of orthogonality with intermediate oxygen  $p$  states, in any orbital state  $|\gamma\rangle$  (e.g.,  $|c\rangle \equiv |xy\rangle$  above), hopping is disallowed between sites separated along the cubic  $\gamma$  ( $c$  above) axis. The ensuing KK Hamiltonian has a  $d = 2$   $SU(2)$  symmetry that corresponds to a uniform rotation of all spins whose orbital state is  $|\gamma\rangle$  in any plane orthogonal to the cubic direction  $\gamma$ . Such a rotation in the  $xy$  plane is indicated by the spins in the figure.

three-dimensional KK system is identical to that in a two-dimensional three-component Heisenberg spin system.

## VII. INTERMEDIATE SYMMETRIES AND FLAT BANDS IN CLASSICAL SPIN-WAVE DISPERSION

In this section, we introduce a new result that is of utility in understanding a number of aspects of the order-by-disorder physics and the role of the large degeneracy of these systems. It pertains to a simple  $k$ -space classical spin-wave-type analysis and sheds light on the relation between spectral structure, degeneracy, and intermediate symmetries in general classical ferromagnetic compass systems in  $D$ -spatial dimensions. In a nutshell, one asks what the consequences are of the existence of real space stratified ground states found in Sec. VIII (schematically illustrated in Figs. 20–24) on the momentum space spectrum of pseudospin excitations.

Application of the low  $d$ -dimensional symmetries (either exact or emergent) that lead to stratified states in real space, on the canonical uniform ( $\mathbf{k} = \mathbf{0}$ ) ferromagnetic state, leads, in momentum space, to a redistribution of weights in  $(D - d)$ -dimensional regions. As all of these states share the same energy, one finds that the existence of  $d$ -dimensional symmetries ensures that there are  $(D - d)$ -dimensional volumes which are flat and share the same mode energy as the  $\mathbf{k} = \mathbf{0}$  point. Although  $d$ -dimensional symmetries imply flat bands in classical systems, the converse is not true—in classical systems with a finite number of pseudospin components, flat bands generally do not imply the existence of  $d$ -dimensional symmetries.

However, in the large- $n$  limit,  $(D - d)$ -dimensional flat bands indeed imply the existence of  $d$ -dimensional real space

symmetries. Large- $n$  analysis of these systems is identical to that of  $d$ -dimensional systems (i.e., in all directions orthogonal to the flat zero-energy regions in  $k$  space). That is, in the large- $n$  system, an effective dimensional reduction occurs (from  $D$  dimensions to  $d$  dimensions). Thus, for systems with, e.g.,  $d = 2$  symmetries (such as the cubic lattice  $120^\circ$  compass model), large- $n$  analysis and related approximate methods relying on simple classical  $k$ -space spin-wave analysis will, incorrectly, predict that the finite- $n$  classical system does not order and that quantum fluctuations are mandatory to explain the observed ordering in these systems. Similar considerations to all of these results concerning the interesting link between symmetries and band structure may apply, in general (i.e., not necessarily ferromagnetic) systems for both ground and excited states.

### A. Uniform states as ground states of classical compass models

In the absence of an external field, the classical ground states corresponding to the general isotropic compass model Hamiltonian of Eq. (4) are fairly trivial. In the anisotropic (nonuniform  $J_\gamma$ ), the pseudospins tend to align along the direction  $\gamma'$ , the direction associated with the highest exchange coupling  $J_{\gamma'}$ . We now first explicitly turn to the isotropic situation where  $J_\gamma = J > 0$  (Nussinov *et al.*, 2004; Biskup, Chayes, and Nussinov, 2005). As discussed in Sec. III.B, in their classical rendition, the pseudospins are normalized at all lattice sites  $T_r^2 = \mathbf{1}$ . In such a case, for the classical rendition of all of the systems that we focus on in this review, up to an irrelevant additive constant  $C$ , the Hamiltonian may be written as a sum of squares:

$$H_{\text{isotropic}}^{\text{compass}} = \frac{J}{2} \sum_i \left[ \sum_\gamma (T_r^\gamma - T_{r+\mathbf{e}_\gamma}^\gamma)^2 - 2C \right]. \quad (93)$$

A direct computation yields the value of  $C = \sum_\gamma (\mathbf{T}_r \cdot \mathbf{e}_\gamma)^2$ , which is independent of the orientation of  $\mathbf{T}_r$ . For all classical compass models on regular lattices with two-component (i.e.,  $XY$ )-type spins whose orientation may be specified by a single angle  $\theta_r$  on the unit disk, the constant  $C = z/2$  with  $z$  being the coordination number of the lattice (the number of nearest neighbors of any given site). Values of the constant  $C$  in Eq. (93) can be readily computed for compass models with a higher number of spin components. For the classical  $d$ -dimensional  $90^\circ$  compass model of Eq. (20), the additive constant  $C$  in Eq. (93) is given by  $C = 2$ . Similarly, for the classical counterpart of the Kitaev model of Eq. (7),  $C = 1$ .

As all terms in the sum of Eq. (93) are positive or zero, minima are achieved when  $\mathbf{T}_r = \mathbf{T}$  for all  $\mathbf{r}$  with  $\mathbf{T}$  an arbitrary orientation. Thus, any uniform state is a ground state and a continuous global rotation may relate one such ground state to another. These rotations are not bona fide symmetries of the Hamiltonian and may emerge as such only in the restricted ground-state subspace. Thus, the ferromagnetic compass models exhibit a continuous emergent symmetry of their ground states. Starting from any uniform state (a ground state of the classical system), any uniform global rotation of all pseudospins will lead to another ground state.

Although perhaps obvious, we remark on the relation between ferromagnetic and antiferromagnetic compass models. On bipartite lattices, the sign of the exchange couplings can be reversed ( $J_\gamma \rightarrow -J_\gamma$ ) for classical systems. The same trivially holds true for quantum  $XY$  spins (such as those in the  $120^\circ$  model) for which a canonical transformation (rotation by  $180^\circ$  about the  $z$  axis) can be performed.

## B. Stratification in classical compass models

The richness of the classical compass models stems from the many possible ground states that they may possess (aside from the uniform state). Such stratified ground states are depicted in Figs. 20–24. Equal-energy states (classical or quantum) are generally related to each other via the symmetries discussed in Sec. VI.B. Emergent (and exact) symmetries of the classical ferromagnetic compass models link the uniform ferromagnetic states discussed in Sec. VII.A to a plethora of other classical ground states. As elaborated on in Sec. VIII, this proliferation of low-energy states leads to high entropic contributions and the failure of the simplest analysis to predict finite-temperature order. We now explicitly determine all classical ground states of ferromagnetic compass models and link those to the earlier depicted ground states. As can be seen from Eq. (93), any configuration for which

$$T_i^\gamma = T_{i+e_\gamma}^\gamma \quad (94)$$

on all sites  $i$  is also a ground-state configuration. That is, in standard compass models, the projections of any two nearest-neighbor  $\mathbf{T}$  along the bond direction  $\gamma$  must be the same. [As noted several times earlier and made explicit in the original compass model definitions in Sec. III.B, the components in Eq. (94) are defined by  $T^\gamma \equiv \mathbf{T} \cdot \mathbf{e}_\gamma$ ; in this scalar product, the corresponding internal pseudospin unit vectors  $\mathbf{e}_\gamma$  are chosen differently for different compass systems.] In Kitaev's model, the direction specified by  $\gamma$  is dictated by the lattice link direction but it is not equal to it. At any rate, generally, the number of conditions that Eq. (94) leads to is equal to the number of links on the lattice ( $Nz/2$ ). Equation (94) states that only the  $\gamma$  component of the pseudospin  $\mathbf{T}$  is important as we examine the system along the  $\gamma$  lattice direction. It may therefore generally allow for numerous other configurations apart from the uniform ferromagnetic states in which one transforms the pseudospins in planes orthogonal to the  $\gamma$  direction in such a way as not to alter the projection  $T^\gamma$  of  $\mathbf{T}$  on the  $\gamma$  axis. This allows for the multitude of ground states discussed in Sec. VI.B that are related to the uniform ground states via an intermediate low-dimensional operation (generally an emergent symmetry of the ground-state sector).

## C. Flat bands: Momentum space consequences of real space stratified ground states

A new prevalent aspect that has apparently not been discussed before in the literature concerns a general relation between the classical ground states of the compass models and the classical spin-wave dispersions. This relation will be introduced shortly. Toward this end, it will be profitable to examine the matrix  $\hat{V}(\mathbf{k})$  of Eq. (34) in its internal pseudospin eigenbasis and write the classical compass Hamiltonians as

$$H = \frac{1}{2} \sum_\alpha \sum_{\mathbf{k}} v_\alpha(\mathbf{k}) |t_\alpha(\mathbf{k})|^2. \quad (95)$$

In Eq. (95), the internal pseudospin space index  $\alpha$  labels the eigenvalues  $v_\alpha(\mathbf{k})$  of the matrix  $\hat{V}(\mathbf{k})$  and  $t_\alpha(\mathbf{k})$  are the internal pseudospin components of the vectors  $\mathbf{T}(\mathbf{k})$  when expressed in this basis.

These emergent symmetries within the ground-state sector lead to an enormous degeneracy of the classical ground states. One can relate this to the eigenvalues of the matrix  $\hat{V}(\mathbf{k})$  of Eq. (34). Before doing so for the compass (and general systems), we reflect on the situation in canonical nearest-neighbor classical ferromagnets. In standard, isotropic, ferromagnetic systems,  $v_\alpha(\mathbf{k})$  attains its global minimum when  $\mathbf{k} = \mathbf{0}$ . Thus, in standard ferromagnets, only the uniform ( $\mathbf{k} = \mathbf{0}$ ) states are ground states. Any other nonuniform state necessarily has nonvanishing Fourier space amplitudes  $t_\alpha(\mathbf{k}) \neq 0$  also for modes  $\mathbf{k} \neq \mathbf{0}$  each of which costs some energy relative to the lowest-energy  $\mathbf{k} = \mathbf{0}$  state.

By contrast, the multitude of nonuniform ground states generated by the stratification operations of Fig. 20 proves that  $v_\alpha(\mathbf{k})$  no longer attains its minimum at a single point in  $\mathbf{k}$  space but rather at many such points. We observe that the application of the general stratification (or stacking) operations of Fig. 20 on the uniform  $\mathbf{k} = \mathbf{0}$  state (one for which the Fourier amplitudes  $T_{\mathbf{k} \neq \mathbf{0}} = 0$  lead to new configurations for which the Fourier amplitudes  $T_{\mathbf{k}} \neq 0$ , where  $\mathbf{k}$  lies along the  $k_z$  axis).

According to Eq. (95), this observation suggests that the lowest values of  $\min_\alpha \{v_\alpha(\mathbf{k})\}$  define lines along the  $k_x$ ,  $k_y$ , or  $k_z$  axes. This can indeed be verified by a direct computation. More generally, if one sets  $\min_{\alpha, \mathbf{k}} v_\alpha(\mathbf{k}) = 0$ , the ground-state energy happens to have a zero value according to Eq. (95). In general, of course, when one applies a general operation  $U$  to get a new ground state, with  $t_{\alpha'}(\mathbf{k}') \neq 0$  then, for all of these values of  $\alpha'$  and  $\mathbf{k}'$  with a nonzero Fourier amplitude  $t_{\alpha'}(\mathbf{k}')$ , one must have that  $v_{\alpha'}(\mathbf{k}') = 0$ . The fact that the uniform ground states at  $\mathbf{k} = \mathbf{0}$  are invariant under global rotation [i.e., a change of basis of the internal indices  $\alpha'$  for all components  $\alpha'$  for which  $t_{\alpha'}(\mathbf{k}' = \mathbf{0})$ ] shows that states having components  $\alpha'$  such that  $\min_\alpha \{v_\alpha(\mathbf{k} = \mathbf{0})\} = v_{\alpha'}(\mathbf{k} = \mathbf{0})$  can, indeed, be materialized. This follows as, whatever  $\alpha'$  happens to be, for  $\mathbf{k} = \mathbf{0}$ , the eigenvector  $\mathbf{t} = (0 \cdots 010 \cdots 0)^T$  corresponding to it will relate to some particular uniform real space vector  $\tilde{\mathbf{T}}$  in the original basis. On the other hand, any uniform state is a ground state and thus such a configuration with a vector  $\tilde{\mathbf{T}}$  can be materialized. That is, the lower bound on the energy stemming from the lowest-energy eigenvector(s) of  $\hat{V}$  of Eq. (34) can be saturated.

Thus, emergent symmetries mandate the appearance of lines of nodes in the dispersion. (The same, of course, also trivially holds for exact symmetries of the Hamiltonian.) The converse is, of course, not true: the existence of flat regions of the dispersion [those with  $v_{\alpha'}(\mathbf{k}') = 0$ ] does not mandate that symmetries appear in the ground-state sector as even for any linear combination involving only  $t_{\alpha'}(\mathbf{k}')$  it might not be possible to construct real space states out of these amplitudes for which  $T_i^2 = 1$  at all sites  $i$ . The discussion above relates the degeneracies brought about by (exact or emergent)

intermediate symmetries to the dispersion of  $v_\alpha(\mathbf{k})$  about its minimum. This general link between intermediate symmetries and (flat) spin-wave-type dispersion applies to many of the other compass models in this review.

If in a general compass model, a  $d$ -dimensional operation relates the different ground states [such as the  $d = 2$  reflections of Fig. 20 and Eq. (87)] then the lowest bands  $v_\alpha(\mathbf{k})$  are zero (or, more generally attain their lowest values) within  $d' = (D - d)$ -dimensional regions in  $k$  space. This follows from the application on a uniform ferromagnetic state of symmetry operators of the form of Eq. (78). Different symmetries [either emergent ( $\hat{O}_P$ ) or exact ( $\hat{O}_P$ )] can be chosen in the string product of Eq. (78) that when acting on the uniform ferromagnetic state lead to disparate configurations that must all share the same energy. Putting all of the pieces together establishes a new theorem:

When a system of the general form of Eq. (95) exhibits a ferromagnetic state then the existence of  $d$ -dimensional symmetries (exact or emergent) implies that  $v_\alpha(\mathbf{k})$  has a flat dispersion in a  $(D - d)$ -dimensional manifold that connects to the ferromagnetic point of  $\mathbf{k} = \mathbf{0}$ .

As explained above, for classical pseudospins  $\mathbf{T}_i$  with a finite number ( $n$ ) of components, that have to be normalized at each lattice site  $i$ , the converse is not guaranteed to be true: if one has flat lowest-energy bands then we are not guaranteed that we can generate real space configurations with normalized pseudospins  $\mathbf{T}_i$  whose sole Fourier amplitudes are associated with wave vectors  $\mathbf{k}$  that belong to these flat bands.

In the large- $n$  limit of the classical models (or, equivalently, in the corresponding spherical models) (Berlin and Kac, 1952; Stanley, 1968; Nussinov, 2001), the local normalization conditions become relaxed and linear superpositions of Fourier modes on the flat band lead to allowed states that share the same energy. That is, in the large- $n$  limit (and, generally, only in that limit), if there is a band  $v_\alpha(\mathbf{k})$  that assumes a constant value  $v_\alpha(\mathbf{k}) = \text{const}$  for wave vectors  $\mathbf{k}$  that belong to a manifold  $\mathcal{M}$  of dimension  $d' = D - d$ , then the system exhibits a  $d$ -dimensional symmetry: any transformation that acts as a unitary transformation on the modes  $\mathbf{k} \in \mathcal{M}$  will not alter the energy of states whose sole nonvanishing Fourier amplitudes  $t_\alpha(\mathbf{k})$  belong to this manifold. For related aspects, see Batista and Nussinov (2005) and Nussinov, Ortiz, and Cobanera (2012b). As the spectrum  $v_\alpha(\mathbf{k})$  is pinned at its minimum value along  $d' = (D - d)$ -dimensional regions in  $k$  space, large- $n$  computations will, up to constant factors associated with the volume of these regions, reproduce results associated with the nonvanishing dispersion in the remaining  $(D - d') = d$ -dimensional regions.

Thus, in the large- $n$  limit, the behavior of compass model ferromagnets in  $D$  spatial dimensions is identical to that of the ferromagnets in the large- $n$  limit in  $d$  dimensions. As the large- $n$  ferromagnet does not exhibit long-range order in  $d = 2$  dimensions (and indeed any pseudovector system with  $n \geq 2$  components), the large- $n$  analysis of the classical cubic lattice  $120^\circ$  model predicts that it does not order at finite temperatures—an erroneous conclusion. As it turns out, simple large- $n$  and other related approximations are not valid for the analysis of the classical  $120^\circ$  model and careful calculations are required for the free energy of the

( $n = 2$ )-component classical system (Nussinov *et al.*, 2004; Biskup, Chayes, and Nussinov, 2005). We return to this point in Sec. VIII.B.1.

In principle, the theorem can be replicated for any other commensurate real space ground-state structure for which the only nonvanishing Fourier components  $t_\alpha(\mathbf{k}) \neq 0$  are those that minimize the kernel  $v_\alpha(\mathbf{k})$  in Eq. (95). Above, we illustrated that the ferromagnetic compass model has, among many other states, the uniform ( $\mathbf{k} = \mathbf{0}$ ) state as a ground state. There are other commensurate structures (e.g., Néel states,  $2 \times 2$  checkerboard states, etc.) that correspond to a particular set of wave vectors (Nussinov, 2001). We proceed by discussing the particular realizations of this theorem in compass models.

### 1. Spin waves of cubic lattice $120^\circ$ compass model

In the case of the  $120^\circ$  model in  $D = 3$  dimensions, this codimension is  $d' = 1$  and the zeros of the modes lie along lines (which happen to be the Cartesian coordinate axes in momentum space). We briefly remark that when local symmetry operations are present (i.e., when  $d = 0$ ) as they are on some of the more frustrated compass models that we review later, there will be flat bands where the corresponding  $v_\alpha(\mathbf{k}) = 0$  for all  $\mathbf{k}$  in the full ( $d' = D$ )-dimensional  $k$  space for some value(s) of the (band) index  $d'$ .

Although it is, of course, of less physical significance, the analysis for the highest-energy state is essentially identical to that for the ground states. When the sign in Eq. (94) is flipped (as on bipartite lattices), the resulting staggered configuration is that of the highest energy possible. Replication of all of the arguments made above, *mutatis mutandis*, shows that if the operations  $U$  do not change the energy of these states then the manifold of highest-energy modes is of the dimensionality  $d'$  of Eq. (79).

### 2. Honeycomb lattice $120^\circ$ compass model

We now discuss the system of Eq. (12) on the honeycomb lattice. As noted from Eq. (95), the existence of emergent  $d$ -dimensional symmetries of ground states that include the ferromagnetic state mandates [Eq. (79)] that a  $d'$ -dimensional subvolume of  $k$  space corresponds to zero modes [ $v_\alpha(\mathbf{k}') = 0$  for one or more bands  $d'$ ].

Given the appearance of the discrete chiral  $d = 0$  symmetries above (Wu, 2008), one sees that  $d' = D$  and thus flat bands may exist corresponding to the highest and lowest possible energy states. Indeed, flat bands exist in the spin-wave dispersion about a state that has these symmetries (Wu, 2008). A more general diagonalization of the  $4 \times 4$  matrix  $\hat{V}(\vec{k})$  of Eq. (34) indeed illustrates that there are two flat bands with (in our convention) values of  $v_{1,2}(\mathbf{k}) = 0, 3J/2$  that correspond to the lowest and highest energies attainable. There are also two dispersing modes. This matrix is of dimension 4 as a result of two factors of 2 as we now explain. Translation invariance appears only for the honeycomb lattice when it is considered as a triangular lattice (belonging to either the A or B sublattices) with a basis of two sites leading to the first factor of 2. The second factor of 2 stems from the number of components of each of the classical pseudospins at each of these sites.

### VIII. ORDER BY DISORDER IN COMPASS MODELS

In Secs. VI and VII, we illustrated how classical (and also quantum) compass systems might exhibit numerous ground states. Aside from emergent global symmetries of the classical ferromagnetic compass model, both the classical and quantum models in  $D$  spatial dimensions exhibit a degeneracy which scales exponentially with  $L^{D-d}$ , where  $d$  is the dimension of the intermediate symmetries [see Eq. (80)]. As we now review, this large degeneracy is generally lifted by the fluctuations process colloquially referred to as order by disorder (Villain *et al.*, 1980; Shender, 1982; Henley, 1989; Moessner, 2001).

Although several states may appear to be equally valid candidate ground states, fluctuations can stabilize those states which have the largest number of low-energy fluctuations about them. These differences can be explicitly captured in values of the free energies for fluctuations about the contending states. Classically, fluctuations are driven by thermal effects and lead to entropic contributions to the free energy. Quantum tunneling processes may fortify such ordering tendencies [“quantum order by disorder” (Rastelli and Tassi, 1987; Henley, 1989; Chubukov, 1992)], especially at zero temperature, and stabilize a particular set of linear combinations of classically degenerate states.

We note that, albeit being very different, somewhat related physics concerning forces deriving from the weight of zero-point “fluctuations” appears in the well-known Casimir effect of quantum electrodynamics (Casimir, 1948; Casimir and Polder, 1948). In the classical arena, similar effects appear—seafarers have long known about the tendency of closely separated ships to pull inward toward each other as a result of hydrodynamic fluctuations. Other notions related to those in order-by-disorder physics concern entropy-driven effects which lead to particular conformations that appear in the funnel model for protein folding (Bryngelson *et al.*, 1995).

#### A. Classical and quantum order out of disorder

Colloquially, quantum and classical systems may be anticipated to exhibit the same qualitative order-out-of-disorder physics. Although this is often the case, there is no fundamental reason for this to be so (and, indeed, the two effects may lead to very different results in some instances). Different sets of states can be stabilized by these fluctuations. An understanding of the quintessential physics may be obtained by considering small (harmonic) fluctuations about classical ground states. To harmonic order, within the quantum arena, the fluctuations will be governed by a Bose distribution (with frequencies  $\omega_i$  that denote the energies of the various independent harmonic modes), whereas the classical fluctuations obey a Boltzmann distribution with the same set of harmonic modes. The two may be radically different at low temperatures especially insofar as they apply to zero-mode fluctuations about the ground states. This intuition is made more precise in Appendix C. The upshot is that in many situations quantum systems may order more readily than their classical counterparts. In the following we review the relevant order-out-of-disorder effects for specific compass models.

#### B. Cubic lattice 120° compass model

When entropic contributions are omitted, the spin-wave spectrum of the standard classical cubic lattice 120° compass model is gapless (van den Brink *et al.*, 1999). This suggests that, on the classical level, these orbital systems exhibit finite-temperature disorder. Indeed the commonly held lore for some time was that quantum fluctuations (tunneling between the different contending classical ground states) are mandatory in order to lift the orbital degeneracy and account for the experimentally detected orbital orders. Most of the work on quantum order out of disorder focused on  $1/S$  corrections (with  $S$  the spin size) to the classical spin-wave spectrum.

##### 1. Thermal fluctuations

The difficulties encountered in the simplest analysis of the classical model stem from the  $d = 2$  symmetries that it exhibits (see Sec. VI.B) as exemplified in Fig. 20. As discussed in Sec. VII, these symmetries lead to flat ( $d' = D - d$ )-dimensional regions in  $\mathbf{k}$  space along which the dispersion  $v_\alpha(\mathbf{k})$  attains its minimum. In the case of the cubic lattice 120° model, there are lines ( $d' = 1$ ) along the Cartesian axis along which the dispersion is nonincreasing. In simple Gaussian calculations (such as those for the large- $n$  or spherical models) (Biskup, Chayes, and Nussinov, 2005) this leads to canonical divergent fluctuations that inhibit low-temperature order. The divergences are identical to those associated with canonical  $D - d' = d$  ferromagnetic systems (or, in cubic lattice 120° compass systems, those associated with two-dimensional continuous spin ferromagnetic systems). In various guises, this dispersion led to early difficulties in the analysis of this system and to the inclusion of quantum or thermal effects to lift this degeneracy. To make this lucid, note that the structure factor  $S(\mathbf{k})$  within spin-wave theory [and classical large- $n$  analysis (Biskup, Chayes, and Nussinov, 2005)] behaves, at low temperatures, as

$$S(\mathbf{k}) \propto \frac{E_x + E_y + E_z}{E_x E_y + E_x E_z + E_y E_z}, \quad (96)$$

with the shorthand  $E_\gamma(\mathbf{k}) \equiv 2 - 2 \cos k_\gamma$ . As can be seen by inspection, the structure factor of Eq. (96) diverges along lines in  $\mathbf{k}$  space (corresponding to momenta along the lattice directions  $k_x$ ,  $k_y$ , or  $k_z$ ). As briefly alluded to in Sec. VIII.A (and elaborated on in Appendix C), as the simplest, large- $n$  spin-wave type is approached, this divergence of the classical system (as opposed to the convergence of the corresponding integral for its quantum large- $n$  counterpart as well as standard  $1/S$  calculations) leads to the false conclusion that there is no finite-temperature ordering in this system. This divergence is removed by the proper inclusion of fluctuations about the ground states of the ( $n = 2$ )-component classical pseudospin system—an item that we turn to next.

We now, in particular, briefly review finite-temperature effects on the classical 120° model of Eq. (85) (Nussinov *et al.*, 2004). The important thing to note is that the *free-energy minima* (not the energy minima) determine the low-energy states at finite temperatures. The classical spins  $\{S_r\}$  are parametrized by the angles  $\{\theta_r\}$  with the  $a$  axis. We may

consider the finite-temperature fluctuations about the uniform ground states where each  $\theta_r = \theta^*$ . At low temperatures, the deviations  $\vartheta_r = \theta_r - \theta^*$  are small, and the quadratic [spin-wave (SW) Hamiltonian corresponding to Eq. (85) becomes (Nussinov *et al.*, 2004; Biskup, Chayes, and Nussinov, 2005)

$$H_{\text{SW}} = \frac{1}{2} J \sum_{r,\gamma} q_\gamma(\theta^*) (\vartheta_r - \vartheta_{r+e_\gamma})^2, \quad (97)$$

where  $\gamma = a, b,$  and  $c$  while  $q_c(\theta^*) = \sin^2(\theta^*)$ ,  $q_a(\theta^*) = \sin^2(\theta^* + 2\pi/3)$ , and  $q_b(\theta^*) = \sin^2(\theta^* - 2\pi/3)$ . On a cubic lattice with periodic boundary conditions with  $\theta^*$  the average of  $\theta_r$  on the lattice, at an inverse temperature  $\beta = 1/k_B T$ , the partition function (Nussinov *et al.*, 2004; Biskup, Chayes, and Nussinov, 2005)

$$Z(\theta^*) = \int \delta\left(\sum_r \vartheta_r = 0\right) e^{-\beta H_{\text{SW}}} \prod_r \frac{d\vartheta_r}{\sqrt{2\pi}}. \quad (98)$$

A Gaussian integration leads to

$$\ln Z(\theta^*) = -\frac{1}{2} \sum_{\mathbf{k} \neq \mathbf{0}} \log \left\{ \sum_\gamma \beta J q_\gamma(\theta^*) E_\gamma(\mathbf{k}) \right\}, \quad (99)$$

where  $\mathbf{k} = (k_x, k_y, k_z)$  is a reciprocal lattice vector. The spin-wave free energy  $\mathcal{F}(\theta^*)$  of Eq. (99) has minima at

$$\theta_n^* = n\pi/3 \quad (100)$$

with integer  $n$  (Nussinov *et al.*, 2004; Biskup, Chayes, and Nussinov, 2005).

The application of the  $d = 2$  stratification operations of Eq. (87) on each of these uniform configurations (see Fig. 20) leads to an interface with an effective surface tension that leads to a free-energy penalty additive in the number of operations. The detailed derivation is provided by Nussinov *et al.* (2004) and Biskup, Chayes, and Nussinov (2005). Next we provide physical intuition concerning the preference for uniform angles of the form of Eq. (100) over all others [i.e., why the free energy  $\mathcal{F}(\theta^*)$  indeed has its minima at the points  $\theta_n^*$ ].

This analysis will build, once again, on the  $d$ -dimensional emergent (i.e., ground-state) symmetries of the problem. We first start with the system where, for all lattice sites  $\mathbf{r}$ , the angle  $\theta_r = \theta_n^*$  of Eq. (100) with a particular value of  $n$ . For concreteness, we set  $\theta_r = 0$  at all  $\mathbf{r}$ . We next ask what occurs when we twist the angle between sequential planes, i.e., apply the operation of Eq. (87) leading to a configuration such as

$$\theta_r = \delta\theta(-1)^{r_z} \quad (101)$$

(all other related configurations in which the angle is uniform within each plane are orthogonal to the  $z$  axis) with  $r_z$  the  $z$  coordinate of the lattice point  $\mathbf{r}$  and  $\delta\theta$  being arbitrary. In this situation, as emphasized earlier, the energy of Eq. (85) does not change. This is the origin of the large degeneracy that we have been alluding to all along. Next we consider the case when the system is uniformly oriented along an angle that differs from the angles of Eq. (100), i.e.,  $\theta_r = \theta^* \neq \theta_n^*$ . Now, if we perform a twist between any two consecutive planes,

e.g.,  $\theta^* + \delta\theta$  on one plane of fixed  $i_z$  and a uniform angle of  $\theta^* - \delta\theta$  on a neighboring plane separated by one lattice constant along the  $z$  axis, then a simple calculation shows that the energy of Eq. (85) will be elevated. This simple picture can be fleshed out in a full detailed calculation for the free energy of the system about a chosen set of angles (Nussinov *et al.*, 2004; Biskup, Chayes, and Nussinov, 2005). Thus, the stratification (or stacking) ground-state symmetry operation of Eq. (87) leads to the preference for the uniform states of Eq. (100) over all others when thermal fluctuations are included. Thus, while for all values of  $\theta^*$ , a uniform spatial twist will lead to no energy cost, a staggered twist in which consecutive planes are rotated by  $\pm\delta\theta$  costs no energy only for the uniform states of Eq. (100).

Along similar lines of reasoning, if we consider the staggered state in which consecutive planes transverse to the  $z$  axis have the angles of Eq. (101) then an additional staggered twist ( $\pm\delta\varphi$ ) of the opposite parity, i.e., one for which  $\theta_{r_z} = \delta\theta(-1)^{r_z} + \delta\varphi(-1)^{r_z+1}$ , elevates the energy for general small  $\delta\theta$  and  $\delta\varphi$  (while, of course, the energy of a uniform state of, e.g.,  $\delta\theta = 0$ , will not). This is, once again, the origin of the lower free energy for a uniform state than for a stratified one—there are more low-energy fluctuations about the uniform states of Eq. (100) than in their stratified counterparts, with this increase being proportional to the number of stratified interfaces for which a twist was applied.

By “blocking” the lattice (i.e., partitioning the lattice into finite size blocks) and employing reflection positivity bounds (Nussinov *et al.*, 2004; Biskup, Chayes, and Nussinov, 2005), it can indeed be proven that the results of the spin-wave analysis are correct: the free energy has strict minima for six uniform orientations (Nussinov *et al.*, 2004; Biskup, Chayes, and Nussinov, 2005):  $\mathbf{T}_r = \pm S e_a$ ,  $\mathbf{T}_r = \pm S e_b$ , and  $\mathbf{T}_r = \pm S e_c$ . Thus, out of the large number of classical ground states, only six are chosen. Orbital order already appears within the classical ( $S \rightarrow \infty$ ) limit (Nussinov *et al.*, 2004; Biskup, Chayes, and Nussinov, 2005) and is not exclusively reliant on subtle quantum zero-point fluctuations [captured by  $1/S$  calculations (Kubo, 2002; Tanaka, Matsumoto, and Ishihara, 2005)] for its stabilization. Indeed, orbital order is detected up to relatively high temperatures [ $\mathcal{O}(100 \text{ K})$ ] (Murakami *et al.*, 1998; Tokura and Nagaosa, 2000). Numerical work (Dorier, Becca, and Mila, 2005) and an analysis with tilted boundary conditions (Nussinov and Shtengel, 2015) shows that quantum fluctuations do not lift the orbital degeneracy in the simplest  $S = 1/2$  systems—the planar orbital compass model of Eq. (1). A 2D pseudospin  $T = 1/2$  analog of the cubic lattice  $120^\circ$  compass model of Eq. (9), a model of far lower symmetry (and less frustration) than the square lattice  $90^\circ$  compass model, has been shown to have an  $S = 0$  order (Biskup, Chayes, and Nussinov, 2005).

## 2. Quantum order out of disorder

In certain geometrically frustrated systems, one encounters quantum order-from-disorder phenomena, that is, quantum fluctuations lifting the degeneracy of the ground states obtained within a mean-field approach. Examples are the Heisenberg antiferromagnet on the triangular and pyrochlore lattices (Chubokov and Golosov, 1991; Tsunetsugu, 2001).

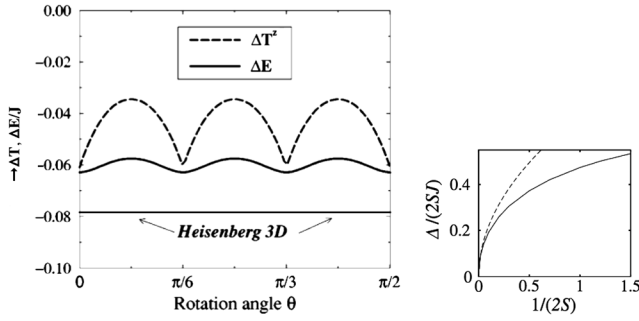


FIG. 25. Left: Quantum corrections for the cubic lattice  $120^\circ$  model system as functions of rotation angle  $\theta$  for the renormalized order parameter  $\Delta T^z$  (full lines) and the ground-state energy  $\Delta E/J$  (dashed lines). From [van den Brink \*et al.\*, 1999](#). Right: The gap  $\Delta$  as a function of  $1/(2S)$  (solid curve) and the square root behavior at small  $1/(2S)$  given by  $\Delta^2/(2SJ)^2 = 0.49/(2S)$ , for pseudospin  $S$  (dashed curve). From [Kubo, 2002](#).

The  $120^\circ$  quantum compass model also exhibits this phenomenon, where quantum fluctuations not only select the ordered state, but also stabilize the selected state against thermal fluctuations which would destroy the ordering at finite temperatures.

If the ground state of the  $120^\circ$  quantum compass model is considered to be ordered, the evaluation of the quantum corrections to the ground-state energy reveals pronounced minima for specific  $\theta^*$ , as illustrated in Fig. 25. The quantum corrections to the energy in a  $1/T$  expansion with  $T$  the pseudospin size (also denoted as  $1/S$  expansion in order to make a clear connection with the equivalent-approach spin models) and the finite order parameter is consistent with the presumed presence of order ([van den Brink \*et al.\*, 1999](#); [Kubo, 2002](#)).

Thus global rotation of the pseudospins does not affect the energy of the classical ground state, which is therefore rotationally invariant, but quantum corrections to the ground-state energy restore the discrete symmetry of the Hamiltonian. When the quantum fluctuations are evaluated to lowest order the excitation spectra are found to be gapless and purely 2D, but higher-order corrections cause the opening of an excitation gap of around  $0.49J$  ([Kubo, 2002](#)), which agrees with the results of quantum Monte Carlo simulations on this model and its extensions ([van Rynbach, Todo, and Trebst, 2010](#)). These are reviewed in Sec. IX.D.2.

### C. $90^\circ$ compass models

We now focus on the planar and three-dimensional realizations of the  $90^\circ$  models in both the classical and quantum cases.

#### 1. Quantum planar $90^\circ$ compass models

We first examine the quantum  $90^\circ$  planar compass model. By the theorem reviewed in Sec. VI.C.2 and, in particular, corollary I therein, at all positive temperatures, the average local “magnetization”  $\langle \tau_r \rangle = 0$ . In the quantum arena, this is so as the system admits the inversion symmetries of Eqs. (84) and (91), and thus, as reviewed in Sec. VI.D.1 and displayed

in Fig. 19, insofar as the breaking of the Ising symmetries of Eqs. (84) and (91) is concerned, the system behaves as though it were one dimensional. As these Ising symmetries cannot be broken in ( $d = 1$ )-dimensional symmetry, the finite-temperature average  $\langle \tau_r \rangle = 0$ . By contrast, any product involving an even number of  $\tau^x$  operators along any horizontal line and an even number of  $\tau^z$  operators along any vertical line is invariant under these  $d = 1$  symmetries and may be used as an order parameter ([Batista and Nussinov, 2005](#); [Nussinov and Fradkin, 2005](#)). In particular, of greatest interest is an order parameter that is invariant under all  $d = 1$  symmetries and may probe a global ( $d = 2$ )-dimensional Ising (reflection) symmetry that may be broken at finite temperature in isotropic compass models ([Nussinov and Ortiz, 2009a](#)). Such a reflection symmetry [as further elaborated in Eq. (105)] interchanges the spin components  $\tau^x \leftrightarrow \tau^z$ . Bilinears such as  $\langle \tau_r^x \tau_{r+e_x}^x - \tau_r^z \tau_{r+e_z}^z \rangle$  are invariant under all of the  $d = 1$  symmetries and can thus attain nonzero values at finite positive temperatures ([Batista and Nussinov, 2005](#); [Nussinov and Fradkin, 2005](#)) when the reflection symmetry is broken. Nematic-type order parameters that probe this Ising symmetry may be constructed as linear combinations of these bilinears. In a general anisotropic compass model [such as that of Eq. (4) without an applied field], which we rewrite here (yet again) for clarity,

$$\mathcal{H}_{\text{compass}} = - \sum_{r,\gamma} J_\gamma \tau_r^\gamma \tau_{r+e_\gamma}^\gamma, \quad (102)$$

the difference between the energy associated with bonds along the two lattice directions,

$$\langle J_x \tau_r^x \tau_{r+e_x}^x - J_y \tau_r^y \tau_{r+e_y}^y \rangle, \quad (103)$$

may be used as an order parameter ([Wenzel and Janke, 2008](#)). In dimensions  $D > 2$ , there are no  $d = 1$  symmetries of the quantum model [the symmetries of Eqs. (84) and (91) are generally  $d = D - 1$  dimensional]. As Ising symmetries can be broken in more than one dimension, the local  $\langle \tau_r \rangle$  may be finite at low temperatures.

#### 2. Classical $90^\circ$ compass models

In the classical version of the  $90^\circ$  compass model in arbitrary spatial dimension, the considerations are identical. We elaborate on these next. As alluded to earlier (Sec. III.B), in considering the classical compass models, the Pauli operators  $\tau$  are replaced by a normalized classical  $XY$  pseudospin  $T$  subject to Eq. (19), and the model becomes once again of the form of Eq. (93). In the planar system, the lattice directions  $e_\gamma = e_1, e_2$ . Along any line  $\ell$  parallel to the lattice  $e_\gamma$  direction, the classical planar system is trivially invariant under the global reflection (an identical Ising symmetry to that in the quantum case) about the  $T_\gamma$  axis:  $T_i^{\gamma \neq \gamma} \rightarrow -T_i^\gamma, T_i^\gamma \rightarrow T_i^\gamma$  for all sites  $i$  that lie along such a line  $\ell$ . As such Ising symmetries cannot be broken in one dimension (for either the quantum or classical system), they also cannot be broken, at finite temperatures, in the planar compass model, and the local magnetization  $\langle T_i \rangle = 0$ . As for the quantum models, it is possible to construct nematic-type two-site bilinears like that of Eq. (103) ([Wenzel and Janke,](#)

2008). It is, in fact, also possible to construct single-site quantities which are identical to those of the standard order parameters for classical nematic liquid crystals (Nussinov and Fradkin, 2005) which would be most appropriate for isotropic planar compass models (with  $J_\gamma = J$  for all  $\gamma$ ). In the planar case, a simple generalization of Eq. (103) is given by  $Q = \langle J_x(T_i^x)^2 - J_y(T_i^y)^2 \rangle$ . It is noteworthy that a quantity such as  $Q$  is meaningful for all pseudospin representations of the planar compass model with a pseudospin of size  $S > 1/2$ . In the pseudospin-1/2 case,  $Q$  is trivially zero.

#### D. 120° honeycomb model

We now discuss the system of Eq. (12) on the honeycomb lattice.

##### 1. Thermal fluctuations

An order-by-disorder analysis for the classical version of the Hamiltonian of Eq. (12) proceeds (Nasu *et al.*, 2008; Wu, 2008) along similar lines as for the cubic lattice 120° model above (Nussinov *et al.*, 2004; Biskup, Chayes, and Nussinov, 2005). By considering thermal fluctuations about a uniform state, it is seen that orientations with the values of Eq. (100) are preferred (Nasu *et al.*, 2008). The underlying physics for the preference of these states (and the larger multitude of low-energy states made possible by stacking operations) is similar to our discussion for the cubic lattice (Nasu *et al.*, 2008).

Work to date has not investigated thermal fluctuations about a nonuniform state that resides in the sector of ground states that, as reviewed previously, are related to each other by a local chiral emergent symmetry operation.

##### 2. Quantum fluctuations

The effect of quantum fluctuations (as seen in 1/ $S$  calculations) has been investigated (Nasu *et al.*, 2008; Wu, 2008; Zhao and Liu, 2008). The analysis is similar to that in the case of the 120° model on the cubic lattice. All investigations concluded that, as for the thermal fluctuation analysis on this system (Nasu *et al.*, 2008) and for the 120° system on the cubic lattice, the preferred ground states are those of Eq. (100).

A detailed calculation for the free energy due to thermal fluctuations (as well as the physical considerations underlying the order-by-disorder mechanism favored the application of these symmetry operations in the ground-state sector) similar to that for the cubic lattice 120° model discussed shows that the low-energy states are, once again, one of the six uniform states of Eq. (100).

Wu (2008) further considered fluctuations about the non-uniform chiral state with emergent chiral gauge symmetries and found that these had a lower free energy than those resulting from fluctuations about the uniform states. The low free energy of these states is in accord with the multitude of low-energy fluctuations about them (Wu, 2008). Wu (2008) and Zhao and Liu (2008) both similarly also investigated the triangular and kagome lattice versions of this system. Earlier work (Mostovoy and Khomskii, 2002) introduced and examined the triangular ferromagnetic 120° model of Eq. (14) to

find that quantum fluctuations lift the degeneracy to favor the six uniform pseudospin states.

#### E. Effect of dilution

We conclude this section with a brief summary of some of the recent results on diluted (or “doped”) orbital compasslike systems (Tanaka, Matsumoto, and Ishihara, 2005; Ishihara, Tanaka, and Matsumoto, 2007; Tanaka and Ishihara, 2007, 2009). It was found that the critical doping fraction ( $x = 1/2$ ) necessary to remove order is smaller than the requisite doping needed to eradicate order in typical diluted magnets (e.g.,  $\text{KCu}_{1-x}\text{Zn}_x\text{F}_3$ ) (Breed *et al.*, 1970; Stinchcombe, 1983); in typical magnetic systems, the decrease in the ordering temperature and its saturation are governed by the percolation threshold (where the ordering temperature vanishes at the critical dopant concentration of  $x_c = 0.69$  for the simple cubic lattice). The faster degradation of orbital order with doping compared to simple percolation physics can be attributed to the directional character of the orbital exchange interactions. Similar effects have been found in related systems, as, e.g., by Honecker *et al.* (2007).

The concept of an orbital-order-driven quantum critical point was introduced (Nussinov and Ortiz, 2008) by an exact solution of diluted 2D and 3D orbital compass models. The solution relies on an exact gauge-type symmetry which results from dilution and the use of a bond algebra mapping (Nussinov and Ortiz, 2008, 2009b; Cobanera, Ortiz, and Nussinov, 2010, 2011; Nussinov, Ortiz, and Cobanera, 2012b; Ortiz, Cobanera, and Nussinov, 2012) wherein the system is mapped onto decoupled one-dimensional transverse-field Ising chains (Nussinov and Ortiz, 2008) that exhibit quantum criticality at their isotropic point. The symmetries associated with the dilution increase the degeneracy of the system. Like charge- and spin-driven quantum critical fluctuations, orbital fluctuations may also drive the system to quantum criticality. The system may be driven to criticality by a combination of doping and uniaxial pressure or strain (Nussinov and Ortiz, 2008). More recently, Chen, Balents, and Schnyder (2009) considered such a quantum critical point for spin-orbital singlets. An overdamped collective mode leading to non-Fermi-liquid-type response functions may emerge in systems that exhibit orbital-ordering-driven quantum critical points (Lo, Lee, and Phillips, 2013). It can be shown that spin-glass-type behavior can arise in doped orbital systems with random exchange constants. Here the orbitals take on the role of spins in the usual spin-glass systems.

In Sec. VIII, we illustrated how low-temperature orders in compass systems may be triggered by thermal and/or quantum fluctuations. We now remark on the opposite limit—that of high temperatures. As illustrated by Chakrabarty and Nussinov (2011) and Nussinov, Ortiz, and Cobanera (2012b) the high-temperature limit of compass (and other) systems as evinced by general correlation functions and thermodynamics coincides with that of the large- $n$  (or spherical model) solution. In the large- $n$  limit, all thermodynamic quantities are directly given by integrals of simple functions involving eigenvalues of the kernel  $\hat{V}(\mathbf{k})$  of Eq. (34). A brief review of some aspects of this limit is provided in

Appendix C. Flat bands, such as those discussed in Sec. VII, in which these eigenvalues  $v_\alpha(\mathbf{k})$  depend on a reduced number of Cartesian components of  $\mathbf{k}$ , lead, in the large- $n$  or high-temperature limit, to exact dimensional reductions to a system whose dimensionality is given by the number of components of  $\mathbf{k}$  on which  $v_\alpha(\mathbf{k})$  depends. Bolstered by their unique high-temperature limit in which compass models may effectively exhibit a reduced dimensionality, all large- $n$  renditions of the compass models that we considered are disordered. In Sec. IX, we discuss the precise character of the transitions in a multitude of compass models between their low- and high-temperature phases.

### F. High-temperature correlations and dimensional reduction

In the previous section, it was illustrated how low-temperature orders in compass systems may be triggered by thermal and/or quantum fluctuations. We now remark on the opposite limit—that of high temperatures. As illustrated by Chakrabarty and Nussinov (2011) and Nussinov, Ortiz, and Cobanera (2012b) the high-temperature limit of compass (and other) systems as evinced by general correlation functions and thermodynamics coincides with that of the large- $n$  (or spherical model) solution. In the large- $n$  limit, all thermodynamic quantities are directly given by integrals of simple functions involving eigenvalues of the kernel  $\hat{V}(\mathbf{k})$  of Eq. (34). A brief review of some aspects of this limit is provided in Appendix C. Flat bands, such as those discussed in Sec. VII, in which these eigenvalues  $v_\alpha(\mathbf{k})$  depend on a reduced number of Cartesian components of  $\mathbf{k}$ , lead, in the large- $n$  or high-temperature limit, to exact dimensional reductions to a system whose dimensionality is given by the number of components of  $\mathbf{k}$  on which  $v_\alpha(\mathbf{k})$  depends. Bolstered by their unique high-temperature limit in which compass models may effectively exhibit a reduced dimensionality, all large- $n$  renditions of the compass models that we considered are disordered. In Sec. IX, we discuss the precise character of the transitions in a multitude of compass models between their low- and high-temperature phases.

## IX. PHASES AND PHASE TRANSITIONS IN COMPASS MODELS

Finite (or zero) -temperature transitions correspond to singularities in the free energy (or energy). When possible, transitions are most easily ascertained when an order parameter is found whose value differs from zero in a symmetry-broken phase. This is not the case for gauge theories that exhibit finite-temperature transitions but do not have a simple corresponding order parameter (Kogut, 1979; Bricmont and Frolich, 1983; Fredenhagen and Marcu, 1986) as they display local ( $d = 0$ ) symmetries which according to our earlier discussion cannot, by Elitzur’s theorem, be broken at any finite temperatures (Elitzur, 1975) due to an effective dimensional reduction (Batista and Nussinov, 2005; Nussinov, Ortiz, and Cobanera, 2012b). Via this extension of Elitzur’s theorem concerning generalized dimensional reduction, topological order (see Sec. VI.A) can be established in numerous systems including, in particular, numerous compass models (Nussinov and Ortiz, 2009a, 2009c).

In systems with topological orders (see Sec. VI.A), analogs (Gregor *et al.*, 2011; Cobanera, Ortiz, and Nussinov, 2013) of the quantities discerning phases in gauge theories (Kogut, 1979; Bricmont and Frolich, 1983; Fredenhagen and Marcu, 1986) may be considered. As reviewed in Secs. VI and VIII, at low temperatures, most compass models exhibit broken-symmetry states in which discrete symmetries of the compass Hamiltonians are broken. While there are notable exceptions the majority of the compass models exhibit low-temperature broken symmetries. While symmetry arguments are powerful, and while, as discussed in Sec. VIII, it may be possible to rigorously prove the existence of a phase transition, it is of great interest to get more insight into the qualitative and quantitative character of the transitions that these systems display by performing direct numerical and analytical analysis of various sorts. Both numerically and analytically, this task is daunting as these systems are highly frustrated. Moreover, numerically, many variants of the compass models currently suffer from the “minus sign” problem.

Many results have been attained, in particular, for the simpler compass models. However, results for many more, including models pertinent to orbital ordering, are currently unknown. Here we review the results known to date on nearly all compass models. We reserve the Kitaev and the related Kitaev-Heisenberg models to another review and start with a summary of results on the classical models and then turn our attention to the quantum systems.

### A. 90° compass models

#### 1. Classical square lattice

For convenience, we provide again the Hamiltonian classical planar 90° model, defined on a square lattice:

$$H_{\square}^{\text{classical } 90^\circ} = -J_x \sum_{\langle ij \rangle_H} T_i^x T_j^x - J_y \sum_{\langle ij \rangle_V} T_i^y T_j^y, \quad (104)$$

with  $\langle ij \rangle_H$  and  $\langle ij \rangle_V$  denoting nearest-neighbor links along the horizontal and vertical directions, respectively. The general dimensional extension of this system was given in Eq. (20). Equation (104) is simply the classical counterpart of the quantum model of Eq. (1).

In the 90° compass model, unlike the 120° compass model, attention is required to examine contending order parameters. The sole symmetry of high dimension which can be broken in the 90° compass model on the square lattice is an Ising-type reflection symmetry of the symmetric compass model [with equal exchange constants along the  $x$  and  $y$  directions  $J_x = J_y (= J)$ ] that involves a global [( $d = 2$ )-dimensional] reflection of all pseudospins in the plane. Formally, such a symmetry is given by

$$O_{\text{reflection}} = \prod_{\mathbf{r}} e^{i\pi(\sqrt{2}/4)(\sigma_r^x + \sigma_r^y)}, \quad (105)$$

where  $\mathbf{r}$  denotes the lattice sites. This global Ising reflection symmetry is related to a duality ( $J_x \leftrightarrow J_y$ ) between the couplings. Along the self-dual line,  $J_x = J_y$ , the duality between the  $x$  and  $y$  bonds becomes a symmetry [as in general self-dual systems (Cobanera, Ortiz, and Nussinov,

2010, 2011]). As a ( $d = 2$ )-dimensional Ising-type symmetry can be broken at finite temperature, this reflection symmetry can (and indeed is) broken at finite temperatures. However, the order parameter cannot be of the usual single-site type. By the symmetry arguments that we outlined in Sec. VI, it is clear that while spontaneous symmetry breaking of the pseudospin on a single site ( $i$ ) is prohibited ( $\langle \mathbf{T}_r \rangle = 0$ ) in the planar  $90^\circ$  compass model, any quantity that is invariant under all ( $d = 1$ )-dimensional symmetries might serve as an order parameter. This implies that one should consider quantities involving more than one on-site operator.

Indeed,  $d = 1$  symmetry-invariant, low-temperature nematic-type order is stabilized in this system by thermal fluctuations (Nussinov *et al.*, 2004); the physical considerations are similar to those presented earlier for the  $120^\circ$  compass model in Sec. VIII.B.1. An elegant study of the classical two-dimensional  $90^\circ$  compass model was pursued by Mishra *et al.* (2004). As in the entropic stabilization in the  $120^\circ$  model, (Nussinov *et al.*, 2004; Biskup, Chayes, and Nussinov, 2005) a (pseudo-)spin-wave-type dispersion about the state with a particular uniform orientation  $\theta^*$  of all of the classical pseudospins  $\mathbf{T}_r$  may be computed. For the  $90^\circ$  square lattice compass model of Eq. (104), the dispersion about  $\theta^* = 0$  is given by  $m + \gamma_x(1 - \cos k_x) + \gamma_y(1 - \cos k_y)$ , with  $m$  and  $\gamma_{x,y}$  denoting a self-consistent (pseudo)spin gap and moduli along the  $x$  and  $y$  axes, respectively. At low temperatures, these scale as (Mishra *et al.*, 2004)  $\gamma_x = 0, \gamma_y = 1 - \mathcal{O}(T^{2/3})$ , and  $m(T) = (1/2)T^{2/3} + \mathcal{O}(T)$ . To emulate the ordering transition in a qualitative way, Mishra *et al.* (2004) studied the “four-state Potts compass model” given by

$$H = -J \sum_{\mathbf{r}} (n_{r\mu} n_{r+\mathbf{e}_x, \mu} \mu_r \mu_{r+\mathbf{e}_x} + n_{r\nu} n_{r+\mathbf{e}_y, \nu} \nu_r \nu_{r+\mathbf{e}_y}),$$

where at each lattice site  $\mathbf{r}$  there are occupation numbers  $n_{r\nu} = 0, 1$  and  $n_{r\mu} = 0, 1$  for which  $n_{r\mu} + n_{r\nu} = 1$  and  $\mu, \nu$  are classical Ising variables ( $\mu = \pm 1, \nu = \pm 1$ ). This Hamiltonian captures the quintessential directionality of the bonds in the compass model. By tracing over the Ising variables  $\mu$  and  $\nu$  at all sites, this four-state Potts compass can be mapped onto the two-dimensional Ising model, from which it can be deduced that the Potts compass model has a critical temperature of (Mishra *et al.*, 2004)  $T_c = 0.4048J$ .

Ordering at lower temperatures corresponds to a dominance of horizontal bonds over vertical ones or vice versa. That is, for temperatures below the critical temperature (Mishra *et al.*, 2004)  $\langle n_{r,\mu} \rangle - \langle n_{r,\nu} \rangle \neq 0$ . In effect, this reflects an order of the nematic type present in the classical  $90^\circ$  compass at low temperatures in which the fourfold rotational symmetry of the square lattice is lifted. A natural nematic-type order is given by (Mishra *et al.*, 2004)

$$q = \langle (T_r^x)^2 - (T_r^y)^2 \rangle. \quad (106)$$

Using Monte Carlo calculations, it was found (Mishra *et al.*, 2004) that this quantity  $q$  becomes nonzero for temperatures lower than an estimated transition temperature of  $T_c = (0.147 \pm 0.001)J$ . Impressive calculations further improved this estimate (Wenzel and Janke, 2008; Wenzel,

Janke, and Läuchli, 2010) to a value for the classical  $90^\circ$  compass model of  $T_c = 0.14612J$ .

In the  $90^\circ$  compass models (whether classical or quantum), related nematic-type order is also characterized by the energy difference between the vertical and horizontal bonds,

$$\langle Q_i \rangle \equiv \langle T_{r_i}^x T_{r_i+\mathbf{e}_x}^x - T_{r_i}^y T_{r_i+\mathbf{e}_y}^y \rangle, \quad (107)$$

where lattice site  $\mathbf{r}$  is indexed by the label  $i$ . The virtue of this form by comparison to that of Eq. (106) is that it can be extended to quantum pseudospins  $T = 1/2$ . Near a general critical point (including the one at hand for the  $90^\circ$  compass model in the vicinity of its critical temperature), the connected correlation function canonically behaves as

$$\langle Q_i Q_j \rangle - \langle Q_i \rangle \langle Q_j \rangle \approx A \frac{e^{-r_{ij}/\xi}}{|r_{ij}|^p}, \quad (108)$$

with  $Q_i$  the corresponding local order parameter which attains a nonzero average value ( $\langle Q_i \rangle$ ) in the ordered phase. In Eq. (108),  $r_{ij}$  is the distance between sites  $i$  and  $j$ , and  $\xi$  is the correlation length,  $A$  is an amplitude, and  $p$  is a power. Typically, a susceptibility  $\chi = \langle Q^2 \rangle - \langle Q \rangle^2$  (with  $Q = \sum_{i=1}^N Q_i/N$ ) diverges at the critical point. The classical  $90^\circ$  compass model was indeed found to fit this form with  $Q_i$  chosen to be the local nematic-type order parameter of Eq. (107). As discussed in Sec. VI, any generally nonzero quantity [as such, involving any number of bonds (Nussinov and Ortiz, 2009b; Cobanera, Ortiz, and Nussinov, 2010)] that is invariant under all low-dimensional gaugelike symmetries can serve as an order parameter. That is, general composites of such bonds can serve as order parameters (Batista and Nussinov, 2005). A similar interesting measure was introduced by Brzezicki and Oleś (2010) for the quantum  $90^\circ$  compass model.

Although order sets in at a temperature far lower than that of the two-dimensional Ising model and its equivalent four-state Potts clock model the transition was numerically found to be in the two-dimensional Ising universality class (Mishra *et al.*, 2004; Wenzel and Janke, 2008; Wenzel, Janke, and Läuchli, 2010). The standard critical exponents that describe the divergence of the correlation length ( $\nu$ ) and susceptibility ( $\gamma$ ) as the temperature approaches the critical temperature  $T_c$ ,

$$\xi \sim |T - T_c|^{-\nu}, \quad \chi \sim |T - T_c|^{-\gamma}. \quad (109)$$

The two-dimensional Ising model and all systems that belong to its universality class are given by  $\nu_{2D\text{Ising}} = 1$  and  $\gamma_{2D\text{Ising}} = 1.75$ . These two exponents were numerically measured by Wenzel, Janke, and Läuchli (2010). From any two exponents, the values of all other exponents follow by scaling relations (in this case the values of all other critical exponents are identical to those of the two-dimensional Ising model). Earlier work (Mishra *et al.*, 2004) found Binder cumulants similar to those in the two-dimensional Ising model as a specific heat collapse which is also similar to that of the two-dimensional Ising model. This two-dimensional Ising-type transition is consistent with the transition in the Potts clock model on the square lattice.

A technical issue that reflects the unusual nature of the system (its high degree of symmetry and proliferation of degenerate and nearly degenerate states) is that finite-size effects are of far greater dominance here than in the usual systems (Wenzel and Janke, 2008; Wenzel, Janke, and Läuchli, 2010). The most successful boundary conditions found to date for numerical study of these systems are the so-called “screw periodic boundary conditions” (Wenzel, Janke, and Läuchli, 2010) in which there is periodicity along a line that wraps around the system with a general non-zero pitch.

## 2. Quantum square lattice 90° compass model

The pseudospin  $T = 1/2$  planar 90° compass model of Eq. (1) was investigated by multiple groups using a variety of tools. The results to date belong to two interrelated subclasses: (i) the character of the finite-temperature transition between a low-temperature ordered state and the disordered high-temperature phase in the symmetric [ $J_x = J_y (= J)$ ] 90° compass model for which the global  $d = 2$  Ising-type reflection symmetry can be broken and (ii) studies of the zero-temperature transition in the extended anisotropic 90° compass model of Eq. (4) in the absence of an external field ( $h = 0$ ) at the point  $J_x = J_y$ . As in the classical system, in the anisotropic 90° quantum compass model,  $J_x \neq J_y$ , the global reflection symmetry is not present. The sole symmetries that remain in the anisotropic model relate to the  $d = 1$  Ising-type symmetries of Eq. (84).

### a. Finite-temperature transitions

A few direct studies have been carried out (Wenzel and Janke, 2008; Wenzel, Janke, and Läuchli, 2010) on the finite-temperature breaking of the ( $d = 2$  Ising-type) reflection symmetries in the symmetric ( $J_x = J_y$ ) 90° compass model. The calculations of Wenzel and Janke (2008) and Wenzel, Janke, and Läuchli (2010) employed an order parameter akin to Eq. (107) and its related susceptibility to find that the two-dimensional quantum pseudospin  $T = 1/2$ , 90° compass system also belongs to the universality class of the classical two-dimensional Ising model. While the exponents characterizing the transition are identical to those in the classical two-dimensional Ising model and thus also those of the classical two-dimensional 90° compass model, the critical temperature is significantly reduced once again. The reduction in the critical temperature is, however, far more severe in the quantum case than in the classical rendition of the 90° compass model. Specifically, within numerical accuracy, Wenzel, Janke, and Läuchli (2010) found the transition temperature for the quantum 90° compass model to be  $T_c = 0.0585J$ .

Different numerical fitting schemes [e.g., allowing the critical (correlation length) exponent  $\nu$  to differ from its value of  $\nu = 1$  and using it as an adjustable parameter] lead to only an incremental shift in the value of the ascertained critical temperature (i.e., a shift only in the last decimal place). The factor of approximately 0.4 between the quantum pseudospin  $T = 1/2$  compass model critical-temperature value and the classical value shows that, at least, in these simple compass models, quantum fluctuations inhibit order rather than fortify

it, contrary to what was thought some time ago to be universally true for compass models (and certain other highly frustrated spin systems).

A slightly less accurate (by comparison to the numerical values above) yet quite insightful and intensive high-temperature series expansion (Oitmaa and Hamer, 2011) to order  $\beta^{24}$  in the inverse temperature  $\beta = 1/k_B T$  led to a similar value for the critical temperature ( $T_c = 0.0625J$ ). This was achieved by determining when the inverse susceptibility  $\chi^{-1}$ , evaluated with Padé approximants, extrapolated to zero. By fitting the determined susceptibility from the high-temperature series expansion with the standard form of Eq. (109) while setting  $T_c$  to the numerical value, the critical exponent  $\gamma$  was found to be 1.3 (of the same order as the value in the two-dimensional Ising value of  $\gamma = 1.75$  yet still slightly removed from it) (Oitmaa and Hamer, 2011). More recent numerical work observed that in finite-size systems the specific heat typically exhibits peaks at two different temperatures (Brzezicki and Oleś, 2013).

### b. Zero-temperature transitions

Before focusing on transitions between ground states, we regress to a very simple discussion concerning the unimportance of the sign of the couplings  $J_x$  and  $J_y$  within the quantum (and classical) 90° model on the square lattice. This is so, as in other two-component pseudospin systems, it is possible to invert the sign of the individual couplings  $J_x$  or  $J_y$  [or both simultaneously as in Eq. (13)] by simple canonical transformations. In order to set  $J_x \rightarrow -J_x$  we may rotate all of the pseudospins that lie on odd-numbered columns (wherein  $r_x$ , the  $x$  component of site  $\mathbf{r}$ , is an odd integer) by 180° about the  $\tau^y$  axis. The simple transformation

$$U = \prod_{r_x=\text{odd}} \exp(i\pi\tau_r^y/2) \quad (110)$$

implements this transformation. One may, of course, similarly rotate by 180° all pseudospins on odd-numbered rows (odd  $i_y$ ) to effect the transformation  $J_y$  to  $-J_y$ . The combined effect of both transformations is encapsulated in the sublattice rotation of Eq. (13) as a result of which all of the exchange couplings have their signs flipped. Below we will at times refer to the system for positive  $J_x$  and  $J_y$  and sometimes for general real  $J_x$  and  $J_y$ . Using the above transformations, the results for positive  $J_x$  and  $J_y$  imply identical conclusions for all  $J_x$  and  $J_y$  when their modulus ( $|J_{x,y}|$ ) is considered.

The very existence of a finite-temperature two-dimensional Ising-type critical point within the symmetric 90° planar compass model ( $J_x = J_y$ )—in both the classical (proven by entropy stabilization with detailed numerical results and further analysis) and quantum (thus far supported by numerical results alone) renditions—allows, but does not prove, that, for temperatures  $T < T_c$  there may be a line of first-order transitions along the temperature axis when  $J_x = J_y$ . Across this line the system may switch from preferring ordering along the  $x$  direction (when  $|J_x| > |J_y|$ ) to ordering of the pseudospin parallel to the  $y$  direction (when  $|J_x| < |J_y|$ ). The situation is reminiscent of, among other systems, the ferromagnetic two-dimensional Ising model in a magnetic field  $h$ ,

$$H = -J \sum_{\langle ij \rangle} \sigma_i \sigma_j - h \sum_i \sigma_i. \quad (111)$$

At  $T = T_c$ , the system is critical with the two-dimensional Ising model critical exponents for small  $|T - T_c|$  for  $h = 0$ . For all temperatures  $T < T_c$ , there is a line of first-order transitions along the temperature axis when  $h = 0$ , where the system switches from preferably order with positive magnetization  $\langle \sigma_i \rangle > 0$  (when  $h > 0$ ) to negative magnetization  $\langle \sigma_i \rangle < 0$  (when  $h < 0$ ). Across the  $h = 0$  line for  $T < T_c$ , there is a discontinuous jump in the value of  $\langle \sigma_i \rangle$  between its values at  $h = 0^+$  and  $h = 0^-$  marking the first-order transition.

Similarly, establishing the existence of a first-order phase transition in the  $T = 0$  system as a function of  $|J_x| - |J_y|$  when  $|J_x| = |J_y|$  would suggest (but not prove) the existence of a finite-temperature critical point  $T_c > 0$  at which the line of phase transitions terminates and above which ( $T > T_c$ ) the system exhibits no order of any kind. At arbitrarily high temperatures  $T \gg J_x, J_y$  the system is, of course, disordered.

A natural question then concerns the direction of investigation of the  $T = 0$  transition at  $J_x = J_y$ . We note that one approach for analyzing the character of the transition at the point  $J_x = J_y$  in the quantum system would be to analyze the  $(2 + 1)$ -dimensional corresponding classical Ising model of Eq. (38). A first-order transition would suggest the possibility of a finite-temperature critical point  $T_c > 0$  as seen by numerical studies.

Many other approaches to investigate the zero-temperature transition have been put forth. The upshot of these studies is that the zero-temperature transition at both  $J_x = J_y$  is indeed first order. As in the classical system,  $J_x \leftrightarrow J_y$  is a self-dual transformation of the quantum system (Nussinov and Fradkin, 2005; Nussinov, Batista, and Fradkin, 2006; Cobanera, Ortiz, and Nussinov, 2010, 2011) and the transition in question pertains to the system at its self-dual point.

Like any other zero-temperature transition, the zero-temperature transition at  $J_x = J_y$  in the  $90^\circ$  compass model corresponds to a ‘‘level crossing’’ at which the low-energy state(s) change from being of one type for  $J_x > J_y$  to another type for  $J_x < J_y$ . At the point  $J_x = J_y$ , their energy levels cross. In order to understand the level crossing, one needs to understand the structure of the low-energy levels in general.

In Sec. VI.B, we reviewed the noncommutativity of the symmetries of Eq. (84) as applied to the two-dimensional  $90^\circ$  model (where the planes  $P_\gamma$  are one-dimensional lines orthogonal to the  $\gamma$  axis) on all lattices as well as time-reversal symmetry as applied to odd-sized lattices, which both imply (at least) twofold degeneracy of the ground-state sector. [As it turns out, the two considerations are not independent. Time-reversal symmetry can be directly expressed in terms of the symmetries of Eq. (84) (Nussinov and Ortiz, 2009c).] This implied twofold degeneracy appears also in the anisotropic case of  $J_x \neq J_y$ . The ground states can be characterized in terms of the set of eigenvalues  $\{\lambda_1, \lambda_2, \dots, \lambda_L\}$  of, say, the  $L$  symmetries of Eq. (84) corresponding to vertical planes  $P$  (Dorier, Becca, and Mila, 2005; Doucot *et al.*, 2005). All of these symmetries commute with one another [while, as highlighted below, anticommute with all of the symmetries

of Eq. (84) corresponding to horizontal planes  $P$ ]. The application of any horizontal plane symmetry will generate another ground state with all of the eigenvalues flipped,  $\lambda_i \rightarrow -\lambda_i$ .

The large number of symmetries [( $2L$ ) for an  $L \times L$  lattice] of the form of Eq. (84) allows for [and, in fact, mandates (Nussinov and Shtengel, 2015)] a degeneracy which is exponential in the perimeter. Crisp numerical results illustrate (Dorier, Becca, and Mila, 2005; Brzezicki and Oleś, 2013) that in the square lattice  $90^\circ$  compass model each level is (asymptotically)  $2^L$ -fold degenerate for  $J_x \neq J_y$  and is  $2^{L+1}$ -fold degenerate when  $J_x = J_y$ . This degeneracy appears in the thermodynamic limit  $L \rightarrow \infty$ . For finite  $L$ , these states split to form a narrow band. There is a gap of size  $\mathcal{O}(e^{-L/L_0})$ , with a fixed length scale  $L_0$ , that separates the ground states from the next excited state (Dorier, Becca, and Mila, 2005; Doucot *et al.*, 2005). In the thermodynamic limit, these sets of  $2^L$  degenerate states further merge at the point  $J_x = J_y$  to form bands of  $2^{L+1}$  degenerate states. Numerical and other analyses illustrate that the level crossing at  $J_x = J_y$  is related to a first-order (or discontinuous) transition of the lowest-energy state as a function of  $(J_x - J_y)$  (Dorier, Becca, and Mila, 2005; Chen *et al.*, 2007; Orús, Doherty, and Vidal, 2009). The two sets of states for positive and negative values  $(J_x - J_y)$  are related to one another by the global Ising-type reflection symmetry of the  $90^\circ$  compass model which exchanges  $J_x \leftrightarrow J_y$ . Particular forms for this global symmetry were written down by Nussinov and Fradkin (2005), Nussinov and Ortiz (2009a), and Orús, Doherty, and Vidal (2009). In essence, these correspond to rotations in the internal pseudospin space about the  $T^z$  axis by an angle of  $90^\circ$  or by  $180^\circ$  about the  $45^\circ$  line in the  $(T^x, T^y)$  plane, compounded by an overall external reflection of the lattice sites about the  $45^\circ$  line on the square lattice or a rotation by  $90^\circ$  about the lattice  $z$  axis that is orthogonal to the square lattice plane. The first-order transition at  $J_x = J_y$  found by various groups represents the crossing of two bands that are related by this global symmetry. Similarly, although by the considerations outlined in earlier sections,  $\langle T_r^{x,y} \rangle = 0$  at any positive temperature, within the ground state,  $T_r$  can attain a nonzero expectation value. It is seen that the ‘‘magnetization components’’  $\langle T^{x,y} \rangle$  exhibit a discontinuous jump at the point  $J_x = J_y$  (Dorier, Becca, and Mila, 2005; Orús, Doherty, and Vidal, 2009). [For  $J_x > J_y$ , the expectation value  $\langle T^x \rangle$  is strictly positive; this expectation value jumps discontinuously to zero when  $J_x = J_y$  (and remains zero for all  $J_x < J_y$ ). Similar results are found when exchanging  $J_x \leftrightarrow J_y$  and  $\langle T^x \rangle \leftrightarrow \langle T^y \rangle$ .] The free energy is similarly found to exhibit a discontinuity in the first derivative relative to  $J_x - J_y$  at the point  $J_x = J_y$  (Orús, Doherty, and Vidal, 2009).

It is also interesting to note that when  $J_x > J_y > 0$ , the ground states  $|\psi\rangle$  were found to be an eigenstate of the  $T^x$  related symmetry operators of Eq. (84) with an eigenvalue of  $+1$ . That is, for the pseudospin  $T = 1/2$  analyzed (Orús, Doherty, and Vidal, 2009),

$$\prod_{r_y, \text{fixed } r_x} \tau_r^x |\psi\rangle = +|\psi\rangle. \quad (112)$$

Similarly, for  $J_y > J_x$  the same occurs with  $x$  and  $y$  interchanged,

$$\prod_{r_x, \text{fixed } r_y} \tau_r^y |\psi\rangle = +|\psi\rangle. \quad (113)$$

A symmetry analysis starting from the decoupled-chain limit is provided by [Dorier, Becca, and Mila \(2005\)](#) and [Doucou et al. \(2005\)](#).

An analytic mean-field-type approximation was invoked ([Chen et al., 2007](#)) to study the fermionic representation of the  $90^\circ$  compass model. In general, fermionization cannot be done in a useful way in dimensions larger than 1. That is, on a general lattice a fermionization procedure (known as the Jordan-Wigner transformation) where pseudospins (or spins) are replaced by spinless fermions, gives rise, in spatial dimensions larger than 1, to a system with arbitrarily long-range interactions. In the case of the  $90^\circ$  compass model, however, the special form of the interactions and consequent symmetries of Eq. (84) enable a reduction to a fermionic system in two dimensions with local terms. The resulting fermionic Hamiltonian ([Chen et al., 2007](#)) contains both hopping and pairing terms along single (e.g., horizontal) chains. The chains interact with one another along a transverse direction (e.g., vertical) via a nearest-neighbor-type density-density attractions ( $J_y > 0$ ) or repulsion ( $J_y < 0$ ). The fermionic Hamiltonian reads

$$H = -\sum_r \left[ J_y n_r n_{r+e_y} - J_y n_r + \frac{J_x}{4} (c_r - c_r^\dagger)(c_{r+e_x} + c_{r+e_x}^\dagger) \right]. \quad (114)$$

The fermionic Hamiltonian of Eq. (114) was analyzed by a self-consistent mean-field-type analysis and the analysis was extended to perturbations beyond mean field ([Chen et al., 2007](#)). This work suggests that a first order is indeed present at  $J_x = J_y$ . The self-consistent mean-field-type calculation suggests that the average values of  $\langle T^{x,z} \rangle$  exhibit a discontinuous jump. This analytical result is in accord with the numerical approaches of [Dorier, Becca, and Mila \(2005\)](#) and [Orús, Doherty, and Vidal \(2009\)](#). We pause to reiterate that while fermionization giving rise to local interactions is generally impossible in canonical systems, in compass-type systems fermionization is possible. A similar occurrence is encountered in Kitaev's honeycomb model where in fact the fermionization enables us to solve the problem exactly in different topological charge sectors. The possibility of fermionization in these systems is rooted in the simple bond algebra which the interactions along different bonds satisfy, giving rise to further symmetries (giving rise to local conserved topological charges in Kitaev's model) ([Nussinov and Ortiz, 2009b](#); [Cobanera, Ortiz, and Nussinov, 2010](#), [2011](#)).

The quantum  $90^\circ$  compass models that we have thus far focused on were of pseudospin  $T = 1/2$ . For integer pseudospin  $T = 1, 2, \dots$ , all of the symmetries of Eq. (84) commute with one another. Unlike the case of all half-odd-integer pseudospins where the anticommutator  $\{\exp(i\pi T_x), \exp(i\pi T_y)\} = 0$  for integer  $T$ , and the commutator  $[\exp(i\pi T_x), \exp(i\pi T_y)] = 0$ . Thus, for integer pseudospin  $T$ , the two types

of symmetry operators of Eq. (84) with the two different possible orientations for the planes (in this case lines)  $P_y$  corresponding to vertical columns and horizontal rows commute with one another. As noted by [Dorier, Becca, and Mila \(2005\)](#), in this case the pseudospin  $T = 1/2$  argument concerning a minimal twofold degeneracy as a result of the incompatibility of the symmetry operators of Eq. (84) no longer holds and a nondegenerate ground state can arise. Indeed, numerical calculations on small finite-size systems ([Dorier, Becca, and Mila, 2005](#)) found the ground state to be nondegenerate. In a similar fashion, time reversal no longer implies a twofold degeneracy for integer pseudospin  $T$  as it does for all half-odd-integer pseudospin values ([Nussinov and Ortiz, 2009a, 2009c](#)). As in the considerations discussed in Sec. VI.C, the  $d = 1$  symmetries of this system imply a degeneracy, for tilted boundary conditions, which is exponential in the system perimeter ([Nussinov and Shtengel, 2015](#)). Such boundary conditions may emulate the square lattice in the thermodynamic limit.

We close this section by remarking that a solution of a one-dimensional (1D) variant of the quantum planar  $90^\circ$  compass model ([Brzezicki, Dziarmaga, and Oleś, 2007](#)) further illustrates how the energy spectrum collapses at the *quantum phase transition* between two possible kinds of order, with either  $\sigma^z$ -like or  $\sigma^x$ -like short-range correlations, and is thus highly degenerate, similarly to the 2D case where the degeneracy scales exponentially in the perimeter size [i.e., as  $\mathcal{O}(2^L)$ ].

### 3. The classical $90^\circ$ model on a cubic lattice

For the classical three-dimensional  $90^\circ$  compass model, the existence of  $d = 1$  symmetry-invariant nematic order can be established, via entropic stabilization calculations along the same lines as for the classical  $120^\circ$  model ([Nussinov et al., 2004](#)). Clear signatures of nematic order were seen in Monte Carlo simulations ([Wenzel and Läuchli, 2011b](#)). A particular three-dimensional extension of Eq. (107) was considered by Wenzel and Läuchli,

$$Q_{\text{WL}} = \frac{1}{N} \left\langle \left( \sum_i T_r^x T_{r+e_x}^x - T_r^y T_{r+e_y}^y \right)^2 + \left( \sum_r (T_r^y T_{r+e_y}^y - T_r^z T_{r+e_z}^z) \right)^2 + \left( \sum_i (T_r^x T_{r+e_x}^x - T_r^z T_{r+e_z}^z) \right)^2 \right\rangle, \quad (115)$$

with (as throughout)  $N$  denoting the total number of sites in the lattice. A discontinuous transition appeared at an ordering transition temperature  $T_o \approx 0.098J$ . That is, the nematic-type order parameter of Eq. (115) was finite just below  $T_o$  and exhibits a discontinuous jump at  $T_o$ . As noted by [Wenzel and Läuchli \(2011b\)](#), when present, the detection of a first-order transition via the vanishing of  $\chi^{-1}$ , as we review next for the quantum model, may lead to null results.

### 4. The quantum $90^\circ$ model on a cubic lattice

Using the same high-temperature-series methods ([Oitmaa and Hamer, 2011](#)) discussed in Sec. IX.A.2.a, [Oitmaa and](#)

Hamer (2011) further examined the pseudospin  $T = 1/2$  three-dimensional  $90^\circ$  compass model. The susceptibility, evaluated with the free energy associated with the inclusion of an external field coupled to a standard three-dimensional version of the nematic order parameter of Eq. (107),

$$Q_3 = \langle 2\tau_r^x \tau_{r+e_x}^x - \tau_r^y \tau_{r+e_y}^y - \tau_r^z \tau_{r+e_z}^z \rangle, \quad (116)$$

did not, to order  $\mathcal{O}(\beta^{20})$  with  $\beta$  the inverse temperature, indicate the existence of a real zero of  $\chi^{-1}$ . This suggested that no finite critical transition temperature exists. The absence of divergence of  $\chi$  does not rule out the existence of a first-order transition similar to that found in the classical model (Wenzel and Läuchli, 2011b).

### B. Classical $120^\circ$ model

Transitions in the  $120^\circ$  compass model on the cubic lattice were numerically examined by various groups. In the most recent study to date, Wenzel and Läuchli (2011a, 2011b) examined the standard  $XY$ -type order parameter

$$m = N^{-1} \sqrt{\left( \sum_{i=1}^N T_i^x \right)^2 + \left( \sum_{i=1}^N T_i^y \right)^2}, \quad (117)$$

and the susceptibility  $\chi = N(\langle m^2 \rangle - \langle m \rangle^2)$  as a function of temperature. In accordance with earlier estimates (Tanaka, Matsumoto, and Ishihara, 2005; van Rynbach, Todo, and Trebst, 2010), the transition temperature between the ordered and disordered states was determined to be (Wenzel and Läuchli, 2011b)

$$T_{c;120^\circ \text{classical}} \approx 0.6775J. \quad (118)$$

This value is, essentially, the same as that reported earlier by van Rynbach, Todo, and Trebst (2010). As the classical  $120^\circ$  model concerns  $XY$ -type pseudospins in  $D = 3$  dimensions, a natural expectation may be that the transition may be in the same universality class as 3D  $XY$  systems but this turned out not to be the case. In fact, the collection of exponents found seems to suggest that the  $120^\circ$  compass model lies in a new universality class. These results beg further analysis. Specifically, by examining the scaling of  $m$  and  $\chi$  with system size, Wenzel and Läuchli (2011a, 2011b) found that the critical exponents associated with the transition at the critical temperature of Eq. (118) are

$$\nu_{120^\circ} = 0.668(6), \quad \eta_{120^\circ} = 0.15. \quad (119)$$

The ‘‘anomalous’’ exponent  $\eta$  governs the algebraic decay of the correlation function at the critical point. That is, the two-point correlation function at the critical point scales as

$$\langle \mathbf{T}_i \cdot \mathbf{T}_j \rangle \sim \frac{1}{|\mathbf{r}_{ij}|^{D-2+\eta}}, \quad (120)$$

with, as in earlier expressions,  $|\mathbf{r}_{ij}|$  denoting the distance between sites  $i$  and  $j$ , and  $D$  being the spatial dimensionality of the lattice. To make a connection with the canonical form of

the correlation function of Eq. (108), which is valid for general parameters, at the critical point  $\xi$  diverges and an algebraic decay of correlations remains. For the bare fields  $T_i$ , at the critical temperature, the form of Eq. (120) appears. These reported exponents do not fall into any of the typical universality classes. In particular, although  $\nu$  of Eq. (119) is not very different from its value in a 3D  $XY$ -type system (where  $\nu_{3DXY} = 0.671$ ), the value of the anomalous exponent is significantly larger ( $\nu_{120^\circ} \gg \nu_{3DXY} \approx 0.038$ ) (Wenzel and Läuchli, 2011a, 2011b). Combined with the hyperscaling relations, these critical exponents are consistent with the seen small specific heat exponent  $\alpha$  ( $C_v \sim |T - T_c|^{-\alpha}$ ) seen in numerical results (Wenzel and Läuchli, 2011a, 2011b).

A similar large discrepancy between the exponents of the  $120^\circ$  model and those of known universality classes appears in the value of an exponent  $a_6$  that will be introduced next for a related discrete version of the  $120^\circ$  model.

### C. Discrete classical $120^\circ$ compass model

A clock model version of the  $120^\circ$  compass model was further introduced and studied by Wenzel and Läuchli (2011a, 2011b). In this variant, the classical Hamiltonian of Eq. (85) is used wherein the classical pseudovectors  $T_i$  at any site  $i$  can point only along six equally spaced discrete directions on the unit disk. These directions correspond to the angles of Eq. (100) along which the system may be oriented at low temperatures (Nussinov *et al.*, 2004; Biskup, Chayes, and Nussinov, 2005). One of the virtues of this system is that it is easier to simulate and enables numerical investigations of larger size systems.

The quantity  $Q_{\text{WL}}$  of Eq. (115) as well as the magnetization  $m$  of Eq. (117) attain nonzero values below a critical temperature  $T_{c;\text{discrete } 120^\circ} \approx 0.67505J$ . This value is numerically close to, yet slightly larger than, the transition for the continuous classical  $120^\circ$  model [Eq. (118)]. As noted by Wenzel and Läuchli (2011a, 2011b), if this deviation in the values of the critical temperature between the discrete version and the original continuous  $120^\circ$  model is indeed precise, it may well be that the entropic stabilization of the  $120^\circ$  model driven by continuous pseudospin fluctuations (Nussinov *et al.*, 2004; Biskup, Chayes, and Nussinov, 2005) can be somewhat larger than in its discrete counterpart where fluctuations are more inhibited.

The critical exponents, as attained numerically, for the discrete  $120^\circ$  compass model are almost identical to those of the continuous  $120^\circ$  model [given by Eq. (119)]. An analysis similar to that of (Lou, Sandvik, and Balents, 2007), for  $T < T_c$ , examined the distribution of the orientations, as seen in the average  $\mathbf{m} = N^{-1} \sum_i \mathbf{m}_i$  for individual systems of sufficiently small size ( $L < \Lambda_6$ ). Similarly to the results of Lou, Sandvik, and Balents (2007), it was found that when examined over an ensemble of such systems the probability  $P(\mathbf{m})$  of attaining a particular  $\mathbf{m}$  was invariant under continuous [i.e.,  $U(1)$ ] rotations. Conversely, for larger systems, this continuous rotational symmetry was lifted. That is, for systems of size  $L > \Lambda_6$ , the probability distribution  $P(\mathbf{m})$  exhibited only the discrete global sixfold global symmetry of the system, with clear peaks along the six angles along which each individual  $T_i$  may point. The system-size length scale  $\Lambda$

for the onset of this change scales with the correlation length  $\xi$  as  $\Lambda_6 \sim \xi^{a_6}$ . This exponent was found to be  $a_{6;\text{discrete } 120^\circ} \approx 1.3$  which is far removed from the corresponding value [ $a_{6;\text{six state clock}} = 2.2$  (Lou, Sandvik, and Balents, 2007)] for XY models perturbed by a term of the type  $-h\sum_i \cos 6\theta_i$ . [Such an external field term renders XY systems to be of the discrete (clock) type.] The lack of breaking of continuous rotational symmetry as evinced in the distribution  $P(\mathbf{m})$  for sufficiently small systems thus allows a new exponent which, like the standard critical anomalous exponent  $\eta$  of Eq. (119), differs from that in known examples thus far.

#### D. Extended 120° model

An extended 120° model on the cubic lattice was recently studied (van Rynbach, Todo, and Trebst, 2010). The model is defined by the Hamiltonian

$$\begin{aligned} H_{120}^{\text{extended}} = & - \sum_{r,\alpha=x,y} \frac{1}{4} [J_z T_r^z T_{r+e_\alpha}^z + 3J_x T_r^x T_{r+e_\alpha}^x] \\ & \pm \sqrt{3} J_{\text{mix}} (T_r^z T_{r+e_\alpha}^x + T_r^x T_{r+e_\alpha}^z) \\ & - J_z \sum_r T_r^z T_{r+e_z}^z. \end{aligned} \quad (121)$$

This model was studied in both its classical and quantum incarnations. The symmetric point  $J_x = J_z = J_{\text{mix}} (= J)$  corresponds to the 120° model of Eq. (9). Next we survey these results.

#### 1. Classical extended 120° model

A free-energy analysis similar to that in Sec. VIII.B.1 found that the six uniform states discussed earlier, at angles  $\theta^* = 0, 60^\circ, 120^\circ, 180^\circ, 240^\circ,$  and  $320^\circ$  relative to the  $T^x$  axis, are the entropically stabilized low-energy states for the extended 120° model over a region of parameter space where  $0.8 \leq J_{\text{mix}}/J_z < 1$ . This region, however, lies at the interface between two other phases (van Rynbach, Todo, and Trebst, 2010). For  $J_{\text{mix}} > J_z$ , low-temperature states are energetically selected (and not entropically selected as discussed earlier for the 120° model) to be states in which there is a preferred angle that alternates in a staggered fashion. Pseudospins in a single  $x$ - $z$  or  $y$ - $z$  plane may have a value of  $\theta^*$  while those on the next parallel plane may assume a value of  $\theta^* + 180^\circ$ , and so on. This value of  $\theta^*$  varies continuously from  $30^\circ$  for  $J_{\text{mix}}/J_z \rightarrow 1^+$  to a value of  $\theta^* = 45^\circ$  for asymptotically large  $J_{\text{mix}}/J_z$ . The transition from the regime with  $J_{\text{mix}}/J_z \leq 1$  (where order is stabilized by entropy) to that where  $J_{\text{mix}}/J_z > 1$  (where order is energetically stabilized) is the first transition at zero temperature in which level crossing occurs. For  $J_{\text{mix}}/J_z \leq 0.8$ , entropic stabilization favors configurations for which the angle  $\theta^*$  is uniform throughout the system and assumes a value that is an integer multiple of  $90^\circ$ . Throughout the entire region  $0 \leq J_{\text{mix}}/J \leq 1$ , the  $d = 2$  emergent symmetries of Eq. (87) found earlier for the classical system remain intact.

Like the 90° compass model, the extended 120° model exhibits finite-temperature critical points concurrent with the first-order transitions at zero temperature at the point of symmetry (the original 120° for which  $J_{\text{mix}} = J_z$ ). In the

extended 120° model, these critical points fuse to form a continuous line as  $J_{\text{mix}}/J_z$  is varied (while  $J_x = J_z$ ). The critical nature is seen by the specific heat divergence and the finite-temperature expectation values of the pseudospins. van Rynbach, Todo, and Trebst (2010) reported that at the symmetric point, the 120° model exhibits a critical transition at a temperature of  $T_c = (0.677 \pm 0.003)J$ , a value which is very close to that of the later study of Wenzel and Läuchli (2011b) [see Eq. (118)].

#### 2. Quantum extended 120° model

One of the major virtues of the extended model, along the line  $J_{\text{mix}} = 0$ , is that it is free of the “sign problem” that plagues quantum Monte Carlo simulations. Along the line  $J_x = J_z = J$  (and  $J_{\text{mix}} = 0$ ), the system was found to undergo a continuous transition at a temperature  $T_c = (0.41 \pm 0.1)J$  into an ordered state in which all pseudospins point up or down along the  $T^z$  direction (the  $\pm T^z$  directions). At zero temperature, as the ratio  $J_x/J_z$  is varied, a first-order transition corresponding to level crossing at  $J_x = J_z$  appears. For  $J_x/J_z < 1$ , the ground state is of the  $\pm T^z$  form. Conversely, for  $J_x/J_z > 1$ , the ground states are of the  $\pm T^x$  type. This situation is reminiscent of the first-order transition found in the 90° compass model on the square lattice. In both cases, elementary excitations corresponding to a pseudospin flip (of either the  $\pm T^z$  or the  $\pm T^x$  type) are gapped. The gap is reduced at the point of symmetry ( $J_x = J_z = J$ ) of this truncated model with  $J_{\text{mix}} = 0$ , where it attains a value equal to  $\Delta \approx (0.34 \pm 0.04)J$ .

The main interest lies in the symmetric 120° angle and its environs. Toward that end, van Rynbach, Todo, and Trebst (2010) computed perturbatively the effect of a finite  $J_{\text{mix}}/J_z$  to find a very interesting suggestive result. These calculations suggest that the gap closes in the vicinity of the symmetry point ( $J_x = J_z = J_{\text{mix}}$ ). If this is indeed the case then the states found in the “unmixed” truncated model ( $J_{\text{mix}} = 0$ ) are adiabatically connected to those near and at the original symmetric 120° model. On either side of the symmetry point, the ground states are of the  $\pm T^x$  and  $\pm T^z$  types as discussed above. These states must somehow evolve and merge into the states at the point of symmetry. This suggests a greater degree of degeneracy within the ground-state sector of the symmetric 120° model. Among other possibilities this raises the possibility (compounded by  $1/S$  calculations) of six states akin to those found classically (Nussinov *et al.*, 2004; Biskup, Chayes, and Nussinov, 2005) in the symmetric 120° model or of having 12 states with pseudospins all uniformly oriented at an angle  $\theta^* = 0, 30^\circ, \dots, 330^\circ$  relative to the  $\tau^x$  direction.

#### E. Honeycomb lattice 120° compass models

In Secs. VI.F and VIII.D we reviewed key physical aspects of the 120° honeycomb model of Eq. (12). This included an analysis of the ground-state sector, its emergent symmetries, and the order-out-of-disorder free-energy calculations. We now turn to other more quantitative aspects.

#### 1. Classical model

Following Nasu *et al.* (2008), Wu (2008), and Zhao and Liu (2008), we reviewed, in Sec. VI.F, the presence of a

continuous global ( $d = 2$ ) and chiral discrete  $d = 1$  emergent symmetries of the  $120^\circ$  compass models on the honeycomb lattice. The low-temperature orders are unconventional. That is, the numerically observed usual pair correlations  $\langle \mathbf{T}_i \cdot \mathbf{T}_j \rangle$  were found to be short ranged (and  $\langle \mathbf{T}_i \rangle$  vanished) as the system size increased (Nasu *et al.*, 2008). Numerically, a continuous (or weakly first-order) low-temperature ordering transition at ca.  $T_c = 0.0064J$  is marked by an order parameter  $q$  defined as (Nasu *et al.*, 2008)  $q = N^{-1} \sum_{i=1}^N q_i$  with  $q_i = \cos 3\theta_i$ . Note that this quantity constitutes an analog to the nematic-type order parameters in the two- and three-dimensional  $90^\circ$  models. The pair correlations  $\langle q_i q_j \rangle$  exhibit a correlation length of size  $\xi$  that scales in accordance with Eq. (109) with an exponent  $\nu = 0.72 \pm 0.04$ . Similarly, the transition at  $T_o$  is evident as a peak in the specific heat. Within the ground states  $|q| = 1$  in accord with the order-out-of-disorder analysis that, as reviewed in Sec. VI.F (similar to that of the  $120^\circ$  model on the cubic lattice), led to the angles of Eq. (100).

## 2. Quantum model

The numerical value of the spectral gap between the ground state and the next excited state was found to progressively diminish as the system size was increased (Nasu *et al.*, 2008). Currently, it is not clear if this reflects the existence of gapless modes or points to a degeneracy of the system. Generally, in many spin (and pseudospin) systems, similar results appear in simpler systems that harbor bona fide SU(2) symmetries where the Lieb-Schultz-Mattis theorem and more recent extensions exist (Lieb, Schultz, and Mattis, 1961; Hastings, 2004). It was furthermore found that the ground states might be approximated by an ansatz wave function of the type (Nasu *et al.*, 2008)

$$|\Psi^{(\pm)}\rangle = \mathcal{N} \sum_l \mathcal{A}_l \{ |\psi_l^{(\uparrow)}\rangle \pm |\psi_l^{(\downarrow)}\rangle \}. \quad (122)$$

In Eq. (122),  $\mathcal{N}$  is a normalization constant,  $\{\mathcal{A}_l\}$  are variational parameters, and the states  $|\psi_l^{(\uparrow/\downarrow)}\rangle$  are schematically represented in Fig. 26.

Explicitly,

$$|\psi_l^{(\uparrow)}\rangle = \prod_{\langle ij \rangle_l} U(\phi_\gamma) |\uparrow \uparrow \cdots \uparrow\rangle. \quad (123)$$

In the above,  $l$  denotes a set of links  $\langle ij \rangle$  for which the fully polarized state  $|\uparrow \uparrow \cdots \uparrow\rangle$  will be rotated so that the pseudospins will be parallel to the links in the set  $l$ . In Eq. (123) we will, specifically, set for a single pair of sites  $i$  and  $j$  on the link  $\langle ij \rangle$  (Nasu *et al.*, 2008)

$$U(\phi_\gamma)_{\langle ij \rangle} = \exp[-i\phi_\gamma(T_i^y + T_j^y)], \quad (124)$$

where  $\gamma$  is set by the spatial direction of the link between  $i$  and  $j$ :  $(\phi_1, \phi_2, \phi_3) = (0, 2\pi/3, 4\pi/3)$ . Thus, the states of Eq. (122) correspond to a linear superposition of ‘‘dimer states,’’ see, e.g., Kivelson, Rokhsar, and Sethna (1987), Rokhsar and Kivelson (1988), Nussinov *et al.* (2007), and Nogueira and Nussinov (2009). In this case, the dimer states

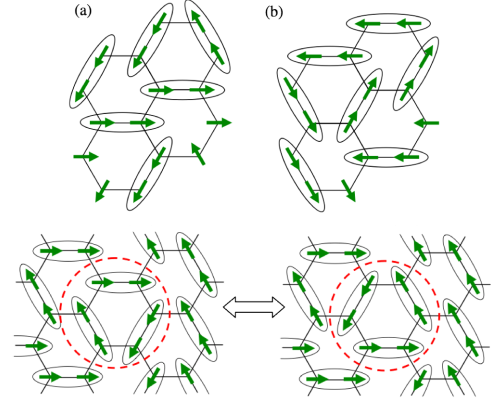


FIG. 26 (color online). Top: Some of the pseudospin configurations where the honeycomb lattice is covered by nearest-neighbor (NN) bonds with the minimum bond energy. One of the  $q = 1$  states in (a) and one of the  $q = -1$  in (b). In NN bonds surrounded by ellipses, the bond energy is the lowest. Bottom: One example for the two pseudospin configurations where a resonance state is possible due to the off-diagonal matrix element. From Nasu *et al.*, 2008.

$|\psi_l^{(\uparrow/\downarrow)}\rangle$  correspond to states wherein the pseudospins are parallel (or antiparallel) to the spatial direction. Kinetic tunneling between different dimer states can lower the energy of such states; see Fig. 26.

Thus, in the space spanned by the dimer states  $\{|\psi_l^{(\uparrow/\downarrow)}\rangle\}$  certain admixtures of these states with certain sets of the amplitudes  $\{\mathcal{A}_l\}$  in Eq. (122) can be selected by quantum fluctuations.

## F. Checkerboard lattice compass models

The most prominent compass models have been inspired by orbital or other interactions on cubic or other geometrically unfrustrated lattices. We briefly touched on some aspects of geometric frustration in different arenas in Secs. V.C, V.B.6, and elsewhere. We now explicitly turn to compass models on the checkerboard lattice. In Sec. III.C.2 [and, in particular, in Eq. (25)], we briefly introduced the checkerboard on the checkerboard lattice (Nasu and Ishihara, 2011b; Nasu, Todo, and Ishihara, 2012b). The checkerboard lattice, a two-dimensional rendition of the pyrcalore lattice, is a prototypical frustrated lattice. The system of Eq. (25) was motivated by examining, within second-order perturbation theory (assuming the kinetic term is small relative to the Coulomb penalty), a spinless Hubbard model on this lattice. This model exhibits  $d = 1$  symmetries in the form (Nasu, Todo, and Ishihara, 2012b) of  $O_l = \prod_{i \in l} \tau_i^z$ , where  $l$  denotes diagonals that run across the system either in the  $\langle 11 \rangle$  or  $\langle 1\bar{1} \rangle$  direction. By the generalization of Elitzur’s theorem (Batista and Nussinov, 2005; Nussinov, Ortiz, and Cobanera, 2012b), these symmetries cannot be broken at finite temperatures. Some limits of the problem are obvious. When  $|J_x| \gg |J_z|$ , as each site lies on only one of the two diagonal directions ( $\langle 11 \rangle$  or  $\langle 1\bar{1} \rangle$ ), the Hamiltonian of Eq. (25) reduces to that of decoupled diagonal chains with Ising  $\tau_i \tau_j$  interactions between nearest neighbors. In the other extreme limit, that of  $|J_z| \gg |J_x|$ , interactions

along the diagonals become negligible and the system becomes a two-dimensional Ising model on the square lattice with nearest-neighbor  $\tau_i^x \tau_j^x$  interactions. In tandem with these limits, it was reported (Nasu and Ishihara, 2011b; Nasu, Todo, and Ishihara, 2012b) that at low temperatures, for  $|J_x| \lesssim 2|J_z|$ , uniform or Néel (depending on the sign of  $J_z$ ) Ising order appears. By contrast, when  $2|J_z| \lesssim |J_x|$ , the decoupled chain-like character leads, on an  $L \times L$  lattice, to a  $2^{2L}$  degeneracy similar to that found for the square lattice  $90^\circ$  compass model. In the antiferromagnetic variant of this system, at zero temperature, a first-order transition between the two low-temperature phases was found at  $J_x \approx 2.7J_z$ . Several approaches (Nasu and Ishihara, 2011b; Nasu, Todo, and Ishihara, 2012b) suggest that there is a finite-temperature tricritical point in the vicinity of  $J_x = 2J_z$ .

### G. Arbitrary-angle compass models

We now discuss the arbitrary-angle square lattice compass models (Cincio, Dziarmaga, and Oleś, 2010) of Eq. (22). The symmetry of the ground states of these systems changes character at an angle  $\theta_c$  which is very close to the right-angle value of the  $90^\circ$  compass model. The second-order transition at  $\theta = \theta_c$  is associated with the doubling of the ground-state degeneracy. Specifically, for  $\theta < \theta_c$ , the system of Eq. (22) has two degenerate ferromagnetic ground states with a spontaneous magnetization that is parallel (antiparallel) to the  $\tau^x$  ( $\pi^x + \pi^y$ ) direction. Conversely when  $\theta > \theta_c$ , there are four degenerate ground states with pseudospins along the  $\pm\pi^x$  or  $\pm\pi^y$  directions. For the pseudospin-1/2 realization of Eq. (22), it was numerically seen that  $\theta_c \approx 84.8^\circ$ . As the pseudospin value increases and the system becomes more classical,  $\theta_c$  monotonically increases and reaches  $90^\circ$  in the classical limit. Thus, the fourfold-degenerate phase is promoted by quantum fluctuations.

### H. XXZ honeycomb compass model

In Sec. II.A.3 [in particular, in Eq. (8)] the XXZ honeycomb compass model (Nussinov, Ortiz, and Cobanera, 2012a) was introduced (see also Fig. 5). This model can be mapped onto a quantum Ising gauge (QIG) theory on a square lattice (Nussinov, Ortiz, and Cobanera, 2012a)

$$H_{\text{QIG}}^{\text{XXZ}} = - \sum_{x \text{ bonds}} J_x^\ell \sigma_\ell^x - \sum_{y \text{ bonds}} J_y^\ell \sigma_\ell^y - \sum_{z \text{ bonds}} J_z^\ell \prod_{\ell \in P_\ell} \sigma_\ell^z. \quad (125)$$

A few explanations are in order concerning this Hamiltonian. The links  $\ell$  and the associated coupling constants  $J^\ell$  refer to the links of the original honeycomb lattice; these links can be oriented along either the  $x$ ,  $y$ , or  $z$  directions of the honeycomb lattice. In Eq. (125), the Pauli operators  $\sigma_\ell^{x,z}$  are located at the centers  $\ell$  of the square lattice which is formed by shrinking all of the vertical (or  $z$ ) links of the honeycomb lattice to an individual point. After such an operation, the resulting (topologically square) lattice is comprised of  $x$ - and  $y$ -type links. As seen in Eq. (125), there is a field  $h = J_x$  that couples to the Pauli  $x$  operator on each such link. This is augmented by a plaquette term [the last term in Eq. (125)]. The plaquette  $P_\ell^j$  is formed by the centers of the four links (two  $x$ -type links and

two  $y$ -type links) that are nearest neighbors to the center of a vertical  $z$ -type link  $\ell$ . The product  $\prod_{\ell \in P_\ell} \sigma_\ell^z$  denotes the product of all four  $\sigma^z$  operators at the centers of links of the square plaquette that surrounds an original vertical link  $\ell$  that has been shrunk to a point. The sum over the original vertical links ( $z$  bonds) becomes, in Eq. (125), a sum over all plaquettes of a square lattice formed by the shrinking of all vertical links. The link center points of this square lattice coincide with those formed by the center points of the  $x$ - and  $y$ -type bonds of the original honeycomb lattice. When all of the coupling constants  $J_{x,z}^\ell$  are isotropic, the system is that of the canonical uniform standard transverse-field Ising gauge theory which, as is well known, maps onto the 3D Ising gauge theory. The 3D Ising gauge theory is dual to the standard 3D Ising model on the cubic lattice (Wegner, 1971; Kogut, 1979). Thus, the uniform XXZ honeycomb compass model is dual to the 3D Ising model and exhibits a finite-temperature phase transition with the standard 3D Ising exponents (Nussinov, Ortiz, and Cobanera, 2012a). As is evident in Eq. (125), not all coupling constants  $J_{x,z}^\ell$  need to be of the same strength. As the disordered transverse-field Ising gauge theory can exhibit a spin-glass-type transition, the XXZ honeycomb model may also correspond to a spin glass when it is nonuniform (Nussinov, Ortiz, and Cobanera, 2012a). Additional information concerning the quantum Ising gauge theory appears in Sec. IX.K.

### I. Plaquette orbital model

Biskup and Kotecky (2010) studied the classical realization of the plaquette orbital model (Wenzel and Janke, 2009) and certain quantum variants. Next these results are reviewed.

#### 1. Exact symmetries

Examining the Hamiltonian of Eq. (24) we note that the inversion of the four pseudospins  $\tau_i^x \rightarrow -\tau_i^x$  on an  $A$  plaquette (while leaving  $\tau_i^y$  unchanged) constitutes a local symmetry. A similar effect occurs with  $x$  and  $y$  interchanged on any of the  $B$ -type plaquettes. These local (i.e., gauge) symmetries are recast in terms of the following four-site symmetry operators of the  $T = 1/2$  quantum Hamiltonian of Eq. (24) ( $[U_{\square_A}, H] = [U_{\square_B}, H] = 0$ ),

$$U_{\square_A} = \prod_{i \in \square_A} \tau_i^y, \quad U_{\square_B} = \prod_{j \in \square_B} \tau_j^x. \quad (126)$$

In Eq. (126),  $\mathcal{A}$  denotes any plaquette of the  $A$  type and, similarly,  $\mathcal{B}$  denotes any plaquette of the  $B$  type. By Elitzur's theorem, at any finite temperature ( $T > 0$ ), all expectation values must be invariant under the symmetries of Eq. (126).

#### 2. Classical ground states and emergent symmetries

As in the analysis for the classical  $120^\circ$  and  $90^\circ$  models, (Nussinov *et al.*, 2004; Biskup, Chayes, and Nussinov, 2005), by rewriting the Hamiltonian of Eq. (24) as a sum of squares and using uniform states as classical “variational states,” Biskup and Kotecky (2010) demonstrated that all classical ground states of Eq. (24) are uniform states up to the application of the classical version of the local symmetries

of Eqs. (126). In particular, for  $J_A > J_B$ , a state which is fully polarized along the  $x$  axis constitutes a ground state; this state can be further mutated by local inversion gauge transformations. Similarly to the situation in the classical  $120^\circ$  and compass models a continuous symmetry emerges in the classical ground-state sector. When  $J_A = J_B$ , any constant uniform state of the pseudospins  $\mathbf{T}_r$  is a ground state of the classical system. As these classical vectors can point anywhere on the unit disk, a continuous rotational symmetry appears.

### 3. Finite-temperature order out of disorder

As in the classical  $120^\circ$  and  $90^\circ$  compass models, a finite-temperature order-out-of-disorder mechanism lifts the ground-state degeneracy (Mishra *et al.*, 2004; Nussinov *et al.*, 2004; Biskup, Chayes, and Nussinov, 2005), and leads, at low positive temperatures ( $0 < T < T_0$ ), to a nematic-type order in the plaquette compass model wherein most of the configurations have a majority of the pseudospins aligned along either the  $(\pm e_x)$  or the  $(\pm e_z)$  direction (Biskup and Kotecky, 2010). Because of the (classical version of the) local symmetries of Eqs. (126), both signs of the orientation ( $\pm$ ) are equally likely.

Following Biskup, Chayes, and Starr (2007), low-temperature order was also proven to hold in the quantum model when the magnitude of the pseudospin is sufficiently large ( $|\mathbf{T}| > c\beta^2$  with  $c$  a positive constant and  $\beta$  the inverse temperature) (Biskup and Kotecky, 2010). The technical reason for requiring a sufficiently large pseudospin is that within the proof of Biskup, Chayes, and Starr (2007) and Biskup and Kotecky (2010) thermal fluctuations were assumed to dominate quantum fluctuations.

## J. Gell-Mann matrix compass models

The two Gell-Mann matrix compass models of Eqs. (67) and (68), derived from Eq. (66), have very interesting and distinct behaviors (Chern and Wu, 2011).

### 1. Cubic lattice Gell-Mann matrix compass model

As the two Gell-Mann matrices  $\lambda^{(3)}$  and  $\lambda^{(8)}$  are diagonal and commute with one another, the quantum model of Eq. (67) is essentially classical (Chern and Wu, 2011).

$T = 0$ : The ground-state energy per site  $E/N = -2J/3$  is consistent with two-thirds of the bonds being minimized and the remaining one-third being frustrated. The two-point correlation function  $\langle \lambda_i \cdot \lambda_j \rangle$  exhibits rapidly decaying oscillations and is essentially vanishing for distances  $|\mathbf{r}_{ij}| \geq 5$  lattice constants (Chern and Wu, 2011).

$T > 0$ : Monte Carlo simulations were performed. An integration from the specific heat curve indicates that there is a large residual entropy at zero temperature. Although not explicit an estimate was given by Chern and Wu (2011) for viable transitions; judging from the data shown the sharp specific heat peak occurs at a temperature  $T \sim 0.7J$ .

### 2. Diamond lattice Gell-Mann matrix compass model

For a single pair of nearest-neighbor sites on the lattice along the  $\mathbf{n}_0$  direction ( $i$  and  $j$ ), the minimum of the corresponding term in Eq. (68) is achieved when the

corresponding orbital states are  $3^{-1/2}(|p_x\rangle + |p_y\rangle + |p_z\rangle)$  and  $2^{-1/2}(|p_x\rangle - |p_y\rangle)$ . As in the case of the Gell-Mann model on the cubic lattice and, more generally, compass models, the system is frustrated and not all interactions can be simultaneously minimized. As shown by Chern and Wu (2011), the ground states are of the form  $|\psi\rangle = \prod_i |\lambda_i\rangle$  with, for site  $i$ , the local state  $|\lambda_i\rangle = |\pm e_x\rangle, |\pm e_y\rangle, \text{ or } |\pm e_z\rangle$  such that for all nearest-neighbor pairs  $\langle ij \rangle$ ,

$$(\lambda_i \cdot e_{ij})(\lambda_j \cdot e_{ij}) = -\frac{1}{3}. \quad (127)$$

When expressed in terms of the original orbital degrees of freedom, the local states are explicitly  $|\pm e_x\rangle = 2^{-1/2}(|p_y\rangle \pm |p_z\rangle)$  and cyclic permutations thereof [i.e.,  $|\pm e_y\rangle = 2^{-1/2}(|p_z\rangle \pm |p_x\rangle)$  and  $|\pm e_z\rangle = 2^{-1/2}(|p_x\rangle \pm |p_y\rangle)$ ].

As shown in Fig. 27, the states  $|\pm e_{x,y,z}\rangle$  at any site  $i$  can be represented by corresponding arrows on the pyrochlore lattice formed by the centers of all nearest-neighbor links  $\langle ij \rangle$ . Specifically, these arrows are given by

$$\mathbf{R}_{\langle ij \rangle} = \sigma_i^j e_{ij} (= -\sigma_j^i e_{ij}), \quad (128)$$

where, with  $e_{ij}$  denoting a unit vector from site  $i$  to site  $j$ , the Ising-type variables  $\sigma_i^j = \pm 1$  are given by  $\sigma_i^j = \sqrt{3}(\lambda_i \cdot e_{ij})$ . Following Chern and Wu (2011), we next focus on the basic tetrahedrons of pyrochlore lattice (that have the vertices of the original diamond lattice at their centers). As a result of the condition of Eq. (127), there are two incoming and two outgoing arrows  $\mathbf{R}$  toward the center of each tetrahedron. This is the so-called ‘‘ice condition’’ which appears in many other systems and leads to an extensive degeneracy (Nagle, 1966; Lieb, 1967) which according to the Pauling estimate would be  $S \approx Nk_B \ln(3/2) \approx 0.405Nk_B$  (Chern and Wu, 2011). [Note that according to the more accurate estimate of Nagle (1966) this would be  $S \approx 0.4102Nk_B$ .] As in the Gell-Mann matrix model on the cubic lattice, two-point correlations within the ground state are decaying. In general, the correlations associated with extensively degenerate ice states are dipolar-type power-law correlations  $\langle \lambda_i \cdot \lambda_j \rangle \sim |\mathbf{r}_{ij}|^{-3}$  (Villain, 1972;

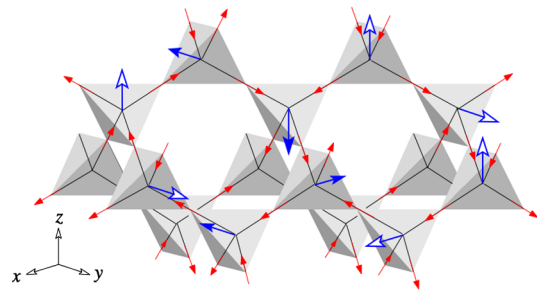


FIG. 27 (color online). A configuration of the pseudovectors on the diamond lattice and its mapping to the spin-ice state on the dual pyrochlore lattice. The pseudovector assumes only six different values  $\langle \mu_i \rangle = \pm \hat{x}, \pm \hat{y}, \pm \hat{z}$  in the ground states, corresponding to  $(p_y \pm p_z)$ ,  $(p_z \pm p_x)$ , and  $(p_x \pm p_y)$  orbitals, respectively. These six orbital configurations are mapped to the six two-in-two-out ice state on a tetrahedron. From Chern and Wu, 2011.

Stillinger and Cotter, 1973; Youngblood and Axe, 1981; Ioffe and Larkin, 1989; Huse *et al.*, 2003; Henley, 2005; Nussinov *et al.*, 2007). Such correlations were indeed numerically verified by Chern and Wu (2011) in their system. The ice condition and its breaking are known to lead to effective fractional charges and related effects as found in different contexts (Fulde, Penc, and Shannon, 2002; Nussinov *et al.*, 2007; Castelnovo, Moessner, and Sondhi, 2008; Powell, 2011; Chang *et al.*, 2012). In particular, when the temperature  $T > 0$ , thermal excitations out of the ground-state ice condition manifold can lead to deconfined fractional charges (with dipolar correlations). It would be interesting to see what is the corresponding physics in this orbital system.

### K. Symmetric extended compass Hubbard models

In Sec. V.A.5, and in Eq. (59), in particular, a compass-type Hubbard model was introduced that, aside from lattice hopping terms, further included electronic pair creation and annihilation terms. Both of these terms (kinetic and pairing) were of the compass type. In Eq. (59), the spatial indices of the electronic creation and annihilation operators involved were determined by the spin polarization. The particular, symmetric, variant written of the extended compass Hubbard model, that of Eq. (59), in which the pairing and hopping amplitudes are of equal strength, is amenable to an exact result. It can be demonstrated (Nussinov, Ortiz, and Cobanera, 2012a) that the square lattice system of Eq. (59) is dual to the QIG theory on the dual lattice. This dual lattice (which is also a square lattice) is formed by regarding each site  $i$  of the original square lattice as the center of a minimal square (or plaquette) of the dual lattice. The QIG theory was already written down as its associated couplings pertain to the XXZ honeycomb compass in Eq. (125). We now do so anew for the symmetric extended compass Hubbard model. The Hamiltonian of the quantum Ising gauge theory which is dual to the theory of Eq. (59) is given by

$$H_{\text{QIG}}^{\text{SECHM}} = -2 \sum_l t_l \sigma_l^x - \sum_P U_i \prod_{l \in P_i} \sigma_l^z. \quad (129)$$

The index  $l$  in Eq. (129) denotes a link of the square lattice. In reference to the symmetric extended compass Hubbard model of Eq. (59),  $t_l$  is the hopping amplitude between two sites in the original electronic system. In the spin Hamiltonian of Eq. (129), a Pauli operator is placed at the center of each link  $l$  of the square lattice. The first term in Eq. (129) thus physically corresponds, at each such link  $l$ , to a magnetic field term along the  $x$  direction which is of strength  $t_l$ . The second term in Eq. (129) is the standard plaquette term of classical gauge theories.  $P_i$  denotes any elementary plaquette of the square lattice on which Eq. (129) is defined [corresponding to a site  $i$  on the original square lattice model of Eq. (59)].  $\prod_{l \in P_i} \sigma_l^z$  is the product of the four  $\sigma^z$  operators on the links  $l$  of such a minimal square plaquette  $P_i$  of the lattice. In the absence of the first (magnetic field) term in Eq. (129), the Hamiltonian is that of the classical square lattice Ising gauge theory (Kogut, 1979) (which is trivially dual to an Ising chain). The field  $t_l$  along the transverse  $x$  direction leads to quantum fluctuations between different classical spin states. These fluctuations are the origin

of the name “quantum Ising gauge theory.” As is well known, the square lattice quantum Ising gauge theory can be mapped onto the 3D classical Ising gauge theory (the theory given solely by square plaquette terms on the cubic lattice). The 3D Ising gauge theory is, in turn, dual to the standard Ising model on the cubic lattice. Thus, similar to the discussion in Sec. IX.H, by the equivalence between the theories of Eqs. (59) and (129), one can adduce much information. These considerations make specific remarks about (i) the spatially uniform and (ii) disordered realizations of this theory.

*The spatially uniform system.* When all of the pairing and hopping amplitudes  $t_l$  and the Hubbard energy terms  $U_i$  in Eq. (59) are spatially uniform and equal to fixed values  $t$  and  $U$ , the system is equivalent to and exhibits canonical 3D Ising behavior. At zero temperature, a 3D Ising transition appears at a critical  $t/U$  ratio of 0.14556.

*Disordered systems.* The mapping (Nussinov, Ortiz, and Cobanera, 2012a) between the symmetric extended compass Hubbard model of Eq. (59) and the quantum Ising gauge theory of Eq. (129) in general applies to any set of couplings  $\{t_l, U_i\}$ . As is well known, sufficiently disordered Ising models (in which couplings are nonuniform) may display a spin-glass-type behavior. Thus, by the correspondence between Eqs. (59) and (129), the electronic system given by a random symmetric extended compass Hubbard model may display spin-glass behavior.

### X. CONCLUSIONS

Complementing more standard theories with isotropic interactions between various fundamental fields (such as spin, charge, color, or more generally pseudospin), there exists a plethora of physical systems in which the couplings between the pertinent internal degrees of freedom are direction dependent. The couplings in these compass models depend on the direction of the vectors connecting the interacting sites relative to a lattice (or continuum Cartesian or other directions). Such anisotropic direction-dependent interactions are ubiquitous. Indeed, the anisotropic components of the interactions between dipoles when these are placed on lattices have precisely such a form.

In compass models, external lattice (or other) directions lift the standard rotational invariance of the interactions. As reviewed here, in recent decades, numerous condensed matter systems have been discovered to host precisely such compass-type interactions. The paradigmatic class of physical systems described by compass interactions is afforded by transition-metal materials where the real space form of the pertinent electronic orbitals leads to exactly such direction-dependent interactions. The associated ordered orbitals have been observed to persist, in some materials, up to temperatures [which can range up to  $\mathcal{O}(10^3 \text{ K})$ ] that may significantly exceed magnetic ordering temperatures (when these are present) in these materials.

Other primary examples of compass-type interactions include diverse spin systems on frustrated lattices, bosonic and fermionic gases on optical lattices, materials with strong spin-orbit interactions, and other systems. The simplicity of the Hamiltonians of even some basic compass-type systems is deceptive. Compass model systems enjoy far fewer currently

known results than their standard isotropic peers. Because of the anisotropic character of the interactions, the study of these systems is, by comparison to more standard rotationally invariant systems, a supremely interesting and challenging problem. Notably, as reviewed here for many particular compass Hamiltonians, some of these systems may be quantum liquids or, conversely, may lead to low-temperature phases of matter in which order is triggered by fluctuation effects. The dichotomy between compass-type and the more standard isotropic interactions is manifest in many physical properties such as the absence of standard symmetry breaking in many compass models (see, e.g., Sec. VI). Broad highlights of currently known results and a concise description of their location in this review have been charted at greater length in the opening outline of Sec. I.B.

Many other systems with directional interactions, such as that of wires with unidirectional hopping and different interactions along the transverse directions, also constitute compass models. For instance, a Jordan-Wigner transformation of the 2D 90° compass model yields such a system (with unidirectional hopping/pairing along one direction and nearest-neighbor charge-charge interactions along the transverse directions). More complicated systems that still retain the same character along different directions abound in many other arenas. This encompasses both general mesoscopic systems as well as, e.g., effective theories for topological insulator surface interfaces (Mross, Essin, and Alicea, 2014).

Augmenting their physical relevance to many different materials, novel rich phenomena appear in compass models, e.g., dimensional reduction and holography that are spawned by unusual (exact or emergent) symmetries. The symmetries and some of the unusual rich behaviors of compass-type systems are strongly intertwined. Within the wide framework of this review, we incorporated new results including a general theorem establishing the intimate relation between flat bands in a very broad class of systems and these unusual symmetries (see Secs. VII and VII.C, in particular). The exploration of the different states of matter of compass models with such symmetries has just begun. Specific items that have only started to be examined include the precise understanding of the nature of the phase transitions that they exhibit. To date, for instance, no effective-field theories of these systems have been studied, or for that matter even been written down (this review actually includes one of the first general forms of these unusual anisotropic field theories). One of the powerful driving forces of this field is the close connections between compass models and topological quantum information (Nussinov and van den Brink, 2013, 2015) (such as in Kitaev's model) and, in particular, topological states of matter (e.g., those displayed by recently discovered topological insulators). This is one of the directions in which the field is bound for the discovery of new physical phenomena and insights.

## ACKNOWLEDGMENTS

We have been fortunate to closely interact with numerous colleagues on some of the systems described in this work. These include, among many others, C. Batista, M. Biskup, L. Chayes, H.-D. Chen, E. Cobanera, M. Daghofer, T.P. Devereaux, E. Fradkin, P. Horsch, G. Khaliullin,

D. Khomskii, S. Kumar, F. Nogueira, F. Mack, M. Mostovoy, A.M. Oleś, K. Shtengel, K. Wohlfeld, J. Zaanen, and P. Zoller. In particular, Z. N. is grateful for a nearly decade-long interaction with G. Ortiz on many aspects of compass models. We are thankful for the understanding of these colleagues in that we did not promptly write other papers that need to be finished. Z. N. is grateful for the support of the National Science Foundation under NSF Grants No. DMR-1106293 and DMR-141122 for work at the Washington University (WU) at St. Louis as well as that of the Center for Materials Innovation of WU. Z. N. is very grateful for the hospitality of the IFW, Dresden where the central parts of this work were done. J. v. d. B. acknowledges the support by the German Science Foundation DFG, in particular, via the Collaborative Research Center SFB 1143.

## APPENDIX A: THE BOND ALGEBRA OF THE PLAQUETTE ORBITAL MODEL

In Eq. (24), following Wenzel and Janke (2009) and Biskup and Kotecky (2010), the *plaquette orbital model* is introduced. Remarkably, its local algebraic structure is similar to that of the 90° compass model on the square lattice [Eq. (1)]. In this Appendix this observation is clarified, invoking the bond algebraic structure (Nussinov and Ortiz, 2008, 2009b; Cobanera, Ortiz, and Nussinov, 2010, 2011; Nussinov, Ortiz, and Cobanera, 2012a, 2012b; Ortiz, Cobanera, and Nussinov, 2012). The Hamiltonian defining the plaquette orbital model is a sum of two types of terms (or “bonds”):

(A)  $\tau_i^x \tau_j^x$  for all links that belong to the  $A$  plaquette sublattice,  $\langle ij \rangle \in A$ . (B)  $\tau_i^y \tau_j^y$  for all links  $\langle ij \rangle$  that belong to the  $B$  plaquette sublattice.

The decomposition into the two plaquette ( $A$  and  $B$  sublattices) is shown in Fig. 8 (Biskup and Kotecky, 2010). The algebra satisfied by these bonds is very simple and is encapsulated by the following relations:

- (i) The square of each bond is 1.
- (ii) Any two bonds that are of different type (i.e., one bond is of type  $A$  and the other is of type  $B$ ) and share one common site anticommute:  $\{\tau_i^x \tau_j^x, \tau_i^y \tau_k^y\} = 0$  with the curly brackets denoting the anticommutator. (By fiat, given the type of the interactions,  $\langle ij \rangle \in A$  and  $\langle ik \rangle \in B$ .)
- (iii) Bonds of different type commute if they share no common site:  $[\tau_i^x \tau_j^x, \tau_k^y \tau_l^y] = 0$  (with  $i, j, k$ , and  $l$  corresponding to four different sites).
- (iv) Any bond of type  $A$  commutes with any other bond of type  $A$  and, similarly, any bond of type  $B$  commutes with all bonds of the  $B$  type. Thus, locally, each bond (having a square that is unity) anticommutes with two other neighboring bonds and commutes with the two other nearest-neighbor bonds (as well as all other bonds on the lattice). The bond algebra associated with the 90° compass model of Eq. (1) is very much like that of the plaquette orbital model. This system has a decomposition into two types of similar bonds:
  - (a)  $\tau_i^x \tau_j^x$  on all horizontal links.
  - (b)  $\tau_i^y \tau_j^y$  on all vertical links.

The algebra satisfied by these bonds is specified by a similar list:

- (i) The square of each bond is 1.
- (ii) Any two bonds that are of different type that share one common site anticommute  $\{\tau_i^x \tau_j^y, \tau_i^y \tau_k^x\} = 0$ .
- (iii) Bonds of different type commute if they share no common site  $[\tau_i^x \tau_j^x, \tau_k^y \tau_l^y] = 0$  (with  $i, j, k$ , and  $l$  corresponding to four different sites).
- (iv) Any horizontal bond commutes with any other horizontal bond and, analogously, any vertical bond commutes with all vertical bonds.

The local algebra is congruent to that of the plaquette orbital model: each bond anticommutes with two out of its four nearest neighbors. This equal structure implies that in their Cayley tree (or Bethe lattice) approximations, the  $90^\circ$  and the plaquette compass model are identical.

### APPENDIX B: GELL-MANN MATRICES

The Gell-Mann matrices are a representation of the infinitesimal generators of the special unitary group  $SU(3)$ . This group has dimension 8 and therefore it has a set with eight linearly independent generators, which can be written as  $\lambda_i$ , with  $i$  taking values from 1 to 8. They obey the commutation relations

$$[\lambda_i, \lambda_j] = \frac{i}{2} f^{ijk} \lambda_k, \quad (\text{B1})$$

where a sum over the index  $k$  is implied. The constants  $f^{ijk}$  are  $f^{123} = 1$ ,  $f^{147} = f^{165} = f^{246} = f^{257} = f^{345} = f^{376} = 1/2$ , and  $f^{458} = f^{678} = \sqrt{3}/2$  and are antisymmetric in the three indices. The Gell-Mann matrix representations involving  $3 \times 3$  matrices act on complex vectors with three entries. They have the additional properties that they are traceless, Hermitian, and obey the relation  $\text{Tr}(\lambda_i \lambda_j) = 2\delta_{ij}$ ,

$$\begin{aligned} \lambda_1 &= \begin{pmatrix} 0 & 1 & 0 \\ 1 & 0 & 0 \\ 0 & 0 & 0 \end{pmatrix}, & \lambda_2 &= \begin{pmatrix} 0 & -i & 0 \\ i & 0 & 0 \\ 0 & 0 & 0 \end{pmatrix}, & \lambda_3 &= \begin{pmatrix} 1 & 0 & 0 \\ 0 & -1 & 0 \\ 0 & 0 & 0 \end{pmatrix}, \\ \lambda_4 &= \begin{pmatrix} 0 & 0 & 1 \\ 0 & 0 & 0 \\ 1 & 0 & 0 \end{pmatrix}, & \lambda_5 &= \begin{pmatrix} 0 & 0 & -i \\ 0 & 0 & 0 \\ i & 0 & 0 \end{pmatrix}, & \lambda_6 &= \begin{pmatrix} 0 & 0 & 0 \\ 0 & 0 & 1 \\ 0 & 1 & 0 \end{pmatrix}, \\ \lambda_7 &= \begin{pmatrix} 0 & 0 & 0 \\ 0 & 0 & -i \\ 0 & i & 0 \end{pmatrix}, & \lambda_8 &= \frac{1}{\sqrt{3}} \begin{pmatrix} 1 & 0 & 0 \\ 0 & 1 & 0 \\ 0 & 0 & -2 \end{pmatrix}. \end{aligned}$$

The matrices  $\lambda_3$  and  $\lambda_8$  commute. Three independent  $SU(2)$  subgroups are formed by the elements of vectors  $\boldsymbol{\mu}^1$ ,  $\boldsymbol{\mu}^2$ , and  $\boldsymbol{\mu}^3$ , where  $\boldsymbol{\mu}^1 = (1/2)(\lambda_1, \lambda_2, \lambda_3)$ ,  $\boldsymbol{\mu}^2 = (1/2)(\lambda_4, \lambda_5, \lambda_+)$ , and  $\boldsymbol{\mu}^3 = (1/2)(\lambda_6, \lambda_7, \lambda_-)$ . Here the  $\lambda_+$  and  $\lambda_-$  are linear combinations of  $\lambda_3$  and  $\lambda_8$ :  $\lambda_\pm = \lambda_3 \cos(2\pi/3) \pm \lambda_8 \sin(2\pi/3)$ , so that, as is expected for an  $SU(2)$  spin-1/2, the commutator  $[\boldsymbol{\mu}_1^\gamma, \boldsymbol{\mu}_2^\gamma] = (i/2)\boldsymbol{\mu}_3^\gamma$ , for each  $\gamma = 1, 2, 3$ .

The operators

$$\hat{R}^+ = \begin{pmatrix} 0 & 0 & 1 \\ 1 & 0 & 0 \\ 0 & 1 & 0 \end{pmatrix}, \quad \hat{R}^- = \begin{pmatrix} 0 & 1 & 0 \\ 0 & 0 & 1 \\ 1 & 0 & 0 \end{pmatrix} \quad (\text{B2})$$

rotate the vectors  $\boldsymbol{\mu}$  onto each other:  $\boldsymbol{\mu}^2 = \hat{R}^- \boldsymbol{\mu}^1 \hat{R}^+$

### APPENDIX C: CLASSICAL AND QUANTUM FLUCTUATIONS IN THE LARGE- $n$ LIMIT

The large- $n$  limit (see Sec. III.B) of the theory of Eq. (95) is exactly solvable. As such, it allows us to easily point out a difference between the classical and quantum theories. In the large- $n$  limit of the classical system, order appears in the  $D$ -dimensional system if and only if the classical (lowest-order  $[\mathcal{O}(1/n)^0]$ ) self-energy diagram stemming from the Boltzmann distribution of harmonic modes (and its related equipartition theorem)

$$\Sigma_{\text{cl}}^{(0)} = \sum_{\alpha} \int \frac{d^D k}{(2\pi)^D} \frac{1}{v_{\alpha}(\mathbf{k}) + \mu} \quad (\text{C1})$$

does not diverge as the “mass”  $\mu$  approaches  $[-\min_{k,\alpha}\{v_{\alpha}(\mathbf{k})\}]$ . The integration in Eq. (C1) is performed over the first Brillouin zone—a region of finite volume. Thus,  $\Sigma_{\text{cl}}^{(0)}$  can diverge only from infrared contributions. In systems in which the mode spectra  $v_{\alpha}(\mathbf{k})$  disperse quadratically about their minimum, the relevant integral converges in dimensions  $D > 2$  but fails to converge in low dimensions due to the large relative phase space volume of low-energy modes. Quantum mechanically, in large  $n$  systems [see, e.g., Nussinov *et al.* (2004) and Serral Gracia and Nieuwenhuizen (2004)], the corresponding self-energy is governed by the Bose function set by the modes  $\omega_k$ . The pertinent zero-temperature dispersion of  $v_{\alpha}(\mathbf{k})$  in the argument of the integrand governing the convergence or divergence of Eq. (C1) in the classical case is replaced in the quantum case by the square root form  $\sqrt{v_{\alpha}(\mathbf{k})}$ . Qualitatively similar Bose-type distributions and dispersions are found in  $1/S$  calculations. As power counting suggests, the convergence of the integral and thus the character of the fluctuations arising from classical and quantum effects are different. It is possible to have ordering of the quantum system at zero temperature while the classical counterpart of Eq. (C1) exhibits an infrared divergence. Such a case arises in two-dimensional ferromagnets. Precisely this sort of situation arises in the  $120^\circ$  compass model—the large- $n$  quantum version of the model exhibits low-temperature order (quantum order out of disorder) yet its classical counterpart exhibits no finite-temperature order. As a result, however, once the  $120^\circ$  system is constrained to its original ( $n = 2$ )-component version, both classical thermal fluctuations and quantum effects lead to similar sorts of ordering.

## REFERENCES

- Anderlini, M., P.J. Lee, B.L. Brown, J. Sebby-Strabley, W.D. Phillips, and J. V. Porto, 2007, *Nature (London)* **448**, 452.
- Andersen, O., and L. Boeri, 2011, *Ann. Phys. (Berlin)* **523**, 8.
- Anderson, P. W., 1959, *Phys. Rev.* **115**, 2.
- Ballhausen, C., 1962, *Introduction to Ligand Field Theory* (McGraw-Hill, New York).
- Batista, C., and S. Trugman, 2004, *Phys. Rev. Lett.* **93**, 217202.
- Batista, C.D., and Z. Nussinov, 2005, *Phys. Rev. B* **72**, 045137.
- Berlin, T. H., and M. Kac, 1952, *Phys. Rev.* **86**, 821.
- Biskup, M., L. Chayes, and Z. Nussinov, 2005, *Commun. Math. Phys.* **255**, 253.
- Biskup, M., L. Chayes, and S. Starr, 2007, *Commun. Math. Phys.* **269**, 611.
- Biskup, M., and R. Kotecky, 2010, *J. Stat. Mech.* P11001.
- Bloch, I., J. Dalibard, and W. Zwerger, 2008, *Rev. Mod. Phys.* **80**, 885.
- Breed, D., K. Gilijamse, J. Sterkenburg, and A. Miedema, 1970, *J. Appl. Phys.* **41**, 1267.
- Bricmont, J., and J. Frolich, 1983, *Phys. Lett.* **122B**, 73.
- Browaeys, A., H. Häffner, C. McKenzie, S.L. Rolston, K. Helmerson, and W.D. Phillips, 2005, *Phys. Rev. A* **72**, 053605.
- Bryngelson, J. D., J. N. Onuchic, N. D. Socci, and P. G. Wolynes, 1995, *Proteins* **21**, 167.
- Brzezicki, W., J. Dziarmaga, and A. M. Oleś, 2007, *Phys. Rev. B* **75**, 134415.
- Brzezicki, W., and A. M. Oleś, 2008, *Eur. Phys. J. B* **66**, 361.
- Brzezicki, W., and A. M. Oleś, 2009, *Phys. Rev. B* **80**, 014405.
- Brzezicki, W., and A. M. Oleś, 2010, *Phys. Rev. B* **82**, 060401.
- Brzezicki, W., and A. M. Oleś, 2013, *Phys. Rev. B* **87**, 214421.
- Budnik, R., and A. Auerbach, 2004, *Phys. Rev. Lett.* **93**, 187205.
- Capponi, S., A. Laeuchli, and M. Mambri, 2004, *Phys. Rev. B* **70**, 104424.
- Casimir, H. B. G., 1948, *Proc. K. Ned. Akad. Wet.* **B51**, 793.
- Casimir, H. B. G., and D. Polder, 1948, *Phys. Rev.* **73**, 360.
- Castelnovo, C., R. Moessner, and S. L. Sondhi, 2008, *Nature (London)* **451**, 42.
- Chakrabarty, S., and Z. Nussinov, 2011, *Phys. Rev. B* **84**, 064124.
- Chaloupka, J., G. Jackeli, and G. Khaliullin, 2010, *Phys. Rev. Lett.* **105**, 027204.
- Chang, L.-J., S. Onoda, Y. Su, Y.-J. Kao, K.-D. Tsuei, Y. Yukio, K. Kakurai, and M. R. Lees, 2012, *Nat. Commun.* **3**, 992.
- Chen, G., L. Balents, and A. P. Schnyder, 2009, *Phys. Rev. Lett.* **102**, 096406.
- Chen, H.-D., C. Fang, J. Hu, and H. Yao, 2007, *Phys. Rev. B* **75**, 144401.
- Chen, H.-D., and Z. Nussinov, 2008, *J. Phys. A* **41**, 075001.
- Chern, G. W., N. Perkins, and Z. Hao, 2010, *Phys. Rev. B* **81**, 125127.
- Chern, G.-W., and C. Wu, 2011, *Phys. Rev. E* **84**, 061127.
- Chubokov, A. V., and D. I. Golosov, 1991, *J. Phys. Condens. Matter* **3**, 69.
- Chubukov, A., 1992, *Phys. Rev. Lett.* **69**, 832.
- Cincio, L., J. Dziarmaga, and A. M. Oleś, 2010, *Phys. Rev. B* **82**, 104416.
- Cobanera, E., G. Ortiz, and Z. Nussinov, 2010, *Phys. Rev. Lett.* **104**, 020402.
- Cobanera, E., G. Ortiz, and Z. Nussinov, 2011, *Adv. Phys.* **60**, 679.
- Cobanera, E., G. Ortiz, and Z. Nussinov, 2013, *Phys. Rev. B* **87**, 041105(R).
- Cvetkovic, V., and Z. Tesanovic, 2009, *Europhys. Lett.* **85**, 37002.
- Daghofer, M., K. Wohlfeld, A. M. Oleś, E. Arrigoni, and P. Horsch, 2008, *Phys. Rev. Lett.* **100**, 066403.
- Dagotto, E., 2005, *New J. Phys.* **7**, 67.
- Dagotto, E., T. Hotta, and A. Moreo, 2001, *Phys. Rep.* **344**, 1.
- Divakarian, U., and A. Dutta, 2009, *Phys. Rev. B* **79**, 224408.
- Dorier, J., F. Becca, and F. Mila, 2005, *Phys. Rev. B* **72**, 024448.
- Doucot, B., M. Feigel'man, L. Ioffe, and A. Ioselevich, 2005, *Phys. Rev. B* **71**, 024505.
- Duan, L., E. Demler, and M. Lukin, 2003, *Phys. Rev. Lett.* **91**, 090402.
- Ederer, C., C. Lin, and A. J. Millis, 2007, *Phys. Rev. B* **76**, 155105.
- Elitzur, S., 1975, *Phys. Rev. D* **12**, 3978.
- Emery, V. J., E. Fradkin, S. A. Kivelson, and T. C. Lubensky, 2000, *Phys. Rev. Lett.* **85**, 2160.
- Eriksson, E., and H. Johannesson, 2009, *Phys. Rev. B* **79**, 224424.
- Fazekas, P., 1999, *Lecture Notes on Electron Correlation and Magnetism* (World Scientific, Singapore).
- Feiner, L. F., and A. M. Oleś, 1999, *Phys. Rev. B* **59**, 3295.
- Feiner, L. F., A. M. Oleś, and J. Zaanen, 1997, *Phys. Rev. Lett.* **78**, 2799.
- Feng, X.-Y., G.-M. Zhang, and T. Xiang, 2007, *Phys. Rev. Lett.* **98**, 087204.
- Ferrero, M., F. Becca, and F. Mila, 2003, *Phys. Rev. B* **68**, 214431.
- Fradkin, E., 1991, *Field Theories of Condensed Matter Systems* (Addison-Wesley, Redwood City).
- Fradkin, E., and S. A. Kivelson, 1999, *Phys. Rev. B* **59**, 8065.
- Fradkin, E., and S. H. Shenker, 1979, *Phys. Rev. D* **19**, 3682.
- Frank, F. C., and J. S. Kasper, 1958, *Acta Crystallogr.* **11**, 184.
- Frank, F. C., and J. S. Kasper, 1959, *Acta Crystallogr.* **12**, 483.
- Fredenhagen, K., and M. Marcu, 1986, *Phys. Rev. Lett.* **56**, 223.
- Fulde, P., K. Penc, and N. Shannon, 2002, *Ann. Phys. (Berlin)* **11**, 892.
- Golubovic, L., and M. Golubovic, 1998, *Phys. Rev. Lett.* **80**, 4341.
- Goodenough, J., 1963, *Magnetism and the Chemical Bond* (Interscience, New York).
- Gregor, K., D. A. Huse, R. Moessner, and S. L. Sondhi, 2011, *New J. Phys.* **13**, 025009.
- Greiner, M., M. O. Mandel, T. Esslinger, T. Hansch, and I. Bloch, 2002, *Nature (London)* **415**, 39.
- Griffith, J., 1971, *The Theory of Transition Metal Ions* (Cambridge University Press, Cambridge, England).
- Harris, A., T. Yildirim, A. Aharony, O. Entin-Wohlman, and I. Korenblit, 2003, *Phys. Rev. Lett.* **91**, 087206.
- Harrison, W., 2004, *Elementary Electronic Structure* (World Scientific, Singapore), revised edition.
- Hastings, M. B., 2004, *Phys. Rev. B* **69**, 104431.
- Henley, C., 1989, *Phys. Rev. Lett.* **62**, 2056.
- Henley, C. L., 2005, *Phys. Rev. B* **71**, 014424.
- Honecker, A., D. Cabra, H.-U. Everts, P. Pujol, and F. Stauffer, 2007, *J. Phys. Condens. Matter* **19**, 145249.
- Horibe, Y., M. Shingu, K. Kurushima, H. Ishibashi, N. N. Ikeda, K. Kato, Y. N. Motome, Furukawa, Mori, and T. Katsufuji, 2006, *Phys. Rev. Lett.* **96**, 086406.
- Hubbard, J., 1963, *Proc. R. Soc. A* **276**, 238.
- Huse, D. A., Krauth, R. Moessner, and S. L. Sondhi, 2003, *Phys. Rev. Lett.* **91**, 167004.
- Imada, M., A. Fujimori, and Y. Tokura, 1998, *Rev. Mod. Phys.* **70**, 1039.
- Ioffe, L. B., and A. I. Larkin, 1989, *Phys. Rev. B* **40**, 6941.
- Isacsson, A., and S. M. Girvin, 2005, *Phys. Rev. A* **72**, 053604.
- Ishihara, S., T. Tanaka, and M. Matsumoto, 2007, *J. Mol. Struct.* **838**, 216.

- Jackeli, G., and G. Khaliullin, 2009, *Phys. Rev. Lett.* **102**, 017205.
- Jahn, H., and E. Teller, 1937, *Proc. R. Soc. A* **161**, 220.
- Jaksch, D., C. Bruder, J. I. Cirac, C. W. Gardiner, and P. Zoller, 1998, *Phys. Rev. Lett.* **81**, 3108.
- Jaksch, D., and P. Zoller, 2005, *Ann. Phys. (N.Y.)* **315**, 52.
- Kanamori, J., 1959, *J. Phys. Chem. Solids* **10**, 87.
- Kanamori, J., 1960, *J. Appl. Phys.* **31**, S14.
- Kargarian, M., A. Langari, and G. A. Fiete, 2012, *Phys. Rev. B* **86**, 205124.
- Khaliullin, G., 2001, *Phys. Rev. B* **64**, 212405.
- Khaliullin, G., 2005, *Prog. Theor. Phys. Suppl.* **160**, 155.
- Khaliullin, G., P. Horsch, and A. M. Oleś, 2001, *Phys. Rev. Lett.* **86**, 3879.
- Khaliullin, G., and S. Maekawa, 2000, *Phys. Rev. Lett.* **85**, 3950.
- Khaliullin, G., and V. Oudovenko, 1997, *Phys. Rev. B* **56**, R14243.
- Khomskii, D., 2010, *Basic Aspects of the Quantum Theory of Solids: Order and Elementary Excitations* (Cambridge University Press, Cambridge, England).
- Kitaev, A. Y., 2003, *Ann. Phys. (Amsterdam)* **303**, 2.
- Kitaev, A. Y., 2006, *Ann. Phys. (Amsterdam)* **321**, 2.
- Kivelson, S. A., D. S. Rokhsar, and J. P. Sethna, 1987, *Phys. Rev. B* **35**, 8865.
- Kogut, J. B., 1979, *Rev. Mod. Phys.* **51**, 659.
- Köhl, M., H. Moritz, T. Stöferle, K. Günter, and T. Esslinger, 2005, *Phys. Rev. Lett.* **94**, 080403.
- Kruger, F., S. Kumar, J. Zaanen, and J. van den Brink, 2009, *Phys. Rev. B* **79**, 054504.
- Kubo, K., 2002, *J. Phys. Soc. Jpn.* **71**, 1308.
- Kugel, K., and D. Khomskii, 1972, *JETP Lett.* **15**, 446.
- Kugel, K., and D. Khomskii, 1973, *Sov. Phys. JETP* **37**, 725.
- Kugel, K., and D. Khomskii, 1982, *Sov. Phys. Usp.* **25**, 231.
- Kuklov, A. B., 2006, *Phys. Rev. Lett.* **97**, 110405.
- Kuklov, A. B., and B. V. Svistunov, 2003, *Phys. Rev. Lett.* **90**, 100401.
- Kuroki, K., S. Onari, R. Arita, H. Usui, Y. Tanaka, H. Kotani, and H. Aoki, 2008, *Phys. Rev. Lett.* **101**, 087004.
- Lai, H.-H., and O. I. Motrunich, 2011, *Phys. Rev. B* **84**, 235148.
- Lieb, E., 1967, *Phys. Rev.* **162**, 162.
- Lieb, E., 1973, *Commun. Math. Phys.* **31**, 327.
- Lieb, E., T. Schultz, and D. Mattis, 1961, *Ann. Phys. (N.Y.)* **16**, 407.
- Lin, F., and V. W. Scarola, 2013, *Phys. Rev. Lett.* **111**, 220401.
- Liu, W. V., and C. Wu, 2006, *Phys. Rev. A* **74**, 013607.
- Lo, K. W., W.-C. Lee, and P. W. Phillips, 2013, *Europhys. Lett.* **101**, 50007.
- Lou, J., A. W. Sandvik, and L. Balents, 2007, *Phys. Rev. Lett.* **99**, 207203.
- Luttinger, J. M., and L. Tisza, 1946, *Phys. Rev.* **70**, 954.
- Lv, W., J. Wu, and P. Phillips, 2009, *Phys. Rev. B* **80**, 224506.
- Lyons, D. H., and T. A. Kaplan, 1960, *Phys. Rev.* **120**, 1580.
- Ma, S.-K., 1973, *Phys. Rev. A* **7**, 2172.
- MacDonald, A. H., and M. P. A. Fisher, 2000, *Phys. Rev. B* **61**, 5724.
- Matsubara, T., and H. Matsuda, 1956, *Prog. Theor. Phys.* **16**, 569.
- Micheli, A., G. K. Brennen, and P. Zoller, 2006, *Nat. Phys.* **2**, 341.
- Mila, F., 1998, *Phys. Rev. Lett.* **81**, 2356.
- Mila, F., F. Vernay, A. Ralko, F. Becca, P. Fazekas, and K. Penc, 2007, *J. Phys. Condens. Matter* **19**, 145201.
- Mishra, A., M. Ma, F.-C. Zhang, S. Guertler, L.-H. Tang, and S. Wan, 2004, *Phys. Rev. Lett.* **93**, 207201.
- Moessner, R., 2001, *Can. J. Phys.* **79**, 1283.
- Mondal, S., D. Sen, and K. Sengupta, 2008, *Phys. Rev. B* **78**, 045101.
- Moore, J. E., and D.-H. Lee, 2004, *Phys. Rev. B* **69**, 104511.
- Mostovoy, M. V., and D. I. Khomskii, 2002, *Phys. Rev. Lett.* **89**, 227203.
- Mostovoy, M. V., and D. I. Khomskii, 2004, *Phys. Rev. Lett.* **92**, 167201.
- Motome, Y., and H. Tsunetsugu, 2004, *Phys. Rev. B* **70**, 184427.
- Mott, N. F., 1990, *Metal-Insulator Transitions* (Taylor & Francis, London).
- Mross, D. F., A. Essin, and J. Alicea, 2014, arXiv:1410.4201.
- Müller, T., S. Fölling, A. Widera, and I. Bloch, 2007, *Phys. Rev. Lett.* **99**, 200405.
- Murakami, Y., H. Kawada, H. Kawata, M. Tanaka, T. Arima, Y. Moritomo, and Y. Tokura, 1998, *Phys. Rev. Lett.* **80**, 1932.
- Nagle, J. F., 1966, *J. Math. Phys. (N.Y.)* **7**, 1484.
- Nakayama, K., *et al.*, 2009, *Europhys. Lett.* **85**, 67002.
- Nasu, J., and S. Ishihara, 2011a, *J. Phys. Conf. Ser.* **320**, 012062.
- Nasu, J., and S. Ishihara, 2011b, *J. Phys. Conf. Ser.* **320**, 012062.
- Nasu, J., and S. Ishihara, 2011c, *J. Phys. Soc. Jpn.* **80**, 033704.
- Nasu, J., and S. Ishihara, 2012, *Europhys. Lett.* **97**, 27002.
- Nasu, J., A. Nagano, M. Naka, and S. Ishihara, 2008, *Phys. Rev. B* **78**, 024416.
- Nasu, J., S. Todo, and S. Ishihara, 2012a, *Phys. Rev. B* **85**, 205141.
- Nasu, J., S. Todo, and S. Ishihara, 2012b, *Phys. Rev. B* **85**, 205141.
- Nogueira, F. S., and Z. Nussinov, 2009, *Phys. Rev. B* **80**, 104413.
- Normand, B., and Z. Nussinov, 2014, *Phys. Rev. Lett.* **112**, 207202.
- Nussinov, Z., 2001, arXiv:cond-mat/0105253.
- Nussinov, Z., 2004, *Phys. Rev. B* **69**, 014208.
- Nussinov, Z., 2005, *Phys. Rev. D* **72**, 054509.
- Nussinov, Z., 2006, arXiv:cond-mat/0606075.
- Nussinov, Z., C. Batista, and E. Fradkin, 2006, *Int. J. Mod. Phys. B* **20**, 5239.
- Nussinov, Z., C. D. Batista, B. Normand, and S. A. Trugman, 2007, *Phys. Rev. B* **75**, 094411.
- Nussinov, Z., M. Biskup, L. Chayes, and J. van den Brink, 2004, *Europhys. Lett.* **67**, 990.
- Nussinov, Z., and E. Fradkin, 2005, *Phys. Rev. B* **71**, 195120.
- Nussinov, Z., and G. Ortiz, 2008, *Europhys. Lett.* **84**, 36005.
- Nussinov, Z., and G. Ortiz, 2009a, *Ann. Phys. (Amsterdam)* **324**, 977.
- Nussinov, Z., and G. Ortiz, 2009b, *Phys. Rev. B* **79**, 214440.
- Nussinov, Z., and G. Ortiz, 2009c, *Proc. Natl. Acad. Sci. U.S.A.* **106**, 16944.
- Nussinov, Z., G. Ortiz, and E. Cobanera, 2012a, *Phys. Rev. B* **86**, 085415.
- Nussinov, Z., G. Ortiz, and E. Cobanera, 2012b, *Ann. Phys. (Amsterdam)* **327**, 2491.
- Nussinov, Z., J. Rudnick, S. A. Kivelson, and L. N. Chayes, 1999, *Phys. Rev. Lett.* **83**, 472.
- Nussinov, Z., and K. Shtengel, 2015, unpublished.
- Nussinov, Z., and J. van den Brink, 2013, arXiv:1303.5922.
- Nussinov, Z., and J. van den Brink, 2015, unpublished.
- O'Hern, C. S., and T. C. Lubensky, 1998, *Phys. Rev. E* **58**, 5948.
- O'Hern, C. S., T. C. Lubensky, and J. Toner, 1999, *Phys. Rev. Lett.* **83**, 2745.
- Oitmaa, J., and C. J. Hamer, 2011, *Phys. Rev. B* **83**, 094437.
- Oleś, A., L. Feiner, and J. Zaanen, 2000, *Phys. Rev. B* **61**, 6257.
- Oleś, A., G. Khaliullin, P. Horsch, and L. Feiner, 2005, *Phys. Rev. B* **72**, 214431.
- Oleś, A. M., 1983, *Phys. Rev. B* **28**, 327.
- Oleś, A. M., 2012, *J. Phys. Condens. Matter* **24**, 313201.
- Ortiz, G., E. Cobanera, and Z. Nussinov, 2012, *Nucl. Phys. B* **854**, 780.
- Orús, R., A. C. Doherty, and G. Vidal, 2009, *Phys. Rev. Lett.* **102**, 077203.
- Paglione, J., and R. L. Greene, 2010, *Nat. Phys.* **6**, 645.
- Paramekanti, A., L. Balents, and M. P. A. Fisher, 2002, *Phys. Rev. B* **66**, 054526.

- Pedrocchi, F. L., S. Chesi, S. Gangadharaiyah, and D. Loss, 2012, *Phys. Rev. B* **86**, 205412.
- Perez-García, D., M. M. Wolf, M. Sanz, F. Verstraete, and J. I. Cirac, 2008, *Phys. Rev. Lett.* **100**, 167202.
- Powell, S., 2011, *Phys. Rev. B* **84**, 094437.
- Rastelli, E., and A. Tassi, 1987, *J. Phys. C* **20**, L303.
- Reitsma, A. J. W., L. F. Feiner, and A. M. Oleś, 2005, *New J. Phys.* **7**, 121.
- Reuther, J., R. Thomale, and S. Trebst, 2011, *Phys. Rev. B* **84**, 100406(R).
- Rokhsar, D. S., and S. A. Kivelson, 1988, *Phys. Rev. Lett.* **61**, 2376.
- Rousochatazakis, I., U. K. Rossler, J. van den Brink, and M. Daghofer, 2013, [arXiv:1209.5895](https://arxiv.org/abs/1209.5895).
- Sachdev, S., 1999, *Quantum Phase Transitions* (Cambridge University Press, London).
- Saket, A., S. R. Hassan, and R. Shankar, 2010, *Phys. Rev. B* **82**, 174409.
- Scarola, V. W., K. B. Whaley, and M. Troyer, 2009, *Phys. Rev. B* **79**, 085113.
- Schneider, U., L. Hackermüller, S. Will, T. Best, I. Bloch, T. A. Costi, R. W. Helmes, D. Rasch, and A. Rosch, 2008, *Science* **322**, 1520.
- Schultz, T. D., D. C. Mattis, and E. H. Lieb, 1964, *Rev. Mod. Phys.* **36**, 856.
- Sen, D., and S. Vishveshwara, 2010, *Europhys. Lett.* **91**, 66009.
- Serral Gracia, R., and T. M. Nieuwenhuizen, 2004, *Phys. Rev. E* **69**, 056119.
- Shender, E., 1982, *Sov. Phys. JETP* **56**, 178.
- Simon, B., 1980, *Commun. Math. Phys.* **71**, 247.
- Stanley, H. E., 1968, *Phys. Rev.* **176**, 718.
- Stillinger, F., and M. A. Cotter, 1973, *J. Chem. Phys.* **58**, 2532.
- Stinchcombe, R., 1983, *Phase Transition and Critical Phenomena*, edited by C. Domb and J. L. Lebowitz, Vol. 7 (Academic Press, London).
- Stöferle, T., H. Moritz, C. Schori, M. Köhl, and T. Esslinger, 2004, *Phys. Rev. Lett.* **92**, 130403.
- Sun, K.-W., Y.-Y. Zhang, and Q.-H. Chen, 2008, *Phys. Rev. B* **78**, 184406.
- Tanaka, T., and S. Ishihara, 2007, *Phys. Rev. Lett.* **98**, 256402.
- Tanaka, T., and S. Ishihara, 2009, *Phys. Rev. B* **79**, 035109.
- Tanaka, T., M. Matsumoto, and S. Ishihara, 2005, *Phys. Rev. Lett.* **95**, 267204.
- Tokura, Y., 2006, *Rep. Prog. Phys.* **69**, 797.
- Tokura, Y., and N. Nagaosa, 2000, *Science* **288**, 462.
- Tokura, Y., and Y. Tomioka, 1999, *J. Magn. Magn. Mater.* **200**, 1.
- Trousselet, F., G. Khaliullin, and P. Horsch, 2011, *Phys. Rev. B* **84**, 054409.
- Trousselet, F., A. M. Oleś, and P. Horsch, 2010, *Europhys. Lett.* **91**, 40005.
- Trousselet, F., A. M. Oleś, and P. Horsch, 2012, *Phys. Rev. B* **86**, 134412.
- Tsunetsugu, H., 2001, *J. Phys. Soc. Jpn.* **70**, 640.
- van den Brink, J., 2004, *New J. Phys.* **6**, 201.
- van den Brink, J., P. Horsch, F. Mack, and A. Oleś, 1999, *Phys. Rev. B* **59**, 6795.
- van den Brink, J., G. Khaliullin, and D. Khomskii, 2004, *Orbital Effects in Manganites and in Colossal Magnetoresistive Manganites*, edited by T. Chatterji (Kluwer Academic Publishers, Dordrecht).
- van den Brink, J., and D. Khomskii, 1999, *Phys. Rev. Lett.* **82**, 1016.
- van den Brink, J., M. B. J. Meinders, J. Lorenzana, R. Eder, and G. A. Sawatzky, 1995, *Phys. Rev. Lett.* **75**, 4658.
- van Rynbach, A., S. Todo, and S. Trebst, 2010, *Phys. Rev. Lett.* **105**, 146402.
- Venderbos, J. W. F., M. Daghofer, J. van den Brink, and S. Kumar, 2011, *Phys. Rev. Lett.* **107**, 076405.
- Vernay, F., K. Penc, and F. Mila, 2004, *Phys. Rev. B* **70**, 014428.
- Villain, J., 1972, *Solid State Commun.* **10**, 967.
- Villain, J., R. Bidaux, J. P. Carton, and R. Conte, 1980, *J. Phys. (Paris)* **41**, 1263.
- Vishwanath, A., and D. Carpentier, 2001, *Phys. Rev. Lett.* **86**, 676.
- Wegner, F., 1971, *J. Math. Phys. (N.Y.)* **12**, 2259.
- Weimer, H., 2013, *Mol. Phys.* **111**, 1753.
- Weisse, A., and H. Fehske, 2004, *New J. Phys.* **6**, 158.
- Wen, X.-G., 2004, *Quantum Field Theory of Many-Body Systems* (Oxford University Press, Oxford).
- Wenzel, S., and W. Janke, 2008, *Phys. Rev. B* **78**, 064402.
- Wenzel, S., and W. Janke, 2009, *Phys. Rev. B* **80**, 054403.
- Wenzel, S., W. Janke, and A. M. Läuchli, 2010, *Phys. Rev. E* **81**, 066702.
- Wenzel, S., and A. M. Läuchli, 2011a, *J. Stat. Mech.* P09010.
- Wenzel, S., and A. M. Läuchli, 2011b, *Phys. Rev. Lett.* **106**, 197201.
- Wohlfeld, K., M. Daghofer, and A. M. Oleś, 2011, *Europhys. Lett.* **96**, 27001.
- Wu, C., 2008, *Phys. Rev. Lett.* **100**, 200406.
- Wu, C., and S. Das Sarma, 2008, *Phys. Rev. B* **77**, 235107.
- Wu, C., W. V. Liu, J. Moore, and S. Das Sarma, 2006, *Phys. Rev. Lett.* **97**, 190406.
- Wu, K., and H. Zhai, 2008, *Phys. Rev. B* **77**, 174431.
- Xu, C., and J. E. Moore, 2004, *Phys. Rev. Lett.* **93**, 047003.
- Xu, C., and J. E. Moore, 2005, *Nucl. Phys.* **B716**, 487.
- You, W.-L., and G.-S. Tian, 2008, *Phys. Rev. B* **78**, 184406.
- Youngblood, R. W., and J. D. Axe, 1981, *Phys. Rev. B* **23**, 232.
- Zaanen, J., G. A. Sawatzky, and J. W. Allen, 1985, *Phys. Rev. Lett.* **55**, 418.
- Zhao, E., and W. V. Liu, 2008, *Phys. Rev. Lett.* **100**, 160403.